BEHAVIOR OF A CRACKED SHAFT DURING PASSAGE THROUGH A CRITICAL SPEED
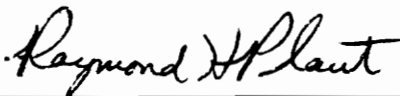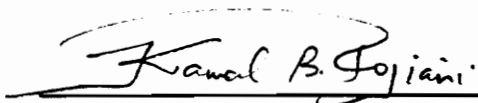
By

Raul Horacio Andruet

Thesis submitted to the Faculty of the

Virginia Polytechnic Institute and State University

in partial fulfillment of the requirements for the degree of

Master of Science

in

Civil Engineering

APPROVED:

_____

Raymond H. Plaut, Chairman

_____
Kamal B. Rojiani

_____
Siegfried M. Holzer

August 15,1991

Blacksburg, Virginia

BEHAVIOR OF A CRACKED SHAFT DURING PASSAGE THROUGH A CRITICAL SPEED

By

Raul Horacio Andruet

Raymond H. Plaut, Chairman

Civil Engineering

(ABSTRACT)

The detection of cracks in structural components and the evaluation of their sizes without the need of removing them from the machine in which they are placed is very important for preventing failures. The objective of this thesis is to study the effects of cracks on the dynamic behavior of shafts under acceleration or deceleration, in order to find methods or procedures capable of detecting the presence of cracks prior to failure.

The equations of motion for a simply supported Bernoulli-Euler shaft are developed following Wauer's formulation. Galerkin's Method is used to obtain five-term approximate solutions. The first two natural frequencies are found for both the uncracked and cracked shaft. A computer program is written to perform the numerical integration of the equations. The shaft is subjected to several constant accelerations and decelerations. Tables and figures showing the results are presented along with discussions and comments related to the different runs made and the results obtained. The effect of the initial position angle of the eccentricity is studied to find the influence of this parameter. The effects of crack

position and crack depth on the dynamic behavior of the shaft are also included in this work. Time histories and summary graphs are presented to make easier the interpretation of the results.

Final conclusions and future research proposals complete the work done in this thesis.

Dedication

To my Parents.

A mis Padres.

Acknowledgements

I would like to express my sincere gratitude to Dr. Raymond Plaut for his patience, understanding, support and guidance during the course of this study.

I would like to thank Marcela Ruiz-Funes and Gustavo Maldonado for their constant support and friendship.

Also, I want to thank Dr. Siegfried Holzer and Dr. Kamal Rojiani for serving on my thesis committee.

Table of Contents

Chapter 5

List of Illustrations

List of Tables

Chapter 1

Introduction

The presence of cracks in structures produces changes in their dynamic behavior. Numerous studies have been made concerning those changes in order to obtain methods to detect cracks and to estimate their sizes.

Many researchers studied rotating shafts with one or more cracks over their lengths, producing many methods and solutions for almost all possible cases. The presence of the cracks was modeled using different approaches. In particular, a crack introduces non-linearity in the structure in both the stiffness and damping terms. In general the structures are considered to be bilinear, but some authors assume the cracks are always open. In the present study a bilinear approach formulated by Wauer is used.

Despite the various works on this topic, the influence of cracks on the dynamic behavior of shafts under angular acceleration or deceleration was not studied previously. Research has been limited to the case of constant angular speed.

It is well known that for rotating structures, there are some angular velocities that produce maximum transverse deflections. These angular velocities are called critical speeds. Many machines, such as generators and compressors, have rotors working above one of these critical speeds at least. The transition from rest to the working rotating speed can produce large-amplitude displacements. Dangerous effects can be the result of this acceleration process. The same problems can arise during deceleration.

It has been observed in experimental studies that the response of a rotating shaft deviates considerably from the steady state during speed-up and slow-down passing through a critical speed. The maximum amplitude is usually found above the critical speed in acceleration and at lower speeds during deceleration. The amplification in the transverse deflection produced during both speed-up and slow-down usually decreases if the acceleration or deceleration increases. Furthermore, the amplitude is considerably larger if the shaft is under a steady critical angular speed.

The presence of mass imbalance in the shaft may cause large deflections, and whirling is very frequently observed. The whirl pattern is in general elliptical considering the possibility of transverse non-symmetric stiffness and damping. The orbits are then ellipses with their centers not coinciding with the line connecting the supports due to gravity.

2

The objective of this thesis is to study the effects of cracks in shafts under angular acceleration and deceleration. The fact that for uncracked shafts the amplitudes of transverse deflection are larger when the angular velocities are close to a critical speed point out the possibility that the amplification can be larger for cracked shafts, making it easier to detect the presence of one or more cracks over the length of the shaft.

This thesis studies the dynamic behavior of a cracked shaft using the mathematical formulation for a Bernoulli-Euler shaft, with one crack modeled following the previous work done by Wauer.

Galerkin's Method is used to solve the differential equations given by Wauer. This method consists of defining the solutions as a summation of functions where each term is the product of an unknown function depending only on time and a known predefined function depending only on the spatial coordinate x. With some algebraic manipulations, a non-dimensional system of differential equations depending only on time can be obtained.

A computer program is developed to compute approximate values for the amplitudes, the unknown functions of time, using the Adams-Moulton numerical multi-step method. Then the amplitudes are multiplied by the functions of the space coordinate and the complete solution is found for the model.

3

Several runs of the mentioned program are made using different parameters and different rates of acceleration and deceleration, in order to obtain the relationships between the various system parameters. Graphs and tables are presented to illustrate the relationships found. Some conclusions and recommendations for further research are presented.

Literature Review

Several works dealing with the behavior of rotating shafts passing through one critical speed have been published. Lewis (1932) published a paper giving an exact solution of the problem of running a one-degree-of-freedom, damped system through the first critical speed.

Although this ideal system was not a rotational shaft, the conclusions and results presented in this paper can be considered an important anteced-ent for the case of this thesis. Dornig (1959) studied the changes in the vibrations of single-degree-of-freedom systems when they are stopped or started with constant acceleration. He gave exact solutions and approxi-mate formulas that include the inertial forces generated. One of the first papers on rotating shafts was published by Baker (1939), in which the author presented the results of his research on unbalanced rotors: amplitudes for different rates of constant acceleration and deceleration and the setup used to obtain these results on the differential analyzer at the Massachusetts Institute of Technology. Capello (1967) studied the

4

influence of external viscous damping and elastic hysteresis on the behavior of a rotor accelerated through a critical speed. Bodger (1967) examined a single-degree-of-freedom rotor under slow deceleration passing through a critical speed, giving closed form solutions. Aiba (1976) investigated the vibration of rotating shafts passing through critical speeds, including gyroscopic effects. Iwatsubo (1976) used the asymptotic method developed by Kononenko to investigate the behavior of a rotor with asymmetric shaft stiffness. Naveh and Brach (1977) considered exponential transition through a critical speed instead of the constant acceleration assumed by the previous researchers as a way to make more realistic simulations. Ying (1987) wrote a paper dealing with the transient whirling of a rotating shaft with an unbalanced disk with different levels of damping, showing that with large damping the response increases with the rate of acceleration. Hassenpflug, Flack and Gunter (1981) examined the effect of angular acceleration on a Jeffcott rotor. Tsuchiya (1982) studied a non-stationary oscillation of a rotor through a critical speed based on the methods of multiple scales and matched asymptotic expansions. Zobnin, Kelzon and Neigebauer (1987) worked on the influence of gyroscopic effects on resonance avoidance during acceleration of unbalanced flexible rotors.

The above mentioned studies have treated the problem of linear systems; but since the presence of cracks introduces some kind of nonlinearity, a brief review of some papers considering non-linear systems is presented. Meuser and Weibel (1948) presented a generalized solution for the effect

of an accelerated sine-wave force on a spring-mass system with linear or cubic stiffness and linear damping. Ishida, Ikeda and Yamamoto (1987) studied the transient vibration of a rotating shaft with nonlinear spring characteristic passing through a critical speed. In all the papers mentioned so far, except in Ying (1987), the maximum amplitude decreases with the rate of acceleration or deceleration. Ishida, Ikeda, Yamamoto and Murakami (1989) investigated the response during constant acceleration or deceleration passing through a critical speed of 1/2-order of a subharmonic oscillation. Differently than in the previous papers, they found that the maximum amplitude depends strongly not only on the rate of acceleration but also on the initial angular position of the shaft.

The influence of a crack in structures has been extensively studied in recent years. The effects on the stiffness were considered as a nonlinearity by Mayes and Davies (1980), and Rogers and Hollingshead (1988) considered that the effects on damping may be important. Many other researchers associate cracks in structures with bilinear oscillators due to the changes in stiffness and damping produced by the presence of the crack.

For cracked shafts it is important to mention Muszynska (1982), who investigated cracked shafts with non-symmetric cross-sections. Schmied and Krämer (1984) modeled the crack and the opening and closing mechanism using continuous functions. Papadopoulos and Dimarogonas (1988) represented the stiffness of the shaft at the crack position by a

6

cosine series. Gasch, Person and Weitz (1988) dealt with hollow shafts and made a comparison between approximate crack models and exact models based on thin-walled shell theory. Wauer (1990a) conducted a literature survey on the dynamics of cracked shafts. Wauer (1990b) derived the equations of motion for a cracked Timoshenko shaft. He considered forces leading to reduced stiffness and damping and simulating the open crack. A term for the closed crack was also included. Wauer also discussed a Bernoulli-Euler beam. Collins, Plaut and Wauer (1991) investigated the detection of cracks in rotating shafts using axial impulses. Finally, Rajab and Al-Sabeeh (1991) studied the dynamic characteristics of a cracked Timoshenko shaft, giving curves of natural frequencies with respect to crack depth and crack position.

Chapter 2

Physical Model

The ideal model, shown in Figure 2.1, consists of a uniform non-circular shaft with length L, rotating at an angular speed φ, a function of time. There is a crack located at a distance b from the end of the shaft, where $0 \leq b \leq L$. . The angle γ measures the slope between the x-axis and a horizontal plane. It was included to consider all possible orientations between the horizontal and the vertical. If γ is 0, the x-axis lies in a horizontal plane and the positive z-axis is in the direction of gravity.

Two coordinate systems are defined for the modeling, one fixed (x,y,z) in which the x axis coincides with the axial direction of the shaft, and the other one (ξ,η,ζ) rotating with the same angular speed as the shaft. In the transverse section there are two axes of symmetry, 1 and 2, also called the principal axes, with the 1-axis always parallel to the ζ-axis and the 2-axis parallel to the η-axis, as shown in Figure 2.2. Two moments of inertia, I_1 and I_2, related to axes 1 and 2, respectively, define the geometric characteristics of the shaft. The centroid of the transverse section is assumed to be different from the mass center. The distance e in Figure 2.2 is the eccentricity and δ the location angle of the center

of mass. The coordinates of motion, V and W, are time- and space-dependent and are measured in the (ξ,η,ζ) coordinate system. The crack is defined by its depth, called a, and it has a straight edge parallel to the 2-axis. This is supposedly the worst orientation (Wauer,1990b; Muszynska, 1982). h_1 is the distance from the center of the uncracked cross-section to the perimeter of the shaft measured in the 2 direction; and h_2 is the same measured in the 1 direction. In this study it is assumed that the 2 direction has a smaller value of moment of inertia than the 1 direction, or in other words, h_2 is less than h_1.

Except for the crack, the shaft is assumed to be uniform with mass per unit length μ, Young's modulus E and moments of inertia I_1 and I_2 with respect to axis 1 and 2, respectively.

Three types of damping are considered: external d_e (viscous), internal d_i (viscoelastic), and damping at the crack d_c when it is closed. Only transverse displacements (V and W) are taken into account in the present study so the model follows the Euler-Bernoulli theory for elastic beams. Gyroscopic effects are also included in the model.

The effect of the crack is represented by two generalized forces (moments) F and f, see Figure 2.3, corresponding to the influence of the crack on the stiffness of the shaft and on the damping, respectively. Figure 2.3 shows these two forces and also the quantities b_- and b_+ which will be defined in the next section. In general, it is supposed that

9
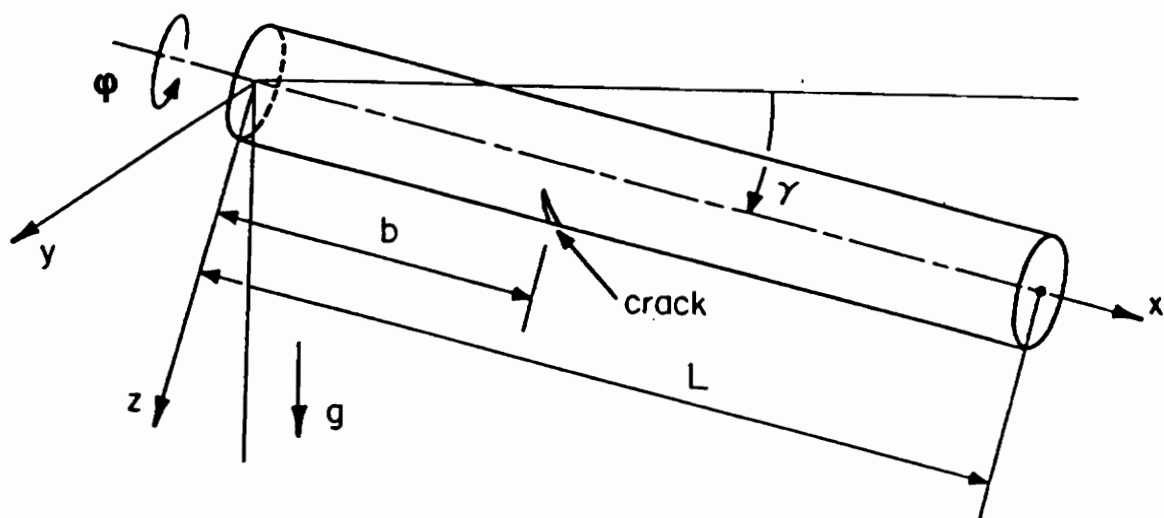
Figure 2.1 Physical model of the cracked shaft.
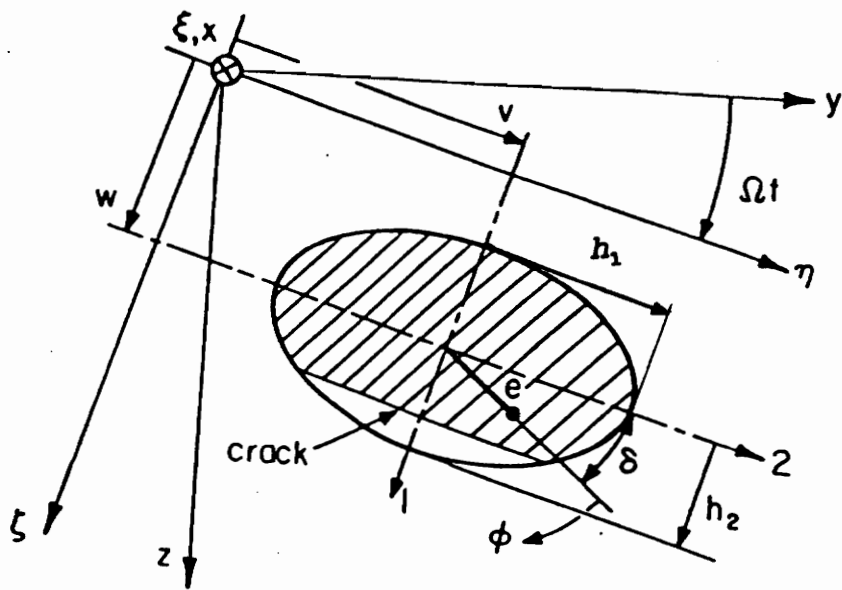
Figure 2.2 Coordinate systems and shaft transverse section parameters at crack position.
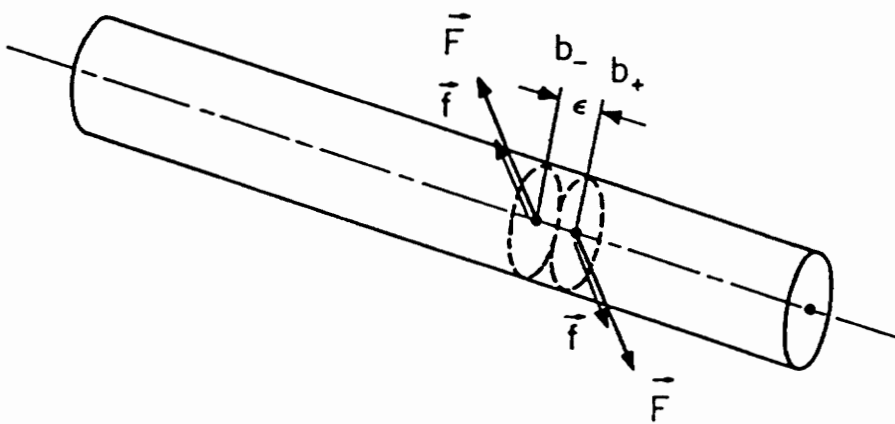
Figure 2.3 Generalized forces F and f.

the crack produces a weakness in the shaft, so the stiffness is smaller in the cracked shaft than in the uncracked one.

Mathematical Model

The governing equations are derived by Wauer (1990b) and therefore the details are not discussed in this thesis. Some comments are presented about this formulation:

· The effect of the crack is considered as a decrease of the stiffness and an increase of the damping of the shaft.

· The shaft is considered uniform along its whole length and the discontinuities in stiffness and damping at the crack are represented by generalized forces F and f, respectively, as depicted in Figure 2.3. This idea was used before by other authors such as Kirmser (1944), Thomson (1949), Petroski (1981), Petroski and Glazik (1980) and Chang and Petroski (1986).

· An Euler-Bernoulli bending shaft is assumed. The gyroscopic effects are considered in the mathematical formulation.

The two following equations of motion used in this work follow those

formulated by Wauer:

$$EI_1V_{xxxx}+\mu V_{tt}-2\varphi\mu W_t-\varphi^2\mu V-\dot{\varphi}\mu W+d_e\mu(V_t-\varphi W)$$

$$+EI_1d_iV_{xxxx}+(1-\Lambda)d_c\mu(V_t-\varphi W)\delta(x-b)$$

$$+\Lambda[\delta'(x-b_+)-\delta'(x-b_-)](M_\zeta+m_\zeta)$$

$$=\mu g\sin(\theta)+e\mu[\varphi^2\cos(\delta)+\dot{\varphi}\cos(\delta)]$$

(2.1)

$$\Gamma EI_1W_{xxxx}+\mu W_{tt}+2\varphi\mu V_t-\varphi^2\mu W+\dot{\varphi}\mu V+d_e\mu(W_t+\varphi V)$$

$$+\Gamma EI_1d_iW_{xxxx}+(1-\Lambda)d_c\mu(W_t+\varphi V)\delta(x-b)$$

$$-\Lambda[\delta'(x-b_+)-\delta'(x-b_-)](M_\eta+m_\eta)$$

$$=\mu g\cos(\theta)+e\mu[\varphi^2\sin(\delta)-\dot{\varphi}\cos(\delta)]$$

(2.2)

The subscripts x and t represent derivatives with respect to x and t, respectively. The crack width parameter ϵ is used to define the coordinates of the two faces of the open crack:

$$b_+=b+(\epsilon/2) \quad ; \quad b_-=b-(\epsilon/2)$$

(2.3)

The open and closed states are handled by the variable Λ. It can take two values:

$$\Lambda=\begin{cases}1:open\ crack\\0:closed\ crack\end{cases}$$

(2.4)

14

The parameter Γ is the ratio between the inertias I_2 and I_1; θ is the rotational angle. φ and ϕ are the rotational velocity and acceleration, respectively, and they are defined by

$$\varphi = \frac{d\theta}{dt} \quad ; \quad \phi = \frac{d^2\theta}{dt^2} \tag{2.5}$$

Having defined the discontinuity produced by the crack in this way, the equations are valid for the whole structure. So, solutions for uniform shafts can be used to solve the cracked shaft.

The generalized forces F and f can be obtained by equating the following expressions of the displacements:

$$V_x(b_+, t) - V_x(b_-, t) = c_{44} EI_1 V_{xx}(b, t)$$

$$W_x(b_+, t) - W_x(b_-, t) = c_{55} EI_2 W_{xx}(b, t)$$

and

$$V_{xx}(b_+, t) - V_{xx}(b_-, t) = c_{44} EI_1 d_i V_{xxx}(b, t)$$

$$W_{xx}(b_+, t) - W_{xx}(b_-, t) = c_{55} EI_2 d_i W_{xxx}(b, t)$$

15

where b can be either b_+ or b_-, and C_{44} and C_{55} are the compliances defined as the inverse of the stiffness coeficients k_{44} and k_{55}. The compliances are functions of the ratio of the crack depth and the bar diameter. The displacements also satisfy:

$$V_x(b_+,t) - V_x(b_-,t) = \varepsilon \frac{M_\zeta}{EI_1}$$

$$W_x(b_+,t) - W_x(b_-,t) = -\varepsilon \frac{M_\eta}{EI_2}$$

$$V_{xx}(b_+,t) - V_{xx}(b_-,t) = \varepsilon \frac{m_\zeta}{d_t EI_1}$$

$$W_{xx}(b_+,t) - W_{xx}(b_-,t) = -\varepsilon \frac{m_\eta}{d_t EI_2}$$

Then, combining these equations,

$$\frac{\varepsilon}{EI_1}(M_\zeta + m_\zeta) = C_{44} EI_1 (V_{xx} + d_t V_{xxx})\big]_{x=b}$$

$$\frac{\varepsilon}{EI_2}(M_\eta + m_\eta) = -C_{55} EI_2 (W_{xx} + d_t W_{xxx})\big]_{x=b}$$

The final expressions for the generalized forces are

$$(M_\zeta + m_\zeta) = C_{44} \frac{(EI_1)^2}{\varepsilon}(V_{xx} + d_t V_{xxx})\bigg]_{x=b}$$

$$(M_\eta + m_\eta) = -C_{55} \frac{(EI_2)^2}{e} (W_{xx} + d_i W_{txx}) \Big]_{x=b}$$

The two equations of motion become

$$EI_1 V_{xxxx} + \mu V_{tt} - 2\varphi\mu W_t - \varphi^2\mu V - \dot\varphi\mu W + d_e\mu(V_t - \varphi W)$$

$$+ EI_1 d_i V_{txxxx} + (1-\Lambda)d_c\mu(V_t - \varphi W)\delta(x-b)$$

$$+ \Lambda[\delta'(x-b_+) - \delta'(x-b_-)]c_{44} \frac{(EI_1)^2}{e}(V_{xx} + d_i V_{txx})\Big]_{x=b} \qquad (2.6)$$

$$= \mu g \sin(\theta) + e\mu[\varphi^2\cos(\delta) + \dot\varphi\sin(\delta)]$$

$$\Gamma EI_1 W_{xxxx} + \mu W_{tt} + 2\varphi\mu Vxbt - \varphi^2\mu W + \dot\varphi\mu V + d_e\mu(W_t - \varphi V)$$

$$+ \Gamma EI_1 d_i W_{txxxx} + (1-\Lambda)d_c\mu(W_t + \varphi V)\delta(x-b)$$

$$+ \Lambda[\delta'(x-b_+) - \delta'(x-b_-)]c_{55}\Gamma^2 \frac{EI_1^2}{e}(W_{xx} + d_i W_{txx})\Big]_{x=b} \qquad (2.7)$$

$$= \mu g\cos(\theta) + e\mu(\varphi^2\sin(\delta) - \dot\varphi\cos(\delta))$$

The crack is supposed to be either completely closed or open at a given time. This means that the equations of motion are linear within each period of time in which the crack remains open or closed. But they can be different from one period of time to another, so that the system is no longer linear but bilinear. The determination of the time when the crack

17

passes from open to closed, and vice versa, can be of relative importance in the behavior of the shaft. This process of changing the state of the crack from open to closed and vice versa is called "breathing". The open or closed condition can be expressed in mathematical terms as follows:

$$W_{xx}\big]_{x=b} = \begin{cases} \leq 0 \ \textit{for open crack} \\ > 0 \ \textit{for closed crack} \end{cases}$$

Solution

As was mentioned previously, the system of differential equations was solved with the use of Galerkin's method. It consists of predefining approximate solutions satisfying the boundary conditions of the system. Since the assumed solutions must satisfy the boundary conditions, these must be defined previously. In this thesis it will be assumed that the shaft is simply supported at its ends. Following is the mathematical expression of the boundary conditions:

$$V(0,t) = W(0,t) = V(L,t) = W(L,t) = 0$$

$$EI_1 V_{xx}(0,t) = EI_2 W_{xx}(0,t) = 0 \qquad\qquad (2.8)$$

$$EI_1 V_{xx}(L,t) = EI_2 W_{xx}(L,t) = 0$$

The proposed approximate solutions, depending on time and on the spatial coordinate x, are:

$$V(x,t)=\sum_{k=1}^{m} V_k(t)\sin\frac{k\pi x}{L}$$

$$W(x,t)=\sum_{k=1}^{m} W_k(t)\sin\frac{k\pi x}{L}$$

(2.9)

where V_k and W_k are unknown functions of time and the sines are the assumed space coordinate dependent functions. It is very simple to prove that these approximate solutions satisfy the boundary conditions.

Once the assumed functions are selected, they are substituted into the equations of motion, which are then made orthogonal to each of the sine functions in the expansions. This leads to a system of differential equations depending only on time. Substituting in the first equation:

$$EI_1\sum_{k=1}^{m} V_k\left(\frac{k\pi}{L}\right)^4\sin\frac{k\pi x}{L}+\mu\sum_{k=1}^{m}\ddot{V}_k\sin\frac{k\pi x}{L}-2\varphi\mu\sum_{k=1}^{m}\dot{W}_k\sin\frac{k\pi x}{L}$$

$$-\varphi^2\mu\sum_{k=1}^{m} V_k\sin\frac{k\pi x}{L}-\dot\varphi\mu\sum_{k=1}^{m} W_k\sin\frac{k\pi x}{L}+d_e\mu(\sum_{k=1}^{m}\dot{V}_k\sin\frac{k\pi x}{L}$$

$$-\varphi\sum_{k=1}^{m} W_k\sin\frac{k\pi x}{L})+EI_1 d_i\sum_{k=1}^{m}\dot{V}_k(\frac{k\pi}{L})^4\sin\frac{k\pi x}{L}$$

(2.10)

$$+(1-\Lambda)d_c\mu(\sum_{k=1}^{m}\dot{V}_k\sin\frac{k\pi x}{L}-\varphi\sum_{k=1}^{m} W_k\sin\frac{k\pi x}{L})\delta(x-b)$$

$$-\Lambda[\delta'(x-b_+)-\delta'(x-b_-)]c_{44}\frac{(EI_1)^2}{\varepsilon}\sum_{k=1}^{m}((V_k+d_i\dot{V}_k)\left(\frac{k\pi}{L}\right)^2\sin\frac{k\pi b}{L})$$

$$=\mu g\sin(\theta)+e\mu[\varphi^2\cos(\delta)+\dot\varphi\sin(\delta)]$$

By multiplying both sides by the sine functions ($\sin(n\pi x/L)$, n=1,...m) and integrating over the whole domain, it is possible to obtain a set of differential equations depending only on time:

$$
\int_0^L [EI_1 \sum_{k=1}^{m} V_k \left(\frac{k\pi}{L}\right)^4 \sin\frac{k\pi x}{L} + \mu \sum_{k=1}^{m} \ddot{V}_k \sin\frac{k\pi x}{L} - 2\varphi\mu \sum_{k=1}^{m} \dot{W}_k \sin\frac{k\pi x}{L}
$$

$$
-\varphi^2\mu \sum_{k=1}^{m} V_k \sin\frac{k\pi x}{L} - \dot{\varphi}\mu \sum_{k=1}^{m} W_k \sin\frac{k\pi x}{L} + d_e\mu(\sum_{k=1}^{m} \dot{V}_k \sin\frac{k\pi x}{L}
$$

$$
-\varphi \sum_{k=1}^{m} W_k \sin\frac{k\pi x}{L}) + EI_1 d_i \sum_{k=1}^{m} \dot{V}_k \left(\frac{k\pi}{L}\right)^4 \sin\frac{k\pi x}{L}
$$

$$
+(1-\Lambda)d_c\mu(\sum_{k=1}^{m} \dot{V}_k \sin\frac{k\pi x}{L} - \varphi \sum_{k=1}^{m} W_k \sin\frac{k\pi x}{L})\delta(x-b) \qquad (2.11)
$$

$$
-\Lambda[\delta(x-b_+)-\delta(x-b_-)]c_{44}\frac{(EI_1)^2}{e}\sum_{k=1}^{m} ((V_k
$$

$$
+d_i\dot{V}_k)\left(\frac{k\pi}{L}\right)^2 \sin\frac{k\pi b}{L})]\sin\frac{n\pi x}{L}dx
$$

$$
=\int_0^L [\mu g\sin(\theta) + e\mu(\varphi^2\cos(\delta) + \dot{\varphi}\sin(\delta))]\sin\frac{n\pi x}{L}dx
$$

Each integral is calculated separately for the n equations:

$$
\int_0^L EI_1 V_k \left(\frac{k\pi}{L}\right)^4 \sin\frac{k\pi x}{L}\sin\frac{n\pi x}{L}dx = \begin{cases} 0 \ \ if \ k \neq n \\ \\ EI_1 V_n \dfrac{L}{2}\left(\dfrac{n\pi}{L}\right)^4 \ \ if \ k=n \end{cases}
$$

$$\int_0^L \mu \ddot{V}_k \sin\frac{k\pi x}{L}\sin\frac{n\pi x}{L}dx = \begin{cases} 0 & \text{if } k \neq n \\ \mu\ddot{V}_n\dfrac{L}{2} & \text{if } k = n \end{cases}$$

$$\int_0^L 2\varphi\mu \dot{W}_k \sin\frac{k\pi x}{L}\sin\frac{n\pi x}{L}dx = \begin{cases} 0 & \text{if } k \neq n \\ 2\varphi\mu\dot{W}_n\dfrac{L}{2} & \text{if } k = n \end{cases}$$

$$\int_0^L \varphi^2\mu \dot{V}_k \sin\frac{k\pi x}{L}\sin\frac{n\pi x}{L}dx = \begin{cases} 0 & \text{if } k \neq n \\ \varphi^2\mu\dot{V}_n\dfrac{L}{2} & \text{if } k = n \end{cases}$$

$$\int_0^L \dot{\varphi}\mu W_k \sin\frac{k\pi x}{L}\sin\frac{n\pi x}{L}dx = \begin{cases} 0 & \text{if } k \neq n \\ \dot{\varphi}\mu W_n\dfrac{L}{2} & \text{if } k = n \end{cases}$$

$$\int_0^L d_e\mu \sum_{k=1}^{m} \dot{V}_k \sin\frac{k\pi x}{L}\sin\frac{n\pi x}{L}dx = \begin{cases} 0 & \text{if } k \neq n \\ d_e\mu\dot{V}_n\dfrac{L}{2} & \text{if } k = n \end{cases}$$

21

$$\int_0^L d_e \mu \varphi W_k \sin\frac{k\pi x}{L}\sin\frac{n\pi x}{L}dx = \begin{cases} 0 & \text{if } k \neq n \\ d_e\mu\varphi W_n\dfrac{L}{2} & \text{if } k = n \end{cases}$$

$$\int_0^L EI_1 d_i \dot{V}_k \left(\frac{k\pi}{L}\right)^4 \sin\frac{k\pi x}{L}\sin\frac{n\pi x}{L}dx = \begin{cases} 0 & \text{if } k \neq n \\ EI_1 d_i \dot{V}_n\dfrac{L}{2}\left(\dfrac{n\pi}{L}\right)^4 & \text{if } k = n \end{cases}$$

and since

$$\int_a^b f(x)\delta(x-\xi)dx = f(\xi) \quad (a \leq \xi \leq b)$$

f(x) being a function defined in the interval (a,b)

$$\int_0^L \sum_{k=1}^m \dot{V}_k\sin\frac{k\pi x}{L}\sin\frac{n\pi x}{L}\delta(x-b)dx = \sum_{k=1}^m \dot{V}_k\sin\frac{k\pi b}{L}\sin\frac{n\pi b}{L}$$

$$\int_0^L \sum_{k=1}^m W_k\sin\frac{k\pi x}{L}\sin\frac{n\pi x}{L}\delta(x-b)dx = \sum_{k=1}^m W_k\sin\frac{k\pi b}{L}\sin\frac{n\pi b}{L}$$

and

$$\int_0^L \Lambda[\delta'(x-b_+)-\delta'(x-b_-)]c_{44}\frac{(EI_1)^2}{e}\sum_{k=1}^m (\frac{k\pi}{L})^2 V_k\sin\frac{k\pi b}{L}\sin\frac{n\pi x}{L}dx$$

$$=\Lambda c_{44}(EI_1)^2\left(\frac{n\pi}{L}\right)^2\sin\frac{n\pi b}{L}\sum_{k=1}^m \left(\frac{k\pi}{L}\right)^2 V_k\sin\frac{k\pi b}{L}$$

$$\int_0^L \Lambda[\delta(x-b_+) - \delta(x-b_-)]c_{44}\frac{(EI_1)^2}{\epsilon}d_i\sum_{k=1}^{m}(\frac{k\pi}{L})^2\dot{V}_k\sin\frac{k\pi b}{L}\sin\frac{n\pi x}{L}dx$$

$$=\Lambda c_{44}(EI_1)^2\left(\frac{n\pi}{L}\right)^2\sin\frac{n\pi b}{L}d_i\sum_{k=1}^{m}\left(\frac{k\pi}{L}\right)^2\dot{V}_k\sin\frac{k\pi b}{L}$$

since

$$\int_0^L \delta'(x-b_+)\sin\frac{n\pi x}{L}dx - \int_0^L \delta'(x-b_-)\sin\frac{n\pi x}{L}dx = [\delta(x-b_+)\sin\frac{n\pi x}{L}]_0^L$$

$$-\int_0^L \delta(x-b_+)\frac{n\pi}{L}\cos\frac{n\pi x}{L}dx - [\delta(x-b_-)\sin\frac{n\pi x}{L}]_0^L + \int_0^L \delta(x-b_-)\frac{n\pi}{L}\cos\frac{n\pi x}{L}dx$$

The first and third terms are 0; then

$$\int_0^L \delta'(x-b_+)\sin\frac{n\pi x}{L}dx - \int_0^L \delta'(x-b_-)\sin\frac{n\pi x}{L}dx = -\frac{n\pi}{L}[\cos\frac{n\pi b_+}{L} - \cos\frac{n\pi b_-}{L}]$$

$$=-\frac{n\pi}{L}(-\frac{n\pi\epsilon}{L}\sin\frac{n\pi b}{L}) = \left(\frac{n\pi}{L}\right)^2\epsilon\sin\frac{n\pi b}{L}$$

On the right hand side

$$\int_0^l \mu(g\sin\theta + e[\dot{\theta}^2\cos\delta + \ddot{\delta}\sin\delta])\sin\frac{n\pi x}{L}dx = \mu[g\sin\theta$$

$$+e(\dot{\theta}^2\cos\delta + \ddot{\delta}\sin\delta)]\frac{(1-(-1)^n)}{n}\frac{L}{\pi}$$

since

$$\int_0^l \sin\frac{n\pi x}{L}dx = \begin{cases} 0 & \textit{if } n \textit{ is even} \\ \dfrac{2L}{n\pi} & \textit{if } n \textit{ is odd} \end{cases}$$

Then the generic final n equation becomes

$$EI_1 V_n(\frac{n\pi}{L})^4\frac{L}{2}+\mu\ddot{V}_n\frac{L}{2}-2\varphi\mu\dot{W}_n\frac{L}{2}-\varphi^2\mu V_n\frac{L}{2}-\dot\varphi\mu W_n\frac{L}{2}+d_e\mu(\dot{V}_n-\varphi W_n)\frac{L}{2}$$

$$+EI_1 d_i\dot{V}_n(\frac{n\pi}{L})^4\frac{L}{2}+(1-\Lambda)d_c\mu\sin\frac{n\pi b}{L}\sum_{k=1}^{m}(\sin\frac{k\pi b}{L}(\dot{V}_k-\varphi W_k))$$

$$-\Lambda c_{44}(EI_1)^2\left(\frac{n\pi}{L}\right)^2\sin\frac{n\pi b}{L}\sum_{k=1}^{m}\left(\frac{k\pi}{L}\right)^2(V_k+d_i\dot{V}_k)\sin\frac{k\pi b}{L}$$

$$=\frac{[1-(-1)^n]}{n\pi}L\mu[g\sin\theta+e(\varphi^2\cos\delta+\dot\varphi\sin\delta)]$$

(2.12)

The generic second n equation in the W direction is obtained following the same procedure:

$$EI_2 W_n(\frac{n\pi}{L})^4\frac{L}{2}+\mu\ddot{W}_n\frac{L}{2}+2\varphi\mu\dot{V}_n\frac{L}{2}-\varphi^2\mu W_n\frac{L}{2}+\dot\varphi\mu V_n\frac{L}{2}+d_e\mu(\dot{W}_n+\varphi V_n)\frac{L}{2}$$

$$+EI_2 d_i\dot{W}_n(\frac{n\pi}{L})^4\frac{L}{2}+(1-\Lambda)d_c\mu\sin\frac{n\pi b}{L}\sum_{k=1}^{m}(\sin\frac{k\pi b}{L}(\dot{W}_k+\varphi V_k))$$

$$-\Lambda c_{55}(EI_2)^2\left(\frac{n\pi}{L}\right)^2\sin\frac{n\pi b}{L}\sum_{k=1}^{m}\left(\frac{k\pi}{L}\right)^2(W_k+d_i\dot{W}_k)\sin\frac{k\pi b}{L}$$

$$=\frac{[1-(-1)^n]}{n\pi}L\mu[g\cos\theta+e(\varphi^2\cos\delta-\dot\varphi\sin\delta)]$$

(2.13)

With the following definitions it is possible to get a set of non-dimensional equations:

24

$$\tilde{V}_n = V_n/L \ ; \ \tilde{W}_n = W_n/L$$

$$\tilde{x} = x/L \ ; \ \tilde{b} = b/L$$

$$\tau = \frac{\pi^2}{L^2}\sqrt{\frac{EI_1}{\mu}}\, t$$

$$\tilde{d}_i = \frac{\pi^2}{L^2}\sqrt{\frac{EI_1}{\mu}}\, d_i \tag{2.14}$$

$$\tilde{d}_e = \frac{L^2}{\pi^2}\sqrt{\frac{\mu}{EI_1}}\, d_e$$

$$\tilde{d}_c = \frac{2L}{\pi^2}\sqrt{\frac{\mu}{EI_1}}\, d_c$$

$$\tilde{c}_{44} = \frac{EI_1}{L}c_{44} \ ; \ \tilde{c}_{55} = \frac{EI_1}{L}c_{55}$$

$$\tilde{\mu} = \frac{2L^3\mu g}{\pi^5 EI_1}$$

$$\Gamma = \frac{I_2}{I_1} \ ; \ \tilde{e} = \frac{2e}{\pi L}$$

$$\Omega = \frac{d\theta}{d\tau} \ ; \ \gamma_n = n\pi\tilde{b} \ ; \ \gamma_k = k\pi\tilde{b}$$

Plugging in (2.12) and (2.13)

$$n^4\tilde{V}_n + \frac{d^2\tilde{V}_n}{d\tau^2} - 2\Omega\frac{d\tilde{W}_n}{d\tau} - \Omega^2\tilde{V}_n - \dot{\Omega}\tilde{W}_n + \tilde{d}_e(\frac{d\tilde{V}_n}{d\tau} - \Omega\tilde{W}_n)$$

$$+ n^4\tilde{d}_i\frac{d\tilde{V}_n}{d\tau} + (1-\Lambda)\tilde{d}_c\sin\gamma_n\sum_{k=1}^{m}\sin\gamma_k(\frac{d\tilde{V}_k}{d\tau} - \Omega\tilde{W}_k) \qquad (2.15)$$

$$- 2\Lambda\tilde{c}_{44}n^2\sin\gamma_n\sum_{k=1}^{m}k^2(\tilde{V}_k + \tilde{d}_i\frac{d\tilde{V}_k}{d\tau})\sin\gamma_k$$

$$= \frac{[1-(-1)^n]}{n}[\tilde{\mu}\sin\theta + \tilde{e}(\Omega^2\cos\delta + \dot{\Omega}\sin\delta)]$$

$$\Gamma n^4\tilde{W}_n + \frac{d^2\tilde{W}_n}{d\tau^2} + 2\Omega\frac{d\tilde{V}_n}{d\tau} - \Omega^2\tilde{W}_n + \dot{\Omega}\tilde{V}_n + \tilde{d}_e(\frac{d\tilde{W}_n}{d\tau} + \Omega\tilde{V}_n)$$

$$+ \Gamma n^4\tilde{d}_i\frac{d\tilde{W}_n}{d\tau} + (1-\Lambda)\tilde{d}_c\sin\gamma_n\sum_{k=1}^{m}\sin\theta_k(\frac{d\tilde{W}_k}{d\tau} + \Omega\tilde{V}_k) \qquad (2.16)$$

$$- 2\Gamma^2\Lambda\tilde{c}_{55}n^2\sin\gamma_n\sum_{k=1}^{m}k^2(\tilde{W}_k + \tilde{d}_i\frac{d\tilde{W}_k}{d\tau})\sin\gamma_k$$

$$= \frac{[1-(-1)^n]}{n}[\tilde{\mu}\cos\theta + \tilde{e}(\Omega^2\sin\delta - \dot{\Omega}\cos\delta)]$$

Then, solving this system of differential equations in time, or in other words, getting functions for the V_n's and W_n's , the complete solution can be obtained by multiplying these functions by sin (nπx/L) and combining terms.

Unfortunately, the complexity of the system makes it difficult to find closed form solutions for the V_n's and W_n's, so numerical integration is used in this thesis. Therefore, approximate values of the time-dependent

26

functions V_n and W_n are obtained.

In order to solve the system of differential equations, a FORTRAN computer program is written. The main features of the program are:

- The numerical integration of the system of differential equations is carried out by the subroutine DIVPAG from IMSL (International Mathematics and Statistical Libraries). This subroutine implements for the computer the multi-step Adams-Moulton predictor-corrector method.

- Determination of the transition point between open and closed conditions using the criterion previously mentioned. A tolerance provided by the user is admitted by the program. In this thesis the value 10^{-5} is used.

- The program includes different rates of rotational acceleration and deceleration.

- For acceleration, the program has the possibility of defining a period of steady angular rotation after the process of acceleration.

- For deceleration, the program looks for a steady state before it initiates the deceleration process. For testing if the

steady state is achieved, the program compares the values of two consecutive peaks; if the difference between the peaks is less than a given tolerance, the steady state is assumed. In this work the tolerance is 1%.

· For both cases, acceleration and deceleration, the program gives values of displacements referred to the rotating system for every time step. The maximum value of the displacement in the Z direction and the time when it is produced are also given by the program.

The system to be solved in this thesis has the following general form:

$$A_v \frac{d^2 \tilde{V}_n}{d\tau^2} + B_v \frac{d\tilde{V}_n}{d\tau} + C_v \frac{d\tilde{W}_n}{d\tau} + D_v \tilde{V}_n + E_v \tilde{W}_n + G_v = F_v(\theta, \Omega, \dot{\Omega})$$

$$A_w \frac{d^2 \tilde{W}_n}{d\tau^2} + B_w \frac{d\tilde{W}_n}{d\tau} + C_w \frac{d\tilde{V}_n}{d\tau} + D_w \tilde{W}_n + E_w \tilde{V}_n + G_w = F_w(\theta, \Omega, \dot{\Omega})$$

The DIVPAG subroutine works only with first-order systems. In order to get a first-order system equivalent to the second order system used in

28

this work, the following definitions are made:

$$Y_{s+1}=\tilde{V}_n \;\; ; \;\; \dot{Y}_{s+1}=\frac{d\tilde{V}_n}{d\tau}=Y_{s+2m+1}$$

$$Y_{s+2}=\tilde{W}_n \;\; ; \;\; \dot{Y}_{s+2}=\frac{d\tilde{W}_n}{d\tau}=Y_{s+2m+2}$$

$$Y_{s+2m+1}=\frac{d\tilde{V}_n}{d\tau} \;\; ; \;\; \dot{Y}_{s+2m+1}=\frac{d^2\tilde{V}_n}{d\tau^2}$$

$$Y_{s+2m+2}=\frac{d\tilde{W}_n}{d\tau} \;\; ; \;\; \dot{Y}_{s+2m+2}=\frac{d^2\tilde{W}_n}{d\tau^2}$$

Then the equivalent system used in the program is

$$\dot{Y}_{s+1}=Y_{s+2m+1}$$

$$\dot{Y}_{s+2}=Y_{s+2m+2}$$

$$A_v\dot{Y}_{s+2m+1}+B_vY_{s+2m+1}+C_vY_{s+2m+2}+D_vY_{s+1}+E_vY_{s+2}+G_v=F_v(\theta,\Omega,\dot{\Omega})$$

$$A_w\dot{Y}_{s+2m+2}+B_wY_{s+2m+2}+C_wY_{s+2m+1}+D_wY_{s+2}+E_wY_{s+1}+G_w=F_w(\theta,\Omega,\dot{\Omega})$$

where s=2(n-1); m is the highest mode considered and n, the number of

the mode corresponding to the equation, ranges between 1 and m.

CHAPTER 3

SHAFT PARAMETERS

The shaft parameters used in this thesis are defined in terms of non-dimensional quantities, in order to make them comparable with previous and future research.

Some values are defined as a function of the ratio L/R, R being the radius for a circular cross section or h_2 for elliptical shafts. A set of parameters is defined as a standard case and some variations over this set are made in the next sections. For the standard case the following parameters are used:

$$L=10'$$
$$R=1'$$
$$\tilde{b}=0.4$$
$$\tilde{e}=0.0016$$
$$\delta=0.75\pi$$
$$a/D=0.2$$

where a is the crack depth and D is the shaft diameter. For a circular cross section the values of damping (see expressions 2.14) are chosen as

$$d_e = 0.1 \frac{L}{\pi R}$$

$$d_1 = 0.1 \pi \frac{R}{L}$$

$$d_c = 0$$

The compliances depend on the ratios a/D and L/R. Table 3.1 (a) shows the adopted expressions for the compliances. These values are based on Papadopoulos and Dimarogonas (1988).

The gravity parameter is given by the expression

$$\beta = \frac{2.99 \times 10^{-7}}{2\pi^2} \frac{L^2}{R^2}$$

Then for L/R=10

$$d_e = 0.32$$

$$d_1 = 0.031$$

$$\beta = 1.5 \times 10^{-6}$$

and the values of compliances for each a/D are presented in Table 3.1 (b). Five terms are used in the expansions (2.9), so that m=5.

Table 3.1 Compliances: (a) expressions; (b) values for L/R=10.

Compliances	a/D		
	0.1	0.2	0.3
$\tilde{c}_{44}$	0.02275R/L	0.0475R/L	0.17225R/L
$\tilde{c}_{55}$	0.09625R/L	0.6375R/L	1.7225R/L

(a)

Compliances	a/D		
	0.1	0.2	0.3
$\tilde{c}_{44}$	0.0023	0.0048	0.0172
$\tilde{c}_{55}$	0.0096	0.0638	0.1723

(b)

33

Natural Frequencies

Since the behavior of the shaft changes when it is under angular rotating speeds close to the critical angular velocity, it seems interesting to know the values of these critical speeds. To achieve this goal, an uncracked , undamped shaft is analyzed. Because the natural frequencies do not depend on the loads, the gravity and eccentricity are also set to zero. Since we are interested in the behavior under a determined rotating speed, the angular acceleration is also taken as zero. These conditions in mathematical terms are

$$\tilde{d}_I = 0 \; ; \; \tilde{d}_e = 0 \; ; \; \tilde{d}_c = 0 \; ; \; \tilde{\varepsilon} = 0$$

$$\beta = 0 \; ; \; \Lambda = 0 \; ; \; \frac{d^2\theta}{d\tau^2} = 0 \tag{3.1}$$

Under these assumptions the equations of motion for mode n become

$$n^4 \tilde{V}_n + \frac{d^2 \tilde{V}_n}{d\tau^2} - 2\Omega \frac{d\tilde{W}_n}{d\tau} - \Omega^2 \tilde{V}_n = 0$$

$$\Gamma n^4 \tilde{W}_n + \frac{d^2 \tilde{W}_n}{d\tau^2} + 2\Omega \frac{d\tilde{V}_n}{d\tau} - \Omega^2 \tilde{W}_n = 0$$

or

$$\frac{d^2 \tilde{V}_n}{d\tau^2} + (n^4 - \Omega^2) \tilde{V}_n - 2\Omega \frac{d\tilde{W}_n}{d\tau} = 0$$

$$(3.2)$$

$$\frac{d^2 \tilde{W}_n}{d\tau^2} + (\Gamma n^4 - \Omega^2) \tilde{W}_n + 2\Omega \frac{d\tilde{V}_n}{d\tau} = 0$$

There are as many pairs of equations like this as modes are considered. To get the first critical speed let n=1 and assume as solutions

$$\tilde{V} = V_1 e^{i\omega\tau} \ ; \ \tilde{W} = W_1 e^{i\omega\tau}$$

Then, using these in (3.2) and considering a circular cross section ($\Gamma=1$),

$$-V_1 \omega^2 e^{i\omega\tau} + (1 - \Omega^2) V_1 e^{i\omega\tau} - 2\Omega W_1 i\omega e^{i\omega\tau} = 0$$

$$-W_1 \omega^2 e^{i\omega\tau} + (1 - \Omega^2) W_1 e^{i\omega\tau} + 2\Omega V_1 i\omega e^{i\omega\tau} = 0$$

In matrix form

$$\begin{pmatrix} (1 - (\omega^2 + \Omega^2)) & -2\Omega\omega i \\ 2\Omega\omega i & (1 - (\omega^2 + \Omega^2)) \end{pmatrix} \cdot \begin{Bmatrix} V_1 \\ W_1 \end{Bmatrix} = \begin{Bmatrix} O \\ O \end{Bmatrix} \qquad (3.3)$$

To get a solution different from zero, the determinant of the matrix must be zero. So, the characteristic equation is found:

$$[1 - (\omega^2 + \Omega^2)]^2 + 4\Omega^2\omega^2 i^2 = 0$$

or

35

$$\Omega^4 - 2\Omega^2(1+\omega^2) + (1-\omega^2)^2 = 0 \qquad (3.4)$$

From this equation it is possible to get Ω^2 (angular frequency squared) as a function of ω^2 (natural frequency squared):

$$\Omega^2 = 1 + \omega^2 \pm 2\omega$$

Figure 3.1 shows this relation.

For a cracked shaft, considering the crack always open and a one-mode analysis, the equations are

$$-V_1\omega^2 e^{i\omega\tau} + (1-\Omega^2) V_1 e^{i\omega\tau} - 2\Omega W_1 i\omega e^{i\omega\tau} - 2\mathcal{C}_{44}\sin^2\phi_1 V_1 e^{i\omega\tau} = 0$$

$$-W_1\omega^2 e^{i\omega\tau} + (1-\Omega^2) W_1 e^{i\omega\tau} + 2\Omega V_1 i\omega e^{i\omega\tau} - 2\mathcal{C}_{55}\sin^2\phi_1 W_1 e^{i\omega\tau} = 0$$

where $\phi_1 = \pi b/L$. The matrix form is

$$\begin{pmatrix} 1-(\omega^2+\Omega^2)-2\mathcal{C}_{44}\sin^2\phi_1 & -2\Omega\omega i \\ 2\Omega\omega i & 1-(\omega^2+\Omega^2)-2\mathcal{C}_{55}\sin^2\phi_1 \end{pmatrix} \cdot \begin{Bmatrix} V_1 \\ W_1 \end{Bmatrix} = \begin{Bmatrix} 0 \\ 0 \end{Bmatrix}$$

and the characteristic equation is

36

$$(1-\omega^2-\Omega^2-2\mathcal{C}_{44}\sin^2\phi)(1-\omega^2-\Omega^2-2\mathcal{C}_{55}\sin^2\phi)-4\Omega^2\omega^2=0 \quad (3.5)$$

Calling

$$a_1=1-\omega^2-2\mathcal{C}_{44}\sin^2\phi_1$$

$$a_2=1-\omega^2-2\mathcal{C}_{55}\sin^2\phi_1$$

the equation becomes

$$(a_1-\omega^2)(a_2-\omega^2)-4\Omega^2\omega^2=0$$

or

$$\Omega^4-\Omega^2(a_1+a_2+4\omega^2)+a_1a_2=0$$

If

$$b_1=a_1+a_2+4\omega^2=2+2\omega^2-2\sin^2\phi_1(\mathcal{C}_{44}+\mathcal{C}_{55})$$

then

$$\Omega^2=\frac{b_1\pm\sqrt{b_1^2-4a_1a_2}}{2} \quad (3.6)$$

Figures 3.2 show this relation graphically.

To find the natural frequency let $\Omega=0$ in the expression (3.5):

$$\omega^2 = 1 - 2\tilde{C}_{44}\sin^2\pi\tilde{b}$$

$$\omega^2 = 1 - 2\tilde{C}_{55}\sin^2\pi\tilde{b}$$

and two values of the natural frequency can be obtained

If

$$\tilde{b} = 1/2 \quad ; \quad \tilde{C}_{44} = 0.0048 \quad ; \quad \tilde{C}_{55} = 0.0638$$

$$\omega^2 \begin{cases} = 0.9904 & \rightarrow \quad \omega = 0.995 \\ = 0.8736 & \rightarrow \quad \omega = 0.9347 \end{cases}$$

Then the lowest natural frequency for the cracked shaft is 0.9347 or 6% lower than the natural frequency for the uncracked shaft. This result agrees with those given by Rajab and Al-Sabeeh (1991).

To determine the second natural frequency, the value of m must be 2 at least. Considering a two-mode approximation with the first two modes, the system of equtions is (from equations 2.15 and 2.16)

$$\tilde{V}_1 + \frac{d^2\tilde{V}_1}{d\tau^2} - 2\Omega\frac{d\tilde{W}_1}{d\tau} - \Omega^2\tilde{V}_1 - 2\tilde{C}_{44}\sin(\pi\tilde{b})\,[\tilde{V}_1\sin(\pi\tilde{b}) + 4\tilde{V}_2\sin(\pi\tilde{b})] = 0$$

$$\tilde{W}_1 + \frac{d^2\tilde{W}_1}{d\tau^2} + 2\Omega\frac{d\tilde{V}_1}{d\tau} - \Omega^2\tilde{W}_1 - 2\tilde{C}_{55}\sin(\pi\tilde{b})\,[\tilde{W}_1\sin\pi\tilde{b} + 4\tilde{W}_2\sin(\pi\tilde{b})] = 0$$

$$16\tilde{V}_2 + \frac{d^2\tilde{V}_2}{d\tau^2} - 2\Omega\frac{d\tilde{W}_2}{d\tau} - \Omega^2\tilde{V}_2 - 8\tilde{C}_{44}\sin(2\pi\tilde{b})\ [\tilde{V}_1\sin(\pi\tilde{b}) + 4\tilde{V}_2\sin(2\pi\tilde{b})] = 0$$

$$16\tilde{W}_2 + \frac{d^2\tilde{W}_2}{d\tau^2} + 2\Omega\frac{d\tilde{V}_2}{d\tau} - \Omega^2\tilde{W}_2 - 8\tilde{C}_{55}\sin(2\pi\tilde{b})\ [\tilde{W}_1\sin(\pi\tilde{b}) + 4\tilde{W}_2\sin(2\pi\tilde{b})] = 0$$

Let

$$\tilde{V}_1 = V_1 e^{i\omega\tau} \quad ; \quad \tilde{W}_1 = \tilde{W}_1 e^{i\omega\tau} \quad ; \quad \tilde{V}_2 = V_2 e^{i\omega\tau} \quad ; \quad \tilde{W}_2 = W_2 e^{i\omega\tau}$$

Plugging into the equations and eliminating $e^{i\omega\tau}$, the following expressions are obtained:

$$V_1 - \omega^2 V_1 - 2\Omega i\omega W_1 - \Omega^2 V_1 - 2\tilde{C}_{44}\sin^2(\pi b)V_1) - 8\tilde{C}_{44}\sin(\pi\tilde{b})\sin(2\pi\tilde{b})V_2 = 0$$

$$W_1 - \omega^2 W_1 + 2\Omega i\omega V_1 - \Omega^2 W_1 - 2\tilde{C}_{55}\sin^2(\pi\tilde{b})W_1 - 8\tilde{C}_{55}\sin(\pi\tilde{b})\sin(2\pi\tilde{b})W_2 = 0$$

$$16 V_2 - \omega^2 V_2 - 2\Omega i\omega W_2 - \Omega^2 V_2 - 8\tilde{C}_{44}\sin(2\pi\tilde{b})\sin(\pi\tilde{b})V_1 - 32\tilde{C}_{55}\sin^2(2\pi\tilde{b})V_2 = 0$$

$$16 W_2 - \omega^2 W_2 + 2\Omega i\omega V_2 - \Omega^2 W_2 - 8\tilde{C}_{55}\sin(2\pi\tilde{b})\sin(\pi\tilde{b})W_1 - 32\tilde{C}_{55}\sin^2(2\pi\tilde{b})W_2 = 0$$

Using the following definitions

$$a_{11} = 1 - 2\tilde{C}_{44}\sin^2\pi\tilde{b} - \omega^2 \quad ; \quad a_{13} = -8\tilde{C}_{44}\sin\pi\tilde{b}\sin2\pi\tilde{b}$$

$$a_{22} = 1 - 2\tilde{C}_{55}\sin^2\pi\tilde{b} - \omega^2 \quad ; \quad a_{24} = -8\tilde{C}_{55}\sin\pi\tilde{b}\sin2\pi\tilde{b}$$

$$a_{31} = -8\tilde{C}_{44}\sin\pi\tilde{b}\sin2\pi\tilde{b} \quad ; \quad a_{33} = 16 - 32\tilde{C}_{55}\sin^2\pi\tilde{b} - \omega^2$$

$$a_{42} = -8\tilde{C}_{55}\sin\pi\tilde{b}\sin2\pi\tilde{b} \quad ; \quad a_{44} = 16 - 32\tilde{C}_{55}\sin^2 2\pi\tilde{b} - \omega^2$$

the system becomes

$$
\begin{bmatrix}
a_{11}-\Omega^2 & -2\Omega\omega i & a_{13} & 0 \\
2\Omega\omega i & a_{22}-\Omega^2 & 0 & a_{24} \\
a_{31} & 0 & a_{33}-\Omega^2 & -2\Omega\omega i \\
0 & a_{42} & 2\Omega\omega i & a_{44}-\Omega^2
\end{bmatrix}
\cdot
\begin{Bmatrix}
V_1 \\ W_1 \\ V_2 \\ W_2
\end{Bmatrix}
=
\begin{Bmatrix}
0 \\ 0 \\ 0 \\ 0
\end{Bmatrix}
\qquad (3.8)
$$

Again, in order to get non-trivial solutions, the determinant of this matrix must be zero. It is possible to find relations between the values of Ω^2 and ω^2 such that non-zero solutions are obtained, expanding the determinant of the matrix and finding its roots. The characteristic equation is

$$A\Omega^8+B\Omega^6+C\Omega^4+D\Omega^2+E=0$$

where:

$$A=1$$

$$B=-(a_{11}+a_{22}+a_{33}+a_{44}+8\omega^2)$$

$$C=a_{33}a_{44}+a_{33}a_{11}+a_{33}a_{22}+a_{44}a_{11}+a_{11}a_{22}+a_{22}a_{44}$$
$$-a_{24}a_{42}-a_{13}a_{31}+4\omega^2(a_{11}+a_{22}+a_{33}+a_{44})+16\omega^4$$

$$D = -(a_{11}a_{33}a_{44} + a_{22}a_{33}a_{44} + a_{11}a_{22}a_{33} + a_{11}a_{22}a_{44}$$

$$+ 4\omega^2 (a_{11}a_{22} + a_{33}a_{44} + a_{31}a_{24} + a_{13}a_{42}) + a_{11}a_{42}a_{24}$$

$$+ a_{24}a_{42}a_{33} + a_{13}a_{31}a_{22} + a_{13}a_{31}a_{44})$$

$$E = a_{11}a_{22}a_{33}a_{44} - a_{11}a_{24}a_{42}a_{33} - a_{13}a_{31}a_{22}a_{44} + a_{13}a_{31}a_{24}a_{42}$$

A computer program to find the roots of this equation was written using the IMSL subroutine DZPLRC, which determines the roots of a polynomial with real coeficients. Numerous runs using the standard parameters were made for different values of ω and the results are shown in Figures 3.3 and 3.4 for the uncracked and cracked shafts, respectively.

The angular velocities Ω corresponding to angular frequencies $\omega = 0$ are the critical speeds. In Figure 3.3 (uncracked shaft) there is one value of Ω for each mode giving $\omega = 0$. For cracked shafts there are more than one as seen in Figure 3.4. Furthermore, for the current shaft parameters there is not a large difference in the critical speeds and consequently in natural frequencies between the cracked and uncracked shaft.

Table 3.2 presents the critical speeds for the uncracked and cracked shaft for the first and second modes using m equal to 1 and 2, for the standard case ($\mathtt{b} = 0.4$, a/D=0.2)

Table 3.2 Critical speeds and natural frequencies: (a) Uncracked shaft; (b) Cracked sahft.

UNCRACKED				
	m=1		m=2	
	$\omega^2=0$		$\omega^2=0$	
	Ω^2	Ω	Ω^2	Ω
Mode 1	1	1	1	1
Mode 2	-	-	16	4

(a)

CRACKED				
	m=1		m=2	
	$\omega^2=0$		$\omega^2=0$	
	Ω^2	Ω	Ω^2	Ω
Mode 1	0.8846	0.9405	0.8790	0.9375
	0.9913	0.9956	0.9913	0.9956
Mode 2	-	-	15.3019	3.9118
	-	-	15.9454	3.9932

(b)
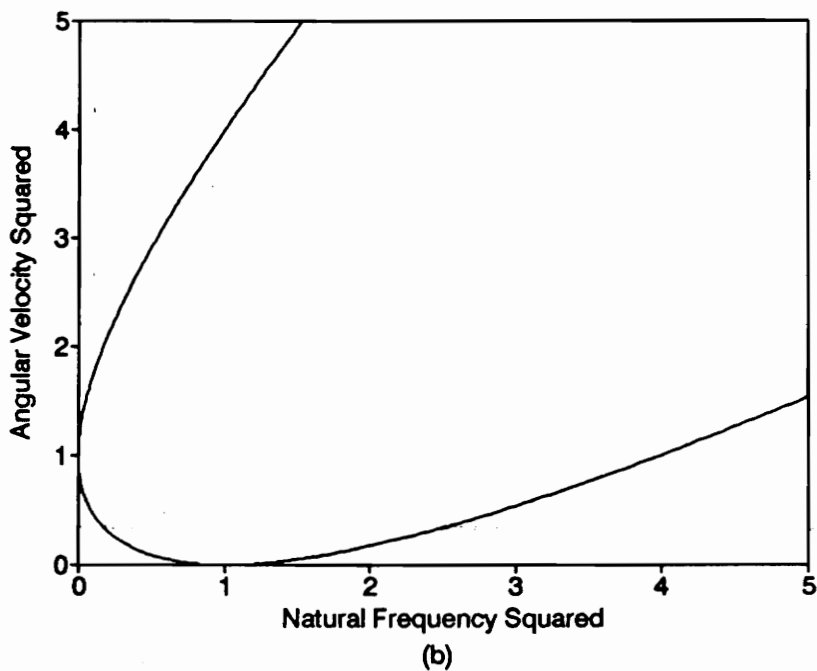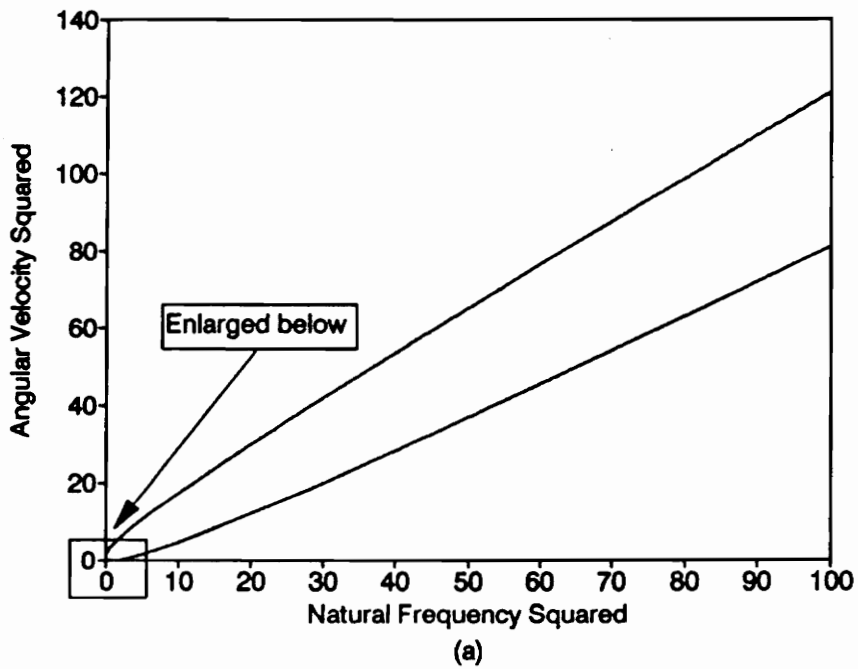
Figure 3.1 Roots of characteristic equation; one mode analysis, uncracked shaft: (a) Complete graph; (b) Enlarged view near the origin.

43

(a)

(b)
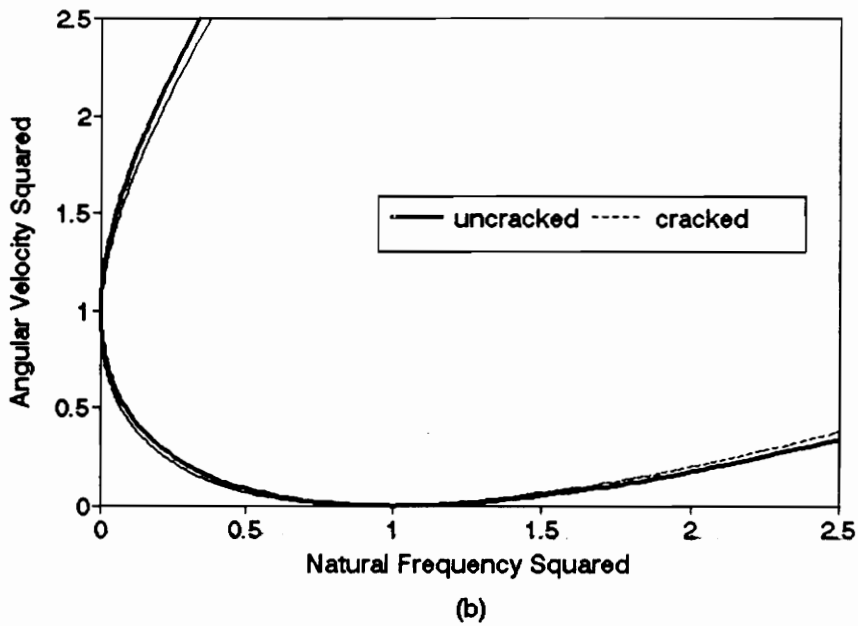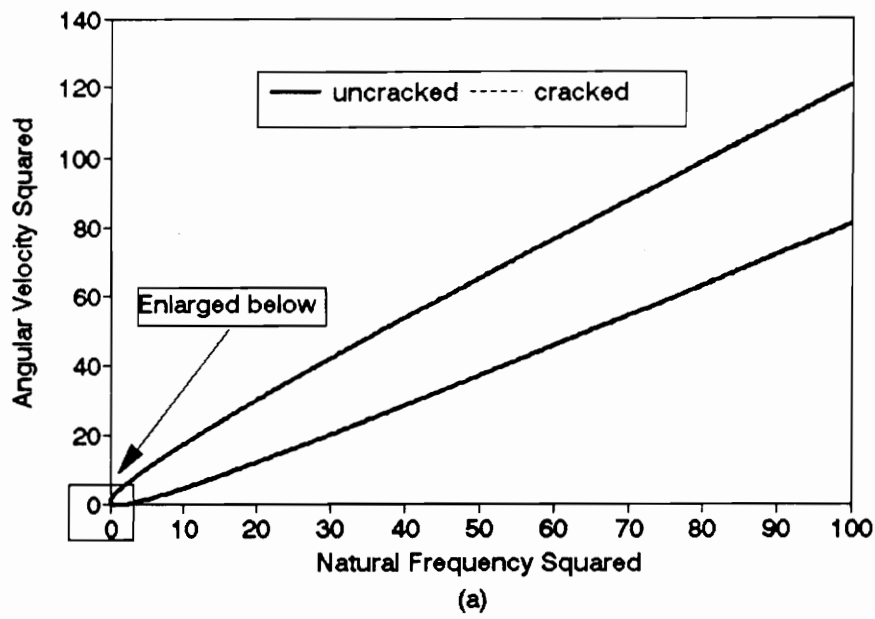
Figure 3.2 Roots of characteristic equation; one mode analysis, cracked shaft: (a) Complete graph; (b) Enlarged view near the origin.

Uncracked Shaft
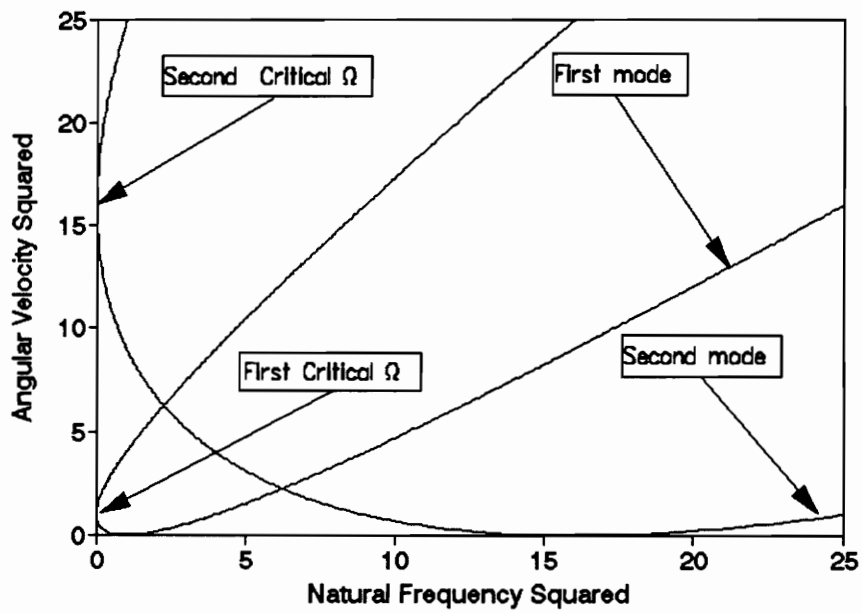
Figure 3.3 Roots of characteristic equation; two modes analysis, uncracked shaft.

Cracked Shaft
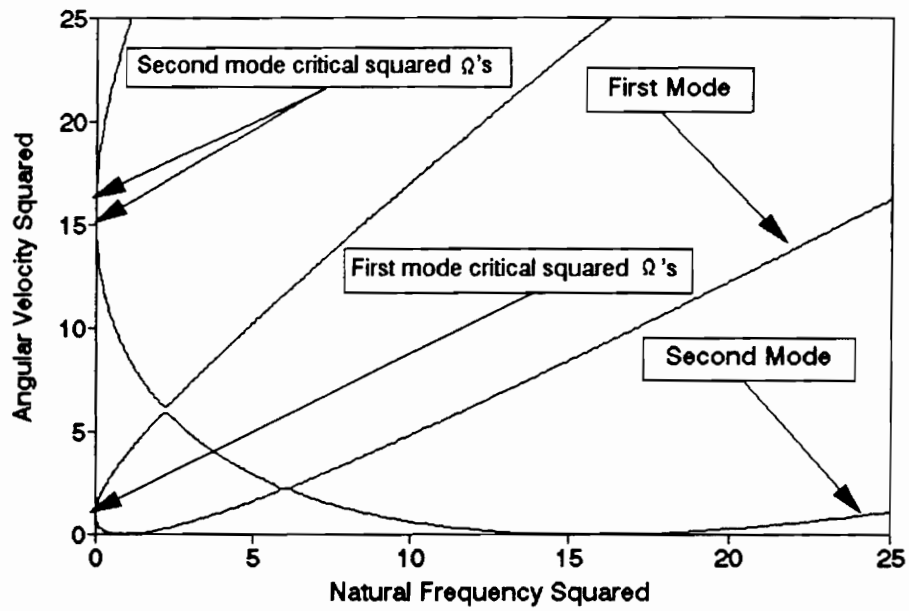
Figure 3.4 Roots of characteristic equation; two modes analysis, cracked shaft.

Chapter 4

Several runs of the program are made in order to determine the influence of the different parameters of the equations of motion on the response of the system.

The first set of processes is intended to study the influence of the rate of acceleration and deceleration on the maximum transverse displacement of the shaft.

For all the cases mentioned, time histories of displacements Z are presented. For selected cases, time histories for Y, V and W displacements are included as well as the orbits followed by the shaft during the motion. Summary figures and tables are also included.

The second set of runs focuses on the importance of the location angle of the center of mass, δ, on the behavior of the shaft; very interesting results are found on this topic.

The influence of crack position and the effect of the crack depth complete the work done in this thesis.

As was mentioned previously, a standard case of parameters is always used unless different values for any of them are specifically stated.

In all the cases presented the expressions for Z and Y are

$$Y = \tilde{V}(\tilde{X}, \tau) \cos\theta - \tilde{W}(\tilde{X}, \tau) \sin\theta$$

$$Z = \tilde{V}(\tilde{X}, \tau) \sin\theta + \tilde{W}(\tilde{X}, \tau) \cos\theta$$

$$(4.1)$$

47

For most of the cases, three kinds of runs are made: without a crack, with a crack always open and with a crack including the breathing process. The second case is not a realistic case, but it is included to have an idea of how the crack can influence the behavior of the shaft. The first and the last cases are, actually, the real situations and consequently those of interest. For the cracked shaft, the more the crack is open during the motion, the more the results are close to the always-open case, and the more the crack is closed, the more the displacements resemble those obtained with the no-crack parameters. As a first impression, the first and second cases should be the upper and lower limits and between them should be the third one, that is, the cracked shaft. But this is not true in all the cases, as the results of this work will show in the next sections. Another predictable result, that is, if the shaft has more stiffness the displacement will be larger, is not absolutely true for all the cases. This will also be seen in the results to be presented.

Influence of acceleration and deceleration

The influence of rate of acceleration is handled by putting a shaft with the standard parameters under a linear acceleration until the angular speed reaches the value of 2 rad/sec; then this steady rotating velocity is held during a period of time long enough so that steady motion is

achieved. The expressions for the angular velocity are

$$\Omega = \lambda \tau \quad \rightarrow \quad 0 \leq \tau \leq t_1$$

$$\text{(4.2)}$$

$$\Omega = 2 \quad \rightarrow \quad \tau > t_1$$

where t_1 is the time when Ω reaches the value 2. Note that the critical angular speed for the first mode of the uncracked shaft is $\Omega = 1$. Figure 4.1 shows graphically these expressions for the different values of λ used.

Figures 4.2 to 4.16 show time histories of the Z displacement measured at $\tilde{x} = 0.7$, for $\lambda = 0.01$, $\lambda = 0.02$, $\lambda = 0.03$, $\lambda = 0.04$ and $\lambda = 0.05$ for the three cases mentioned: no crack, always open crack and breathing. For $\lambda = 0.02$, time histories of Y, V and W displacements and the orbits followed by the shaft during the motion are also presented in Figures 4.17 – 4.19 for the uncracked shaft case, Figures 4.20 – 4.22 for the always open crack case, and Figures 4.23 – 4.25 for the breathing case. In all the cases the initial condition is rest or, in other words, all the initial displacements and velocities equal zero.

The value τ_{crit} is defined as the time when the shaft reaches the critical angular speed. So, for the uncracked shaft under angular acceleration, it is the time when $\Omega = 1$, and for the always open crack it is when $\Omega = 0.9374$ (see section 3.6). For the deceleration case, τ_{crit} is the same for the uncracked shaft and occurs when $\Omega = 0.995$ for the always open crack.

τ_{max} is the time when the maximum displacement, positive or negative, occurs. As the time histories show, τ_{crit} is smaller than τ_{max} in all the cases and as the rate of acceleration increases, τ_{crit} and τ_{max} become closer. The solid lines in the graphs mean closed crack or no crack and the dashed lines represent an open crack. This convention is used in all the time history graphs except in those showing the V and W displacements, where the solid lines are V and the dashed represent W.

An inspection of these figures shows that the uncracked shaft has τ_{max}'s larger than the cracked shaft as a direct result of the difference in their respective τ_{crit}'s. Also, it is noted that for the breathing case, the crack is open until the maximum displacement occurs, and when the steady motion is reached the crack remains closed. This situation produces very close values of the maximum displacement for both cases of always open crack and breathing.

A view of the V and W displacements shows that both have maximum values at times close to the already mentioned τ_{max}, but once the steady motion is reached there is no longer an important oscillatory motion with positive and negative values, but a small oscillation about the equilibrium point, relatively negligible if it is compared with the Z and Y displacements. This means that the whirling motion is the most important when the angular velocity becomes a constant.

Tables 4.1 and 4.2 present a summary of the results shown in the previous figures. They show the maximum values of the vertical displace-

ment Z found for each case: no crack, crack always open and crack with breathing.

The observation of these tables and figures makes clear that for the cracked shaft, changes in the rate of acceleration produce changes in the maximum displacement Z, usually making it smaller as the value of λ increases. The opposite happens for the uncracked shaft; usually the maximum Z displacement increases with the rate of acceleration. Almost the same effect is obtained in both values of Z: at $\tilde{x}=0.7$ and the maximum over the whole length. The irregularities in the values are caused by the numerical method used for the computation of Z. It should be noted that there is an appreciable difference between cracked and uncracked shafts, resulting in a possible means for detecting the presence of cracks. Figures 4.26 and 4.27 show graphically the same results presented in Tables 4.1 and 4.2.

For the deceleration case, it seems important to find a steady state of motion and then start the deceleration. For this reason, a modification in the computer program is made in order to get the time when two successive peaks in the displacement Z differ from each other by less than a given tolerance. For the runs made for this work, this tolerance is 0.0001.

Once the steady state is achieved, the deceleration process is started and it follows the rule

$$\Omega = 2 - \lambda\tau \qquad\qquad (4.3)$$

Figure 4.28 shows Ω as a function of τ for the values of λ used in the time histories.

As was done in the acceleration case, time histories are presented for some values of λ in Figures 4.29 to 4.43, and for $\lambda = 0.02$, time histories of Y, V and W displacements and the orbits followed by the shaft are also shown in Figures 4.44 - 4.46 for an uncracked shaft, in Figures 4.47 - 4.49 for an always open crack , and in Figures 4.50 - 4.52 for a breathing crack.

The effect of the crack seems to be more predictable in deceleration than in acceleration. An observation of the time history graphs shows that the response is larger with smaller stiffness of the shaft. So, the more the crack is open, the greater is the response. There is also a very clear decrease in the maximum amplitude with an increase in the value λ or rate of deceleration. Another highlight is the fact that as the shaft leaves the steady condition, the breathing crack passes from closed to open, as seen in Figures 4.39 - 4.43.

Figures 4.53 and 4.54 present graphically Z_{max} at $\tilde{x} = 0.7$ (the maximum Z displacement at $\tilde{x} = 0.7$) and Z_{max} (the maximum Z displacement over the whole shaft) as a function of λ. As was mentioned in the previous paragraph, in deceleration, as the value of λ increases, the response

decreases and, differently than in acceleration, this is valid for all the cases, with and without crack. The cause for this behavior may be the fact that in acceleration the force applied to the system increases with λ, producing larger displacements that equilibrate the decrease due to the larger acceleration. So, as Figures 4.26 and 4.27 show, the final change in the response is not important. But in deceleration, as the rotating velocity decreases, the force decreases and this, added to the lower time for building up the resonance phenomenon, produces a bigger difference than in acceleration.

The similarity between the values for breathing and always- open cracks is due to the fact that the shaft is always open until the maximum displacement is reached, as the time histories show. In the next section it will be shown that for other values of δ, the results for breathing differ from those obtained for the crack always open.

The time histories show that there is not a process of breathing but a change in the state of the crack from open to closed or vice versa. The reason for this may be the fact that all the processes were started from rest and with values of damping different from zero.

ANGULAR VELOCITIES
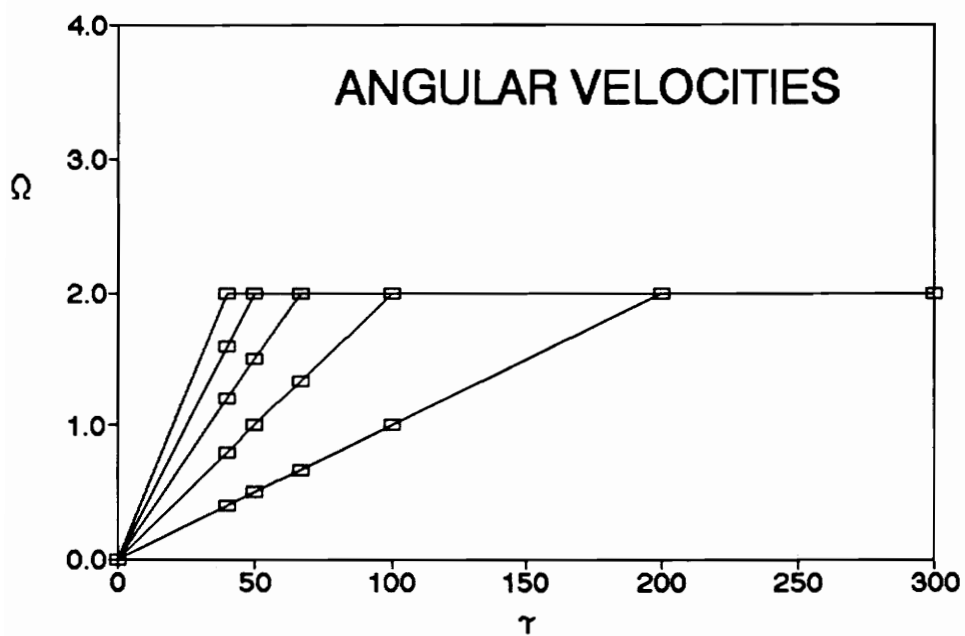
Figure 4.1 Rates of acceleration.
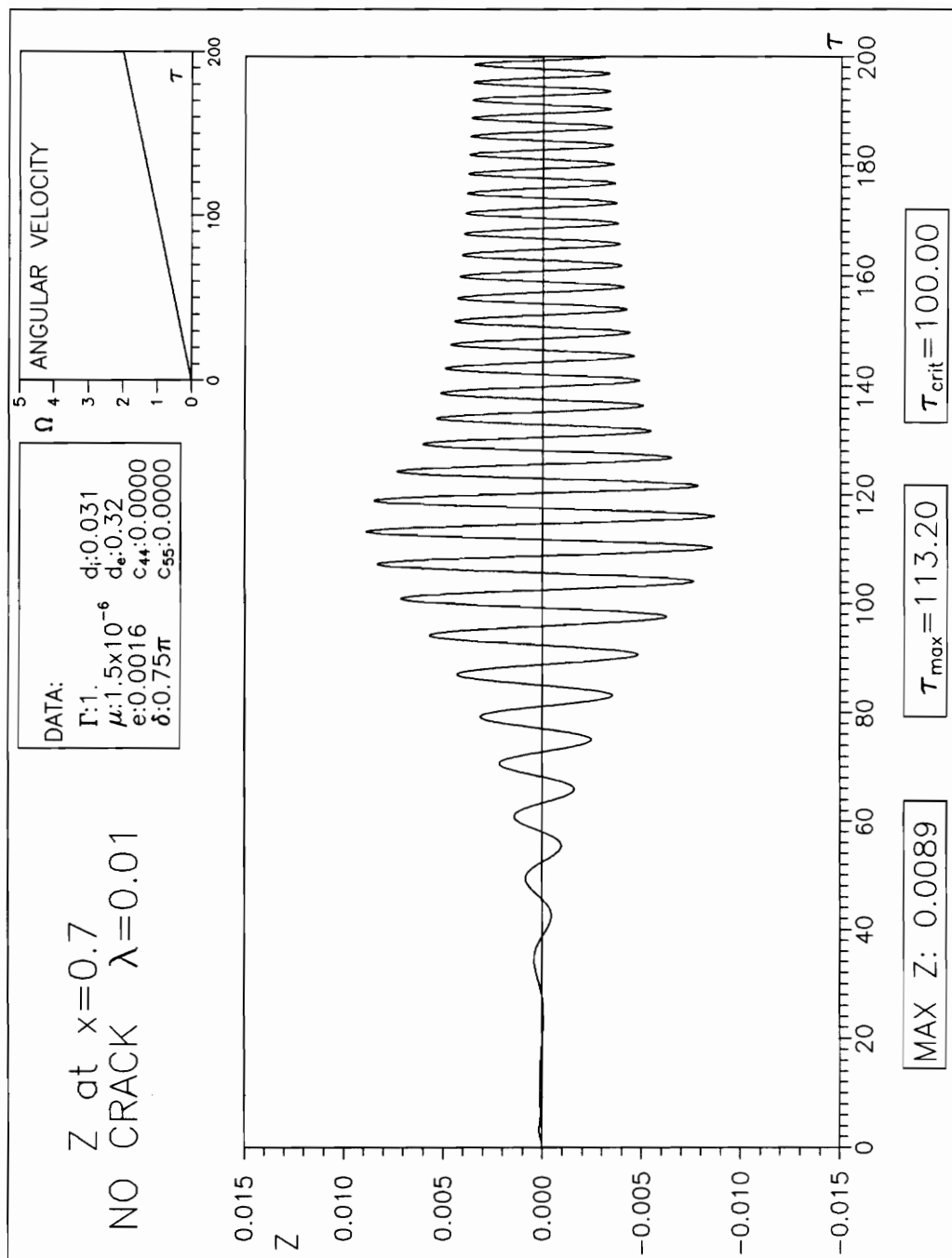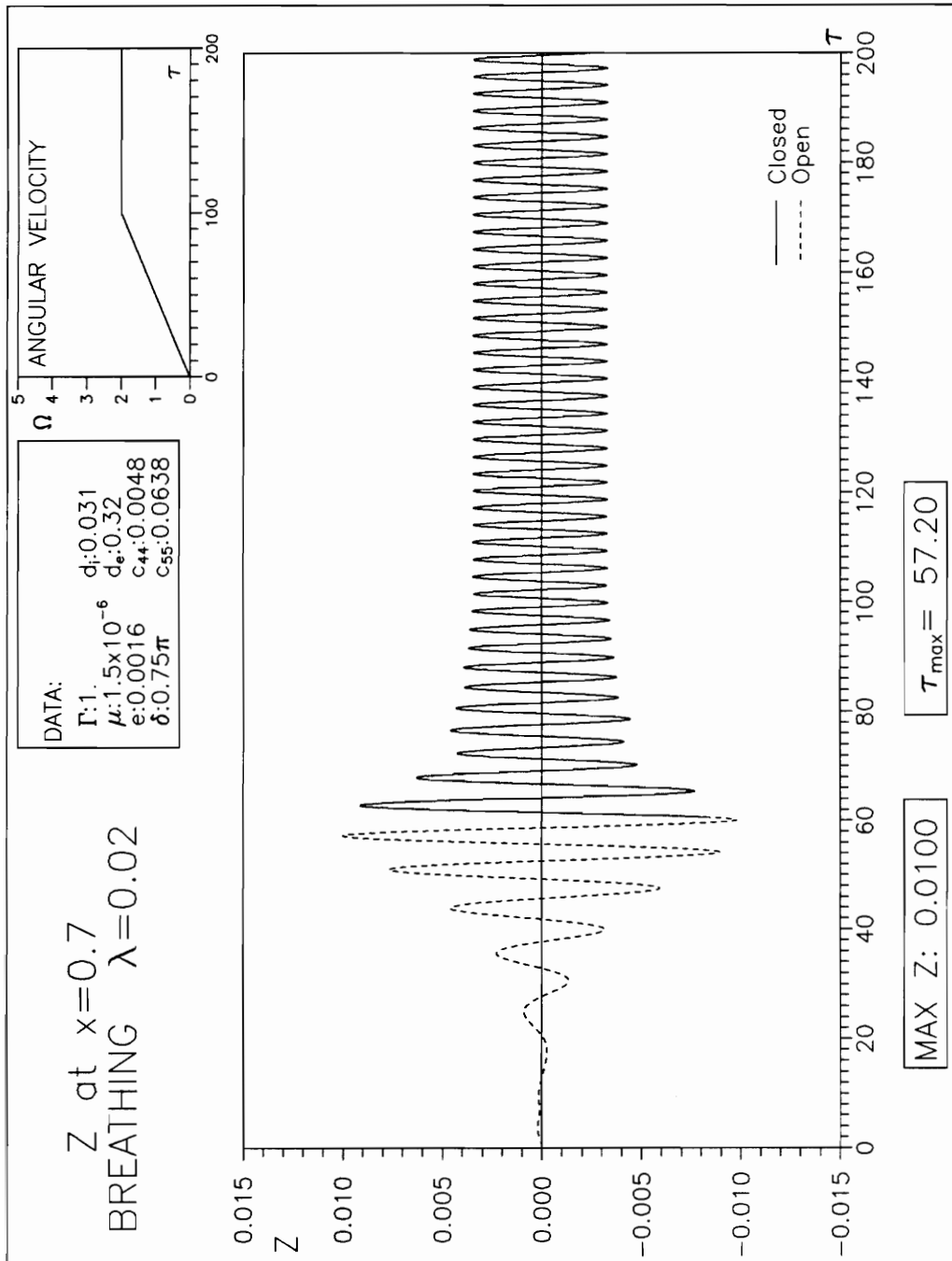
Figure 4.2 Time history of z displacement at x̄=0.7 for λ=0.01 - No crack.
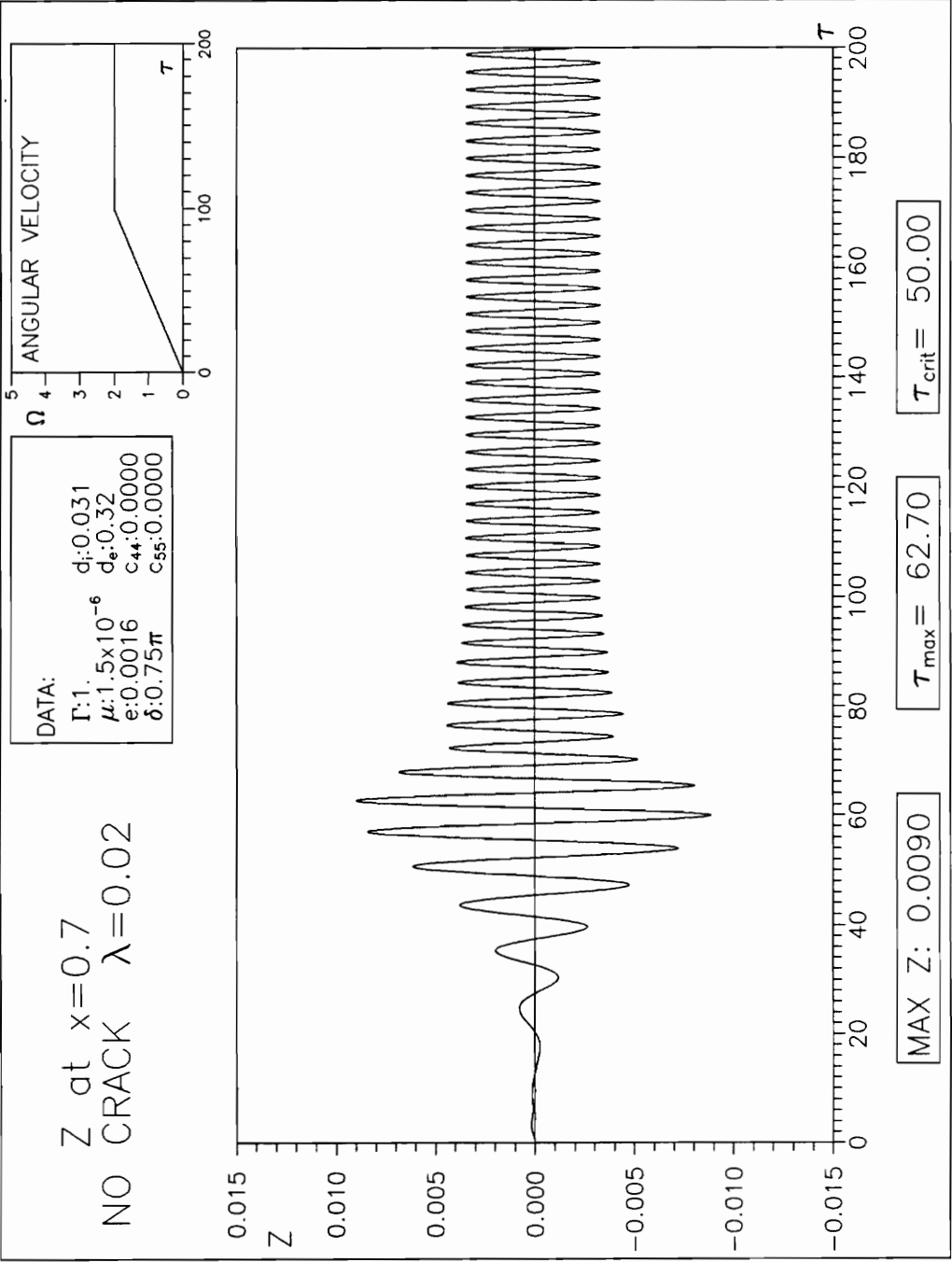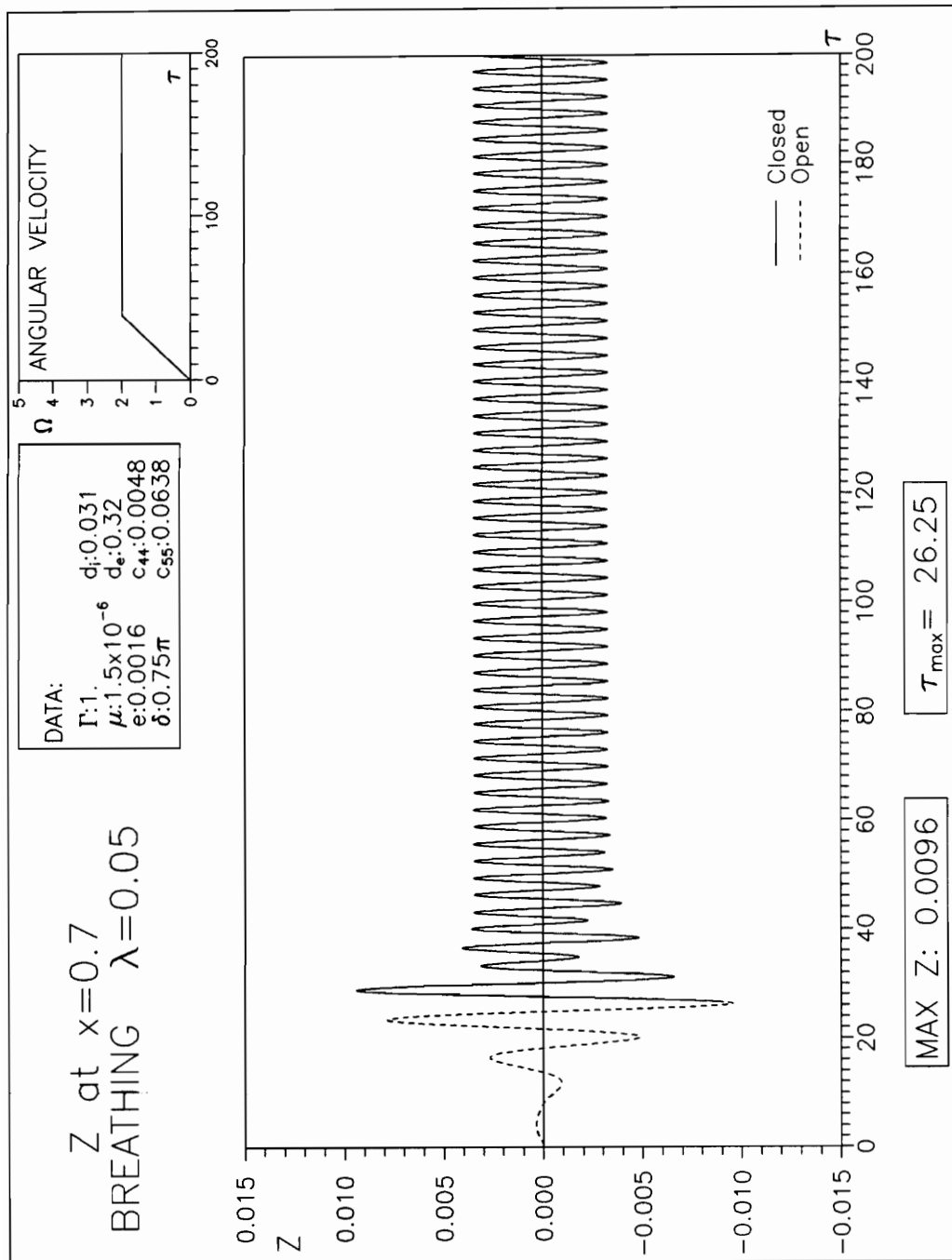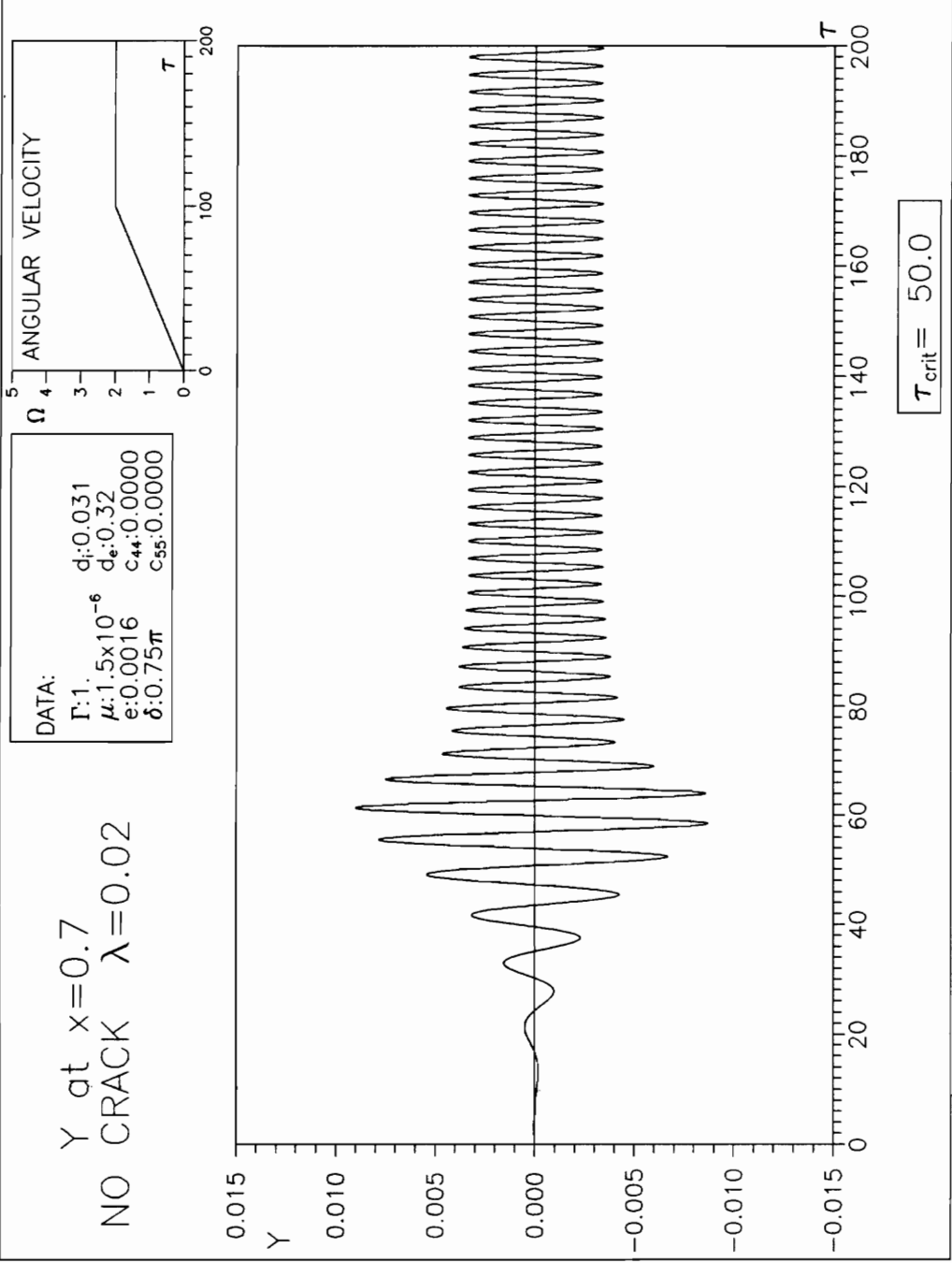
Figure 4.3 Time history of Z displacement at x̄=0.7 for λ=0.02 - No crack.
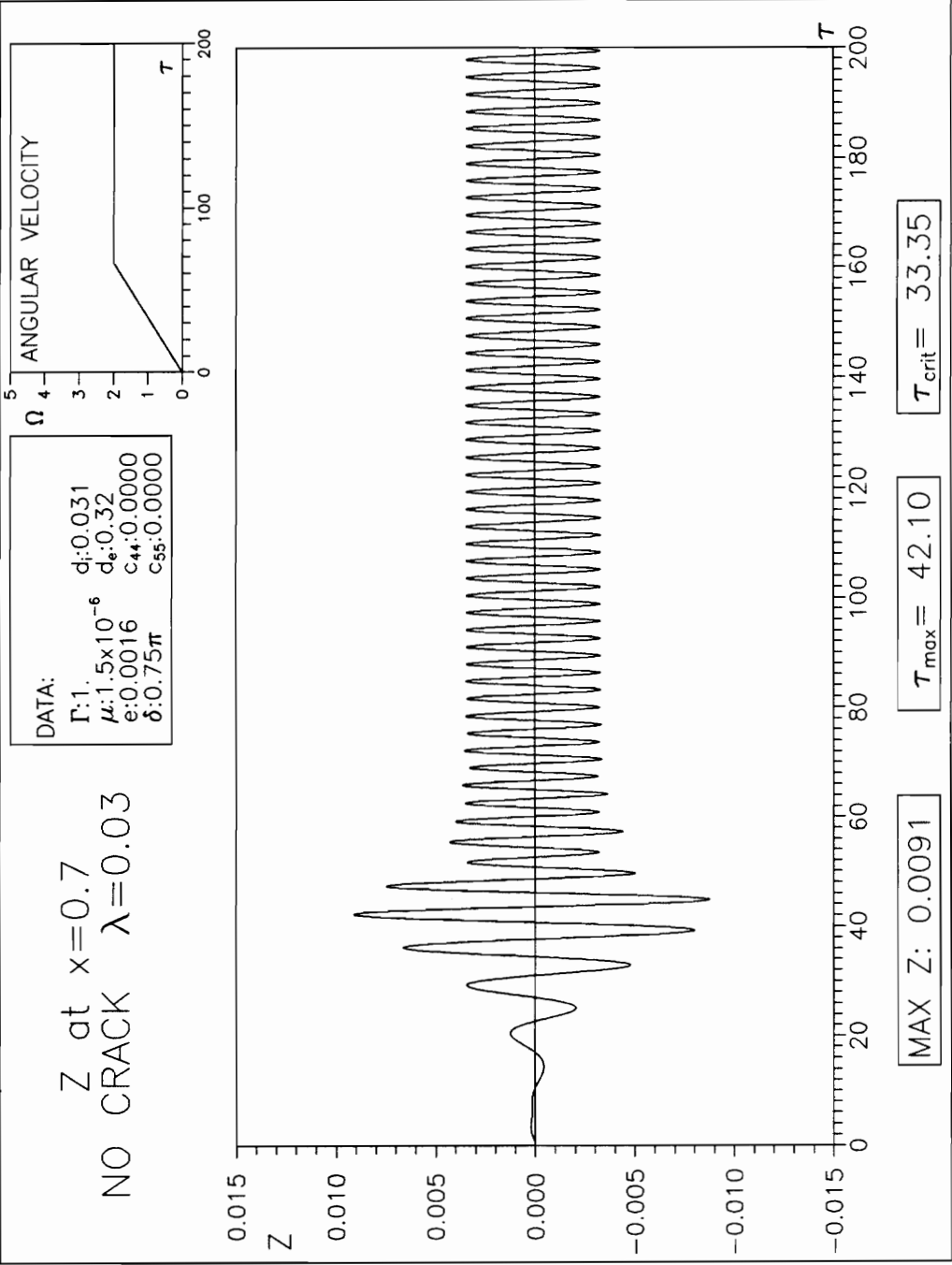
Figure 4.4 Time history of z displacement at x̄=0.7 for λ=0.03 - No crack.
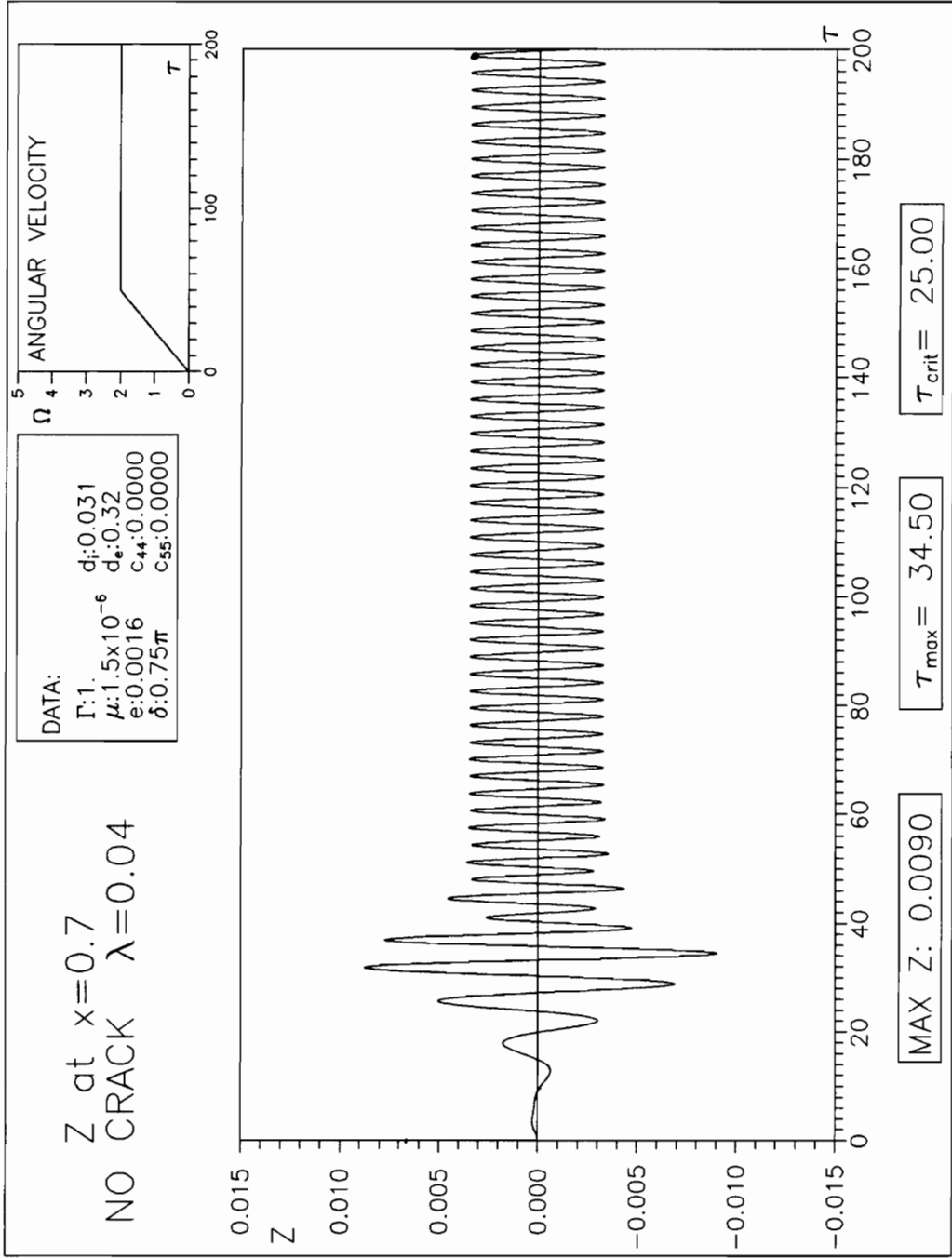
Figure 4.5 Time history of z displacement at x̃=0.7 for λ=0.04 - No crack.
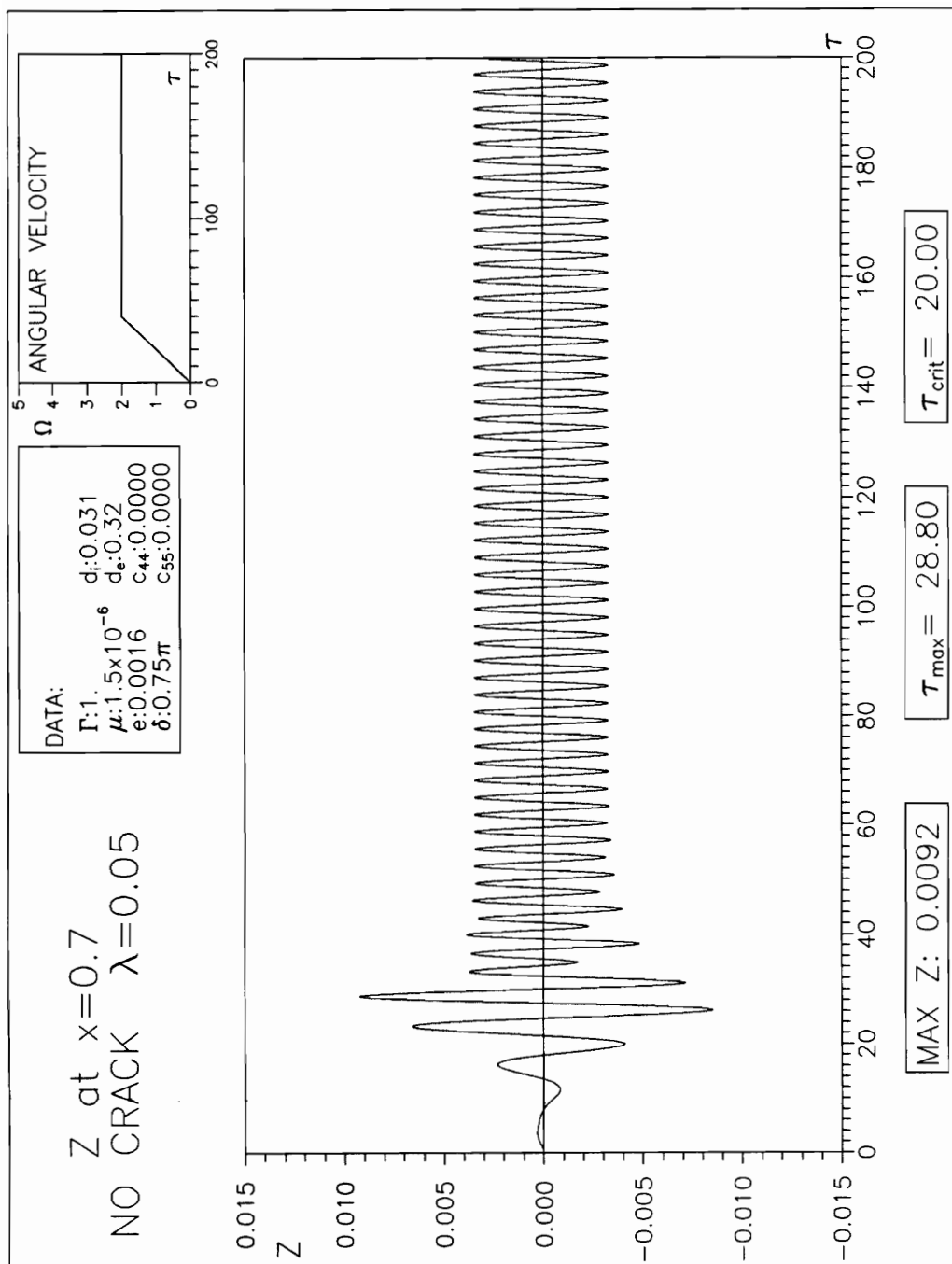
Figure 4.6 Time history of z displacement at x̄=0.7 for λ=0.05 - No crack.

Z at x=0.7
OPEN CRACK λ=0.01

DATA:
Γ:1. d_i:0.031
μ:1.5x10^{-6} d_e:0.32
e:0.0016 c_{44}:0.0048
δ:0.75π c_{55}:0.0638

ANGULAR VELOCITY

MAX Z: 0.0102 τ_{max}=107.40 τ_{crit}= 93.47
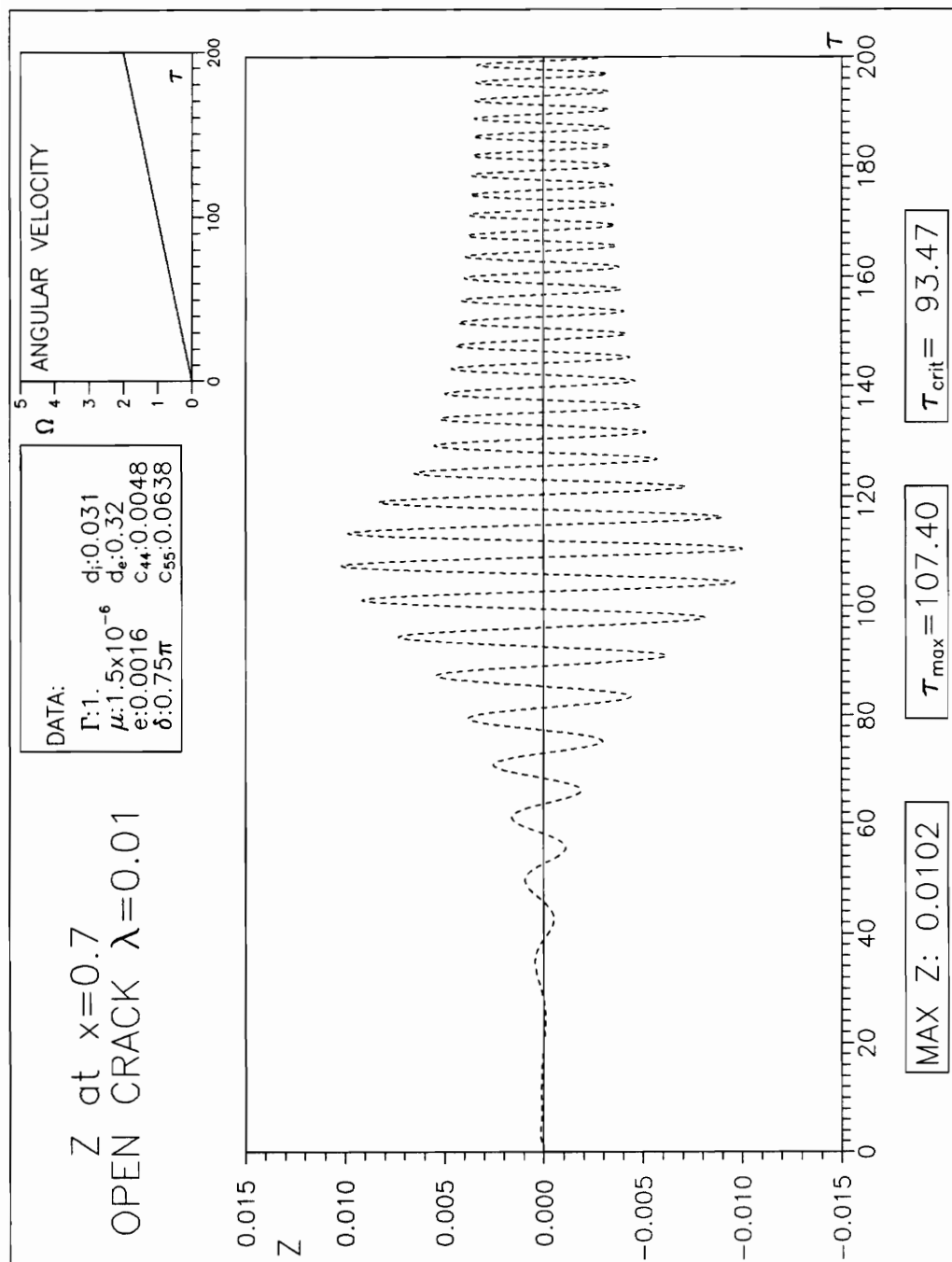
Figure 4.7 Time history of z displacement at x̄=0.7 for λ=0.01 - Open crack.
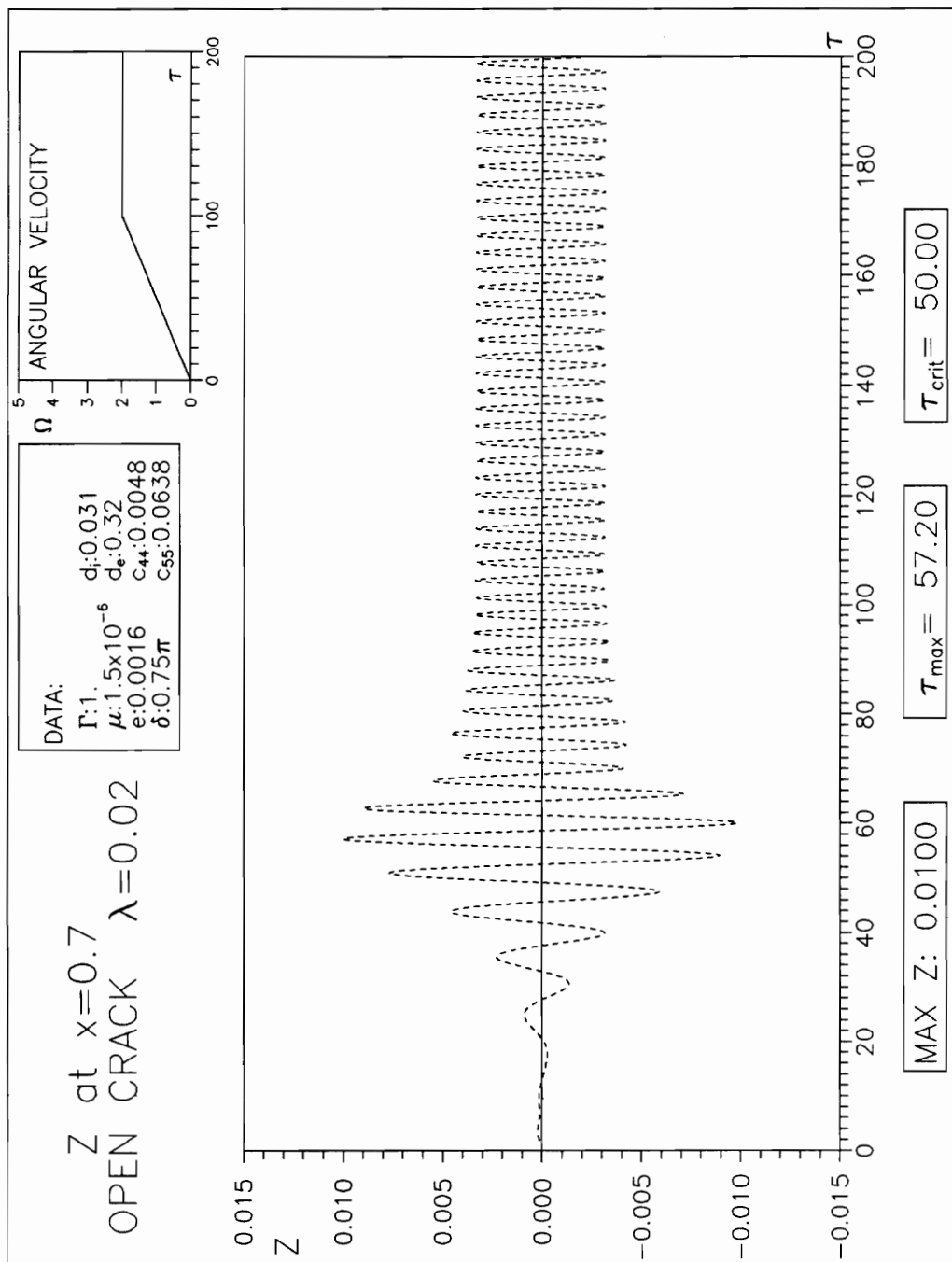
Figure 4.8 Time history of Z displacement at $\tilde{x}=0.7$ for $\lambda=0.02$ - Open crack.

61

Z at x=0.7
OPEN CRACK λ=0.03

DATA:
Γ:1. d_i:0.031
μ:1.5x10^{-6} d_e:0.32
e:0.0016 c_{44}:0.0048
δ:0.75π c_{55}:0.0638

ANGULAR VELOCITY

MAX Z: 0.0099 $\tau_{max}=$ 42.20 $\tau_{crit}=$ 31.17
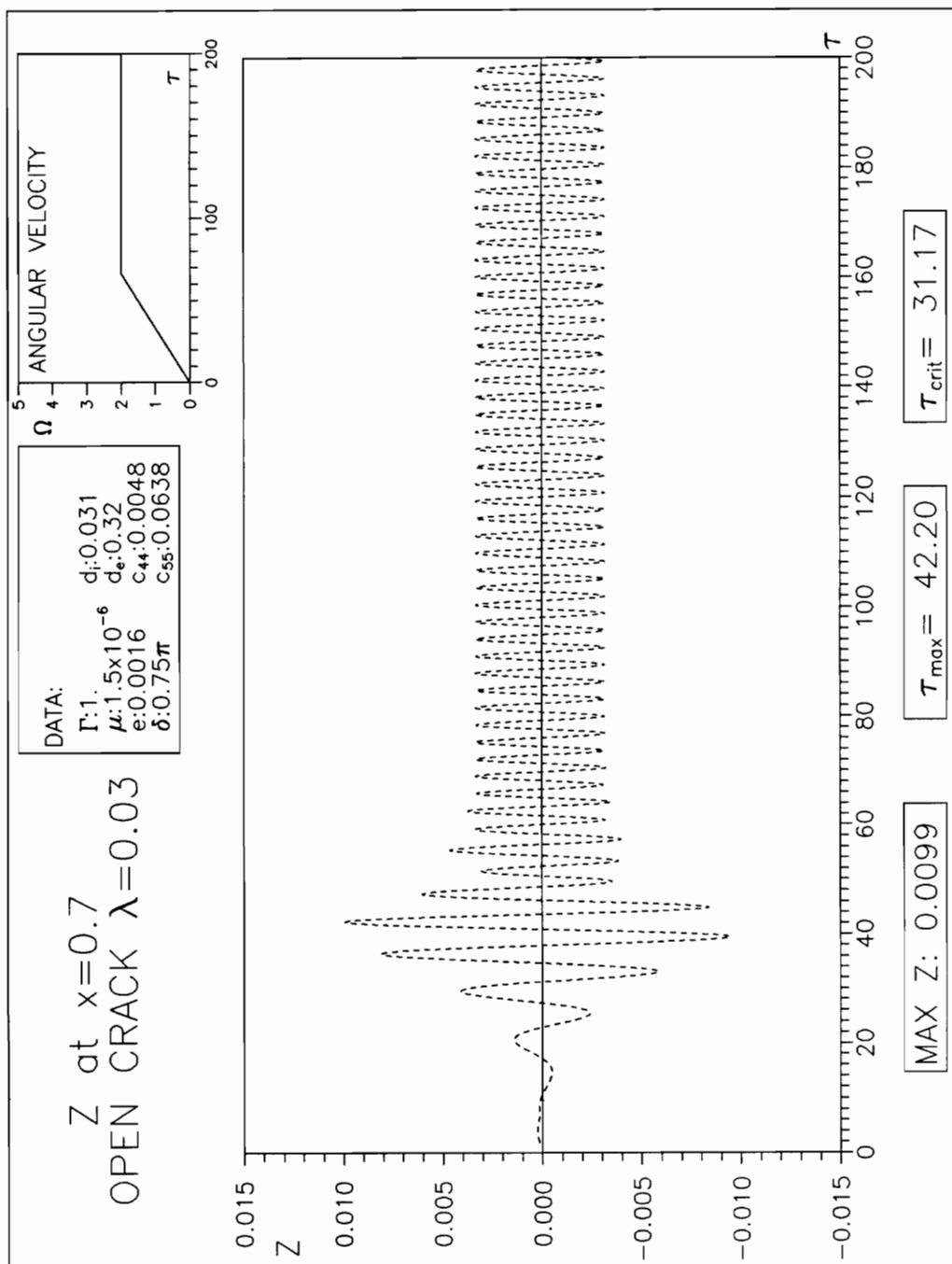
Figure 4,9 Time history of z displacement at x̄=0.7 for λ=0.03 — Open crack.
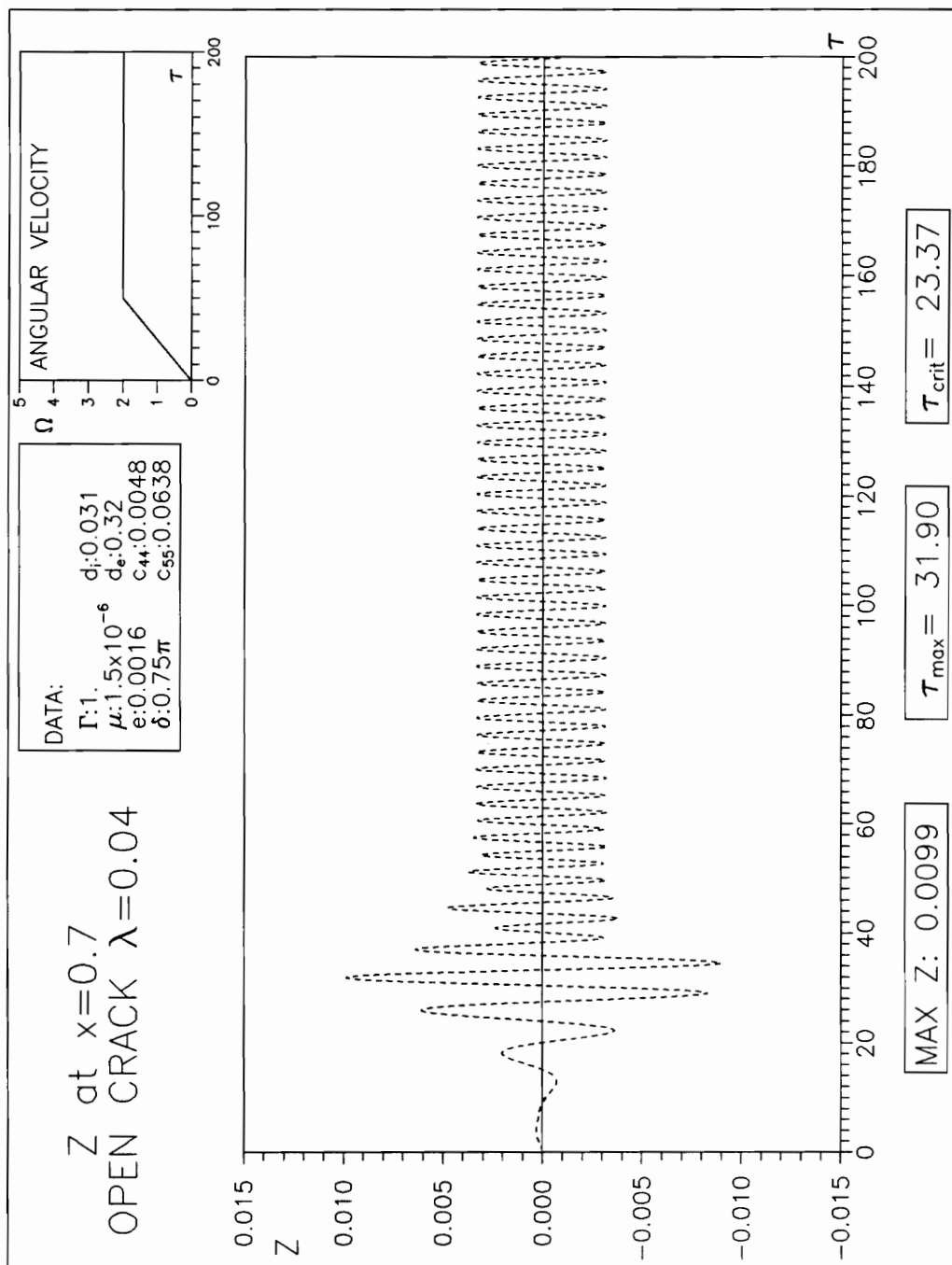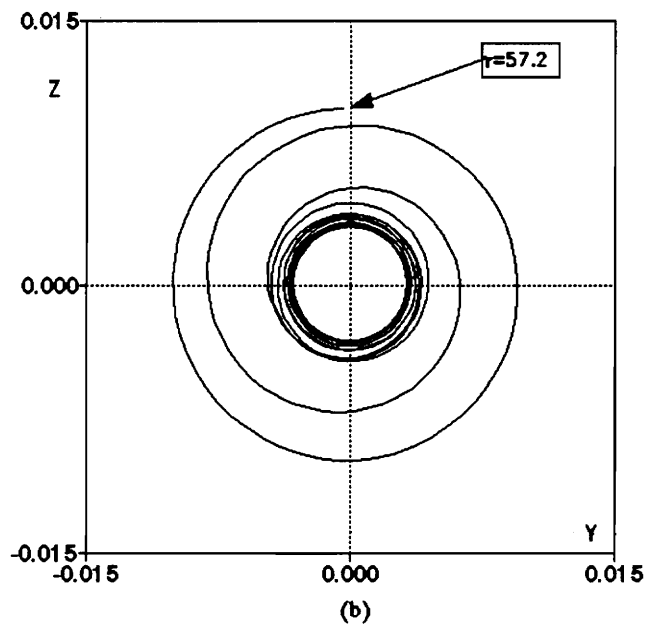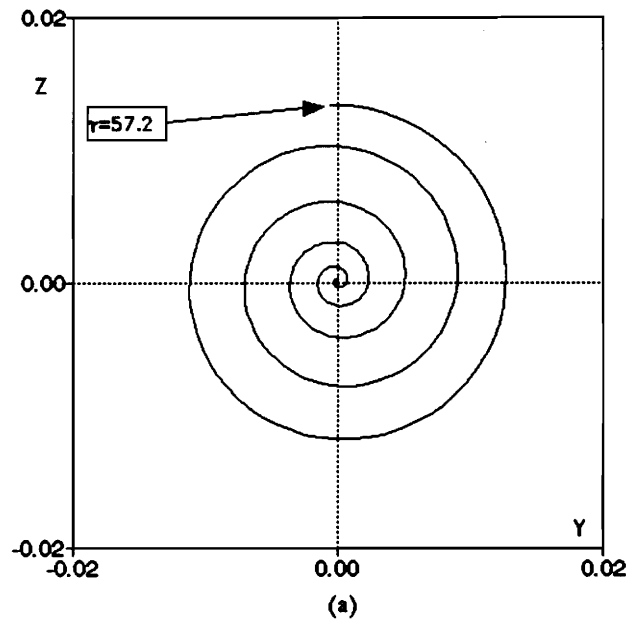
Figure 4.10 Time history of Z displacement at $\tilde{x}=0.7$ for $\lambda=0.04$ – Open crack.

63
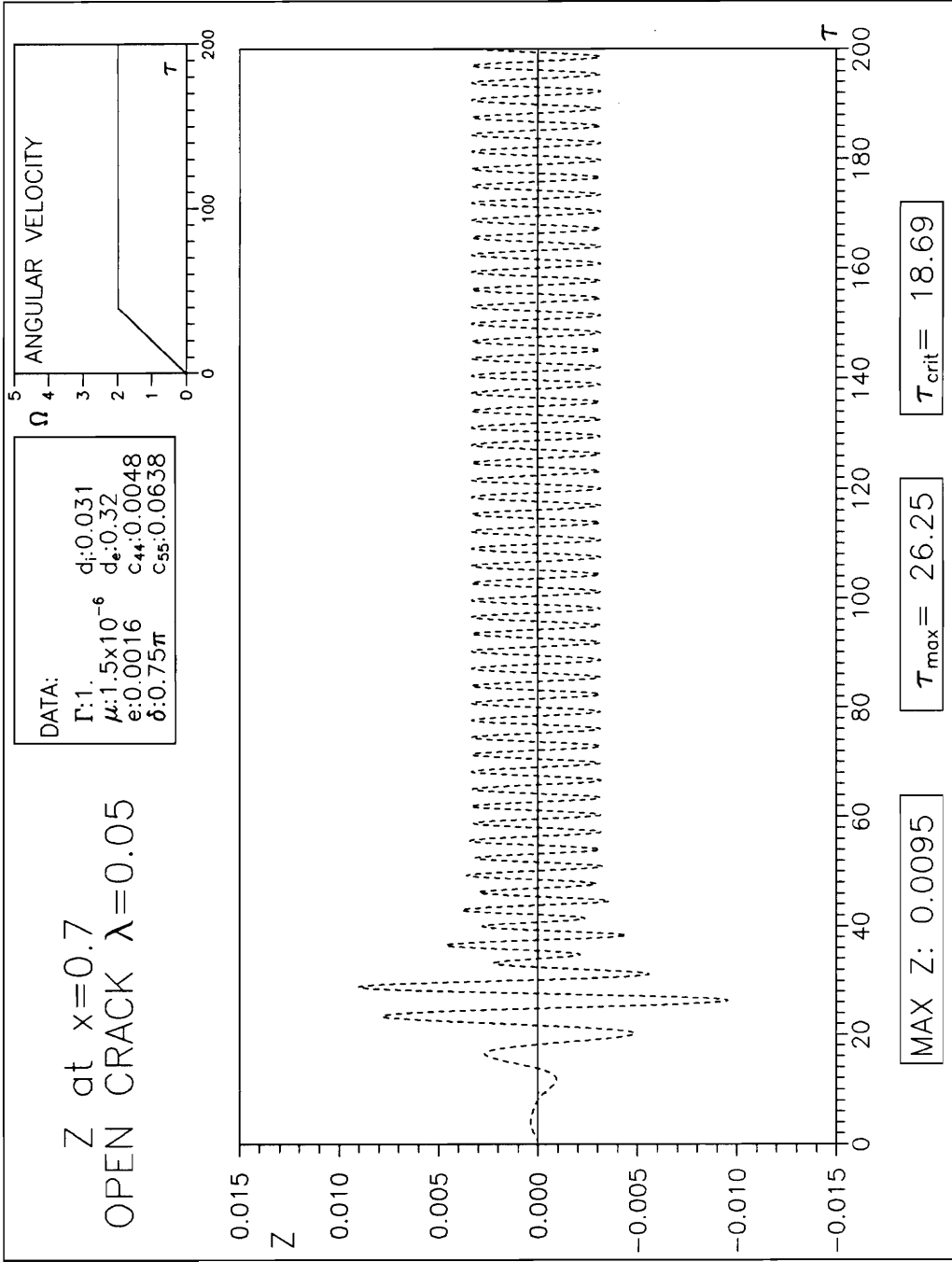
Figure 4.11 Time history of z displacement at x̄=0.7 for λ=0.05 – Open crack.

64
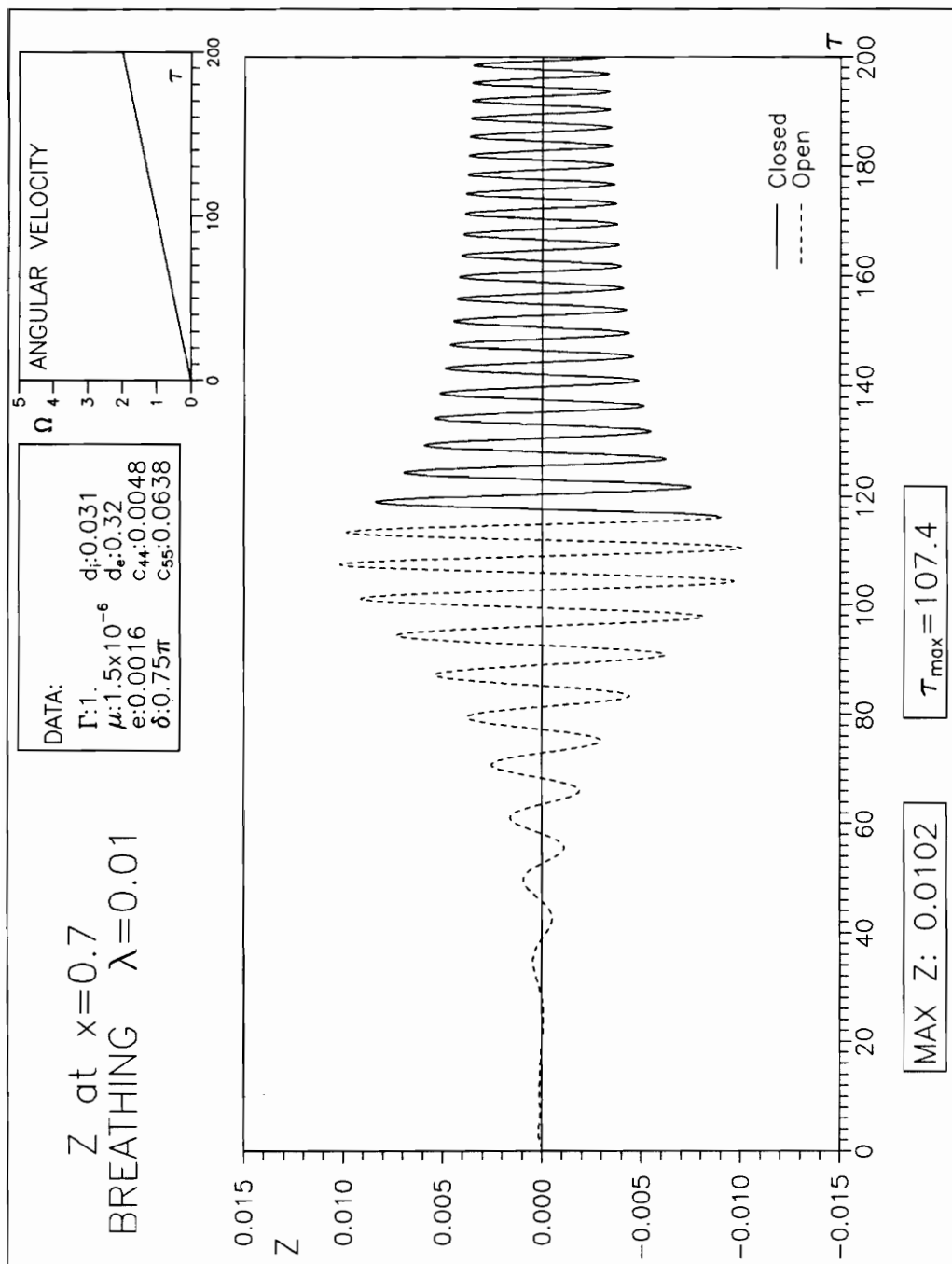
Figure 4.12 Time history of z displacement at $\tilde{x}=0.7$ for $\lambda=0.01$ — Breathing.

65

Figure 4.13 Time history of z displacement at x̄=0.7 for λ=0.02 - Breathing.
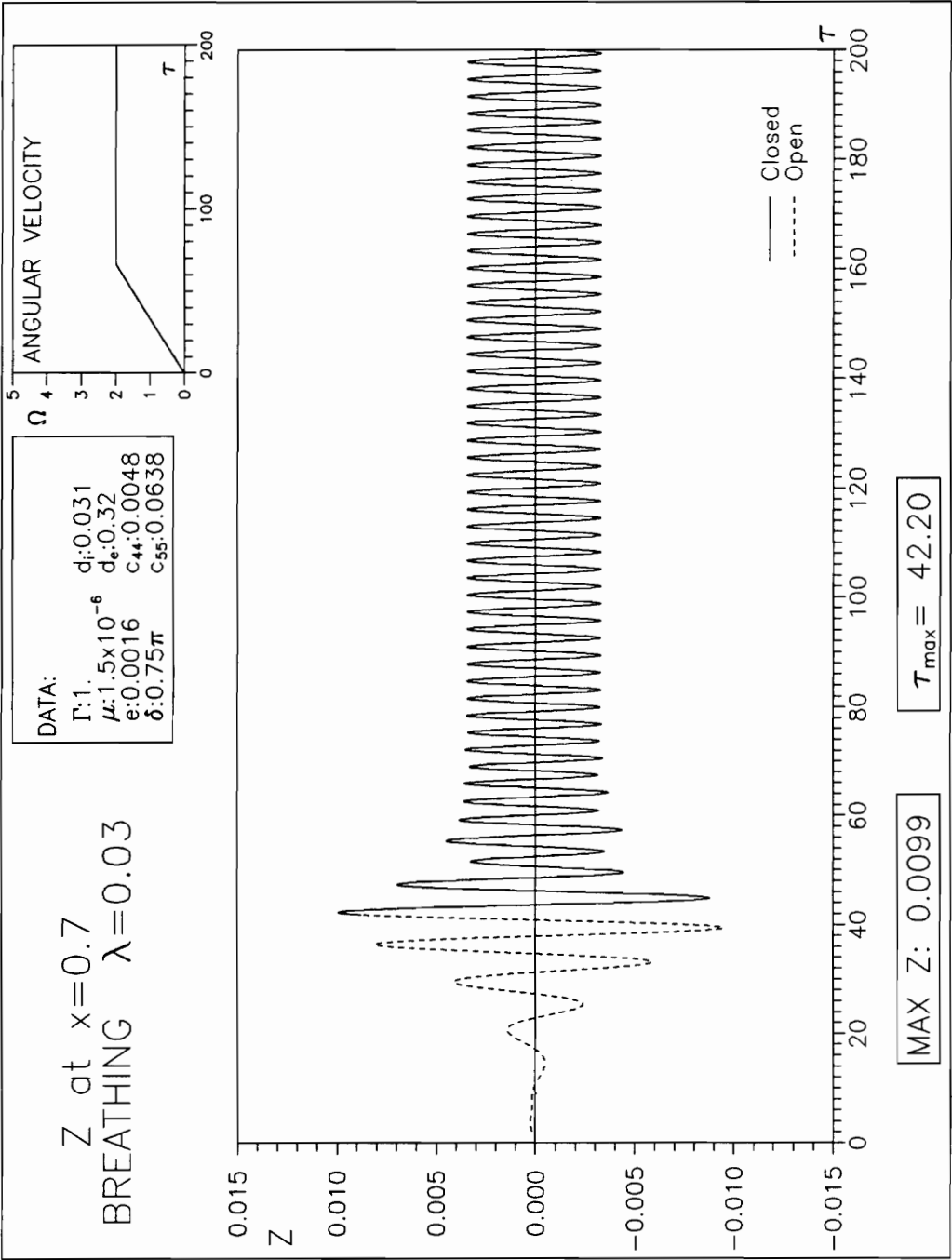
Figure 4.14 Time history of Z displacement at x̄=0.7 for λ=0.03 - Breathing.
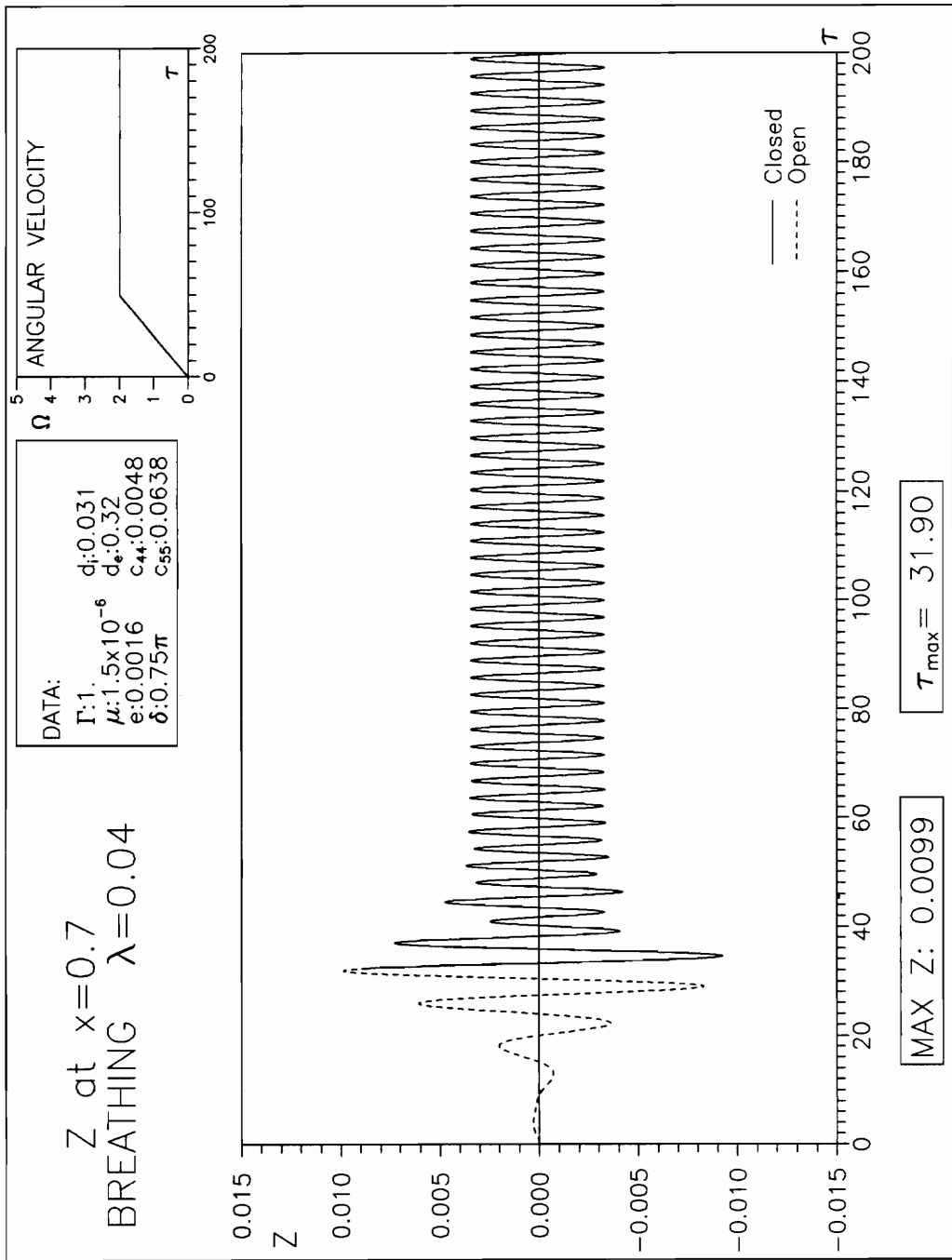
Figure 4.15 Time history of z displacement at $\bar{x}=0.7$ for $\lambda=0.04$ – Breathing.

Figure 4.16 Time history of Z displacement at x̄=0.7 for λ=0.05 – Breathing.

Figure 4.17 Time history of Y displacement at x̆=0.7 for λ=0.02 – No crack.

70
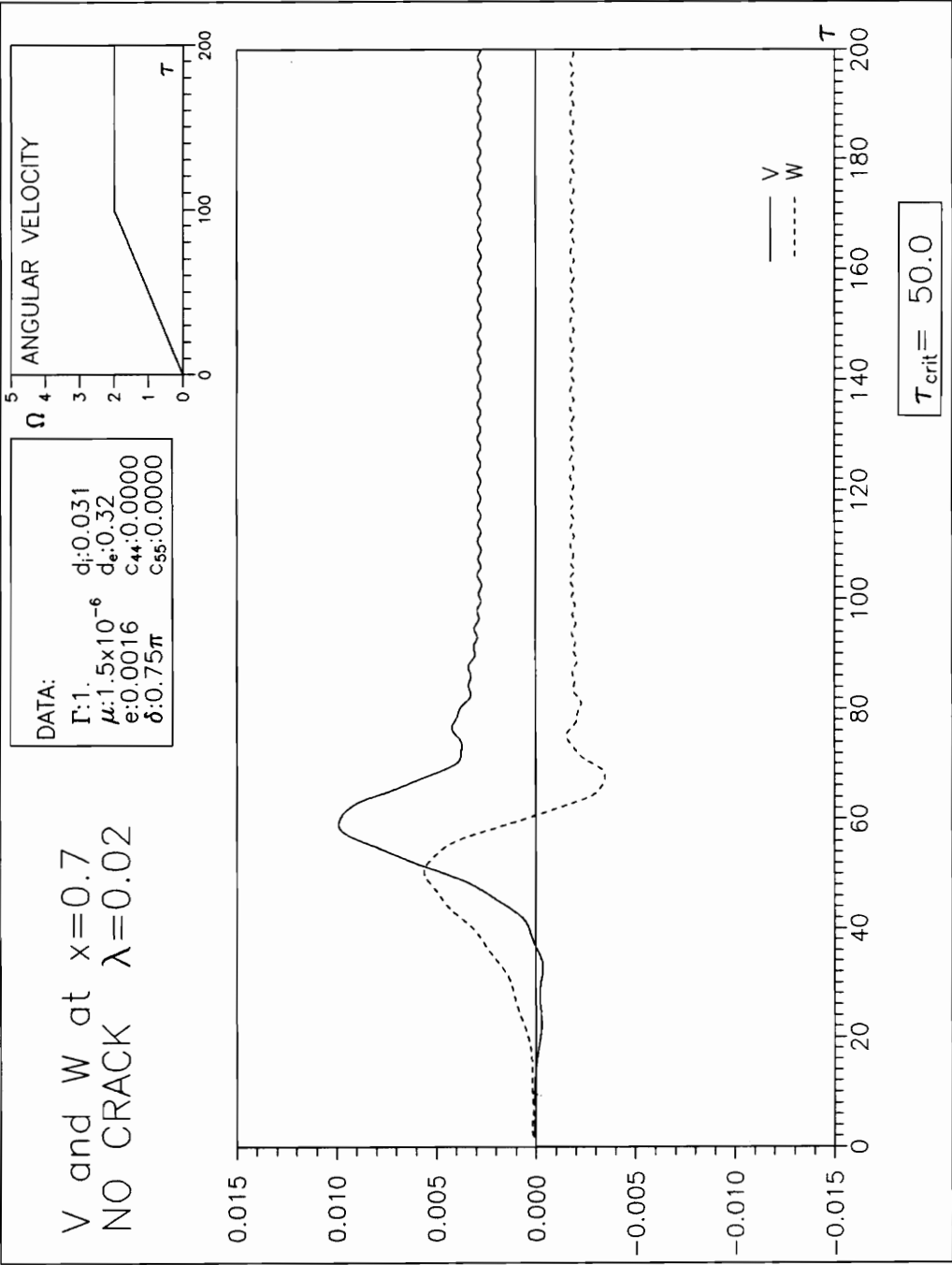
**Figure 4.18** Time history of V and W displacement at x̃=0.7 for λ=0.02 – No crack.
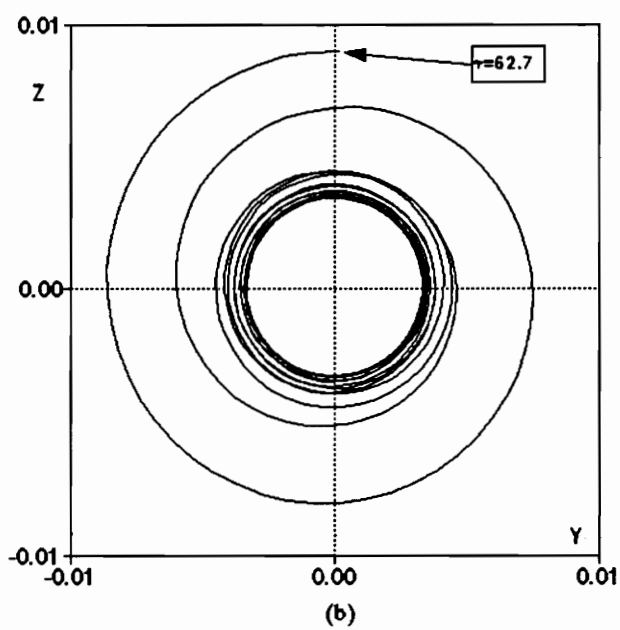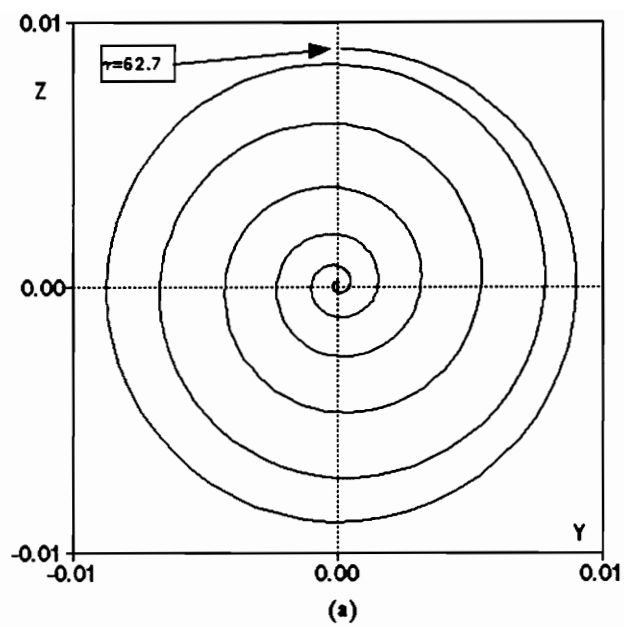
Figure 4.19 Orbits No crack, acceleration: (a) before τ_{max}; (b) after τ_{max}.
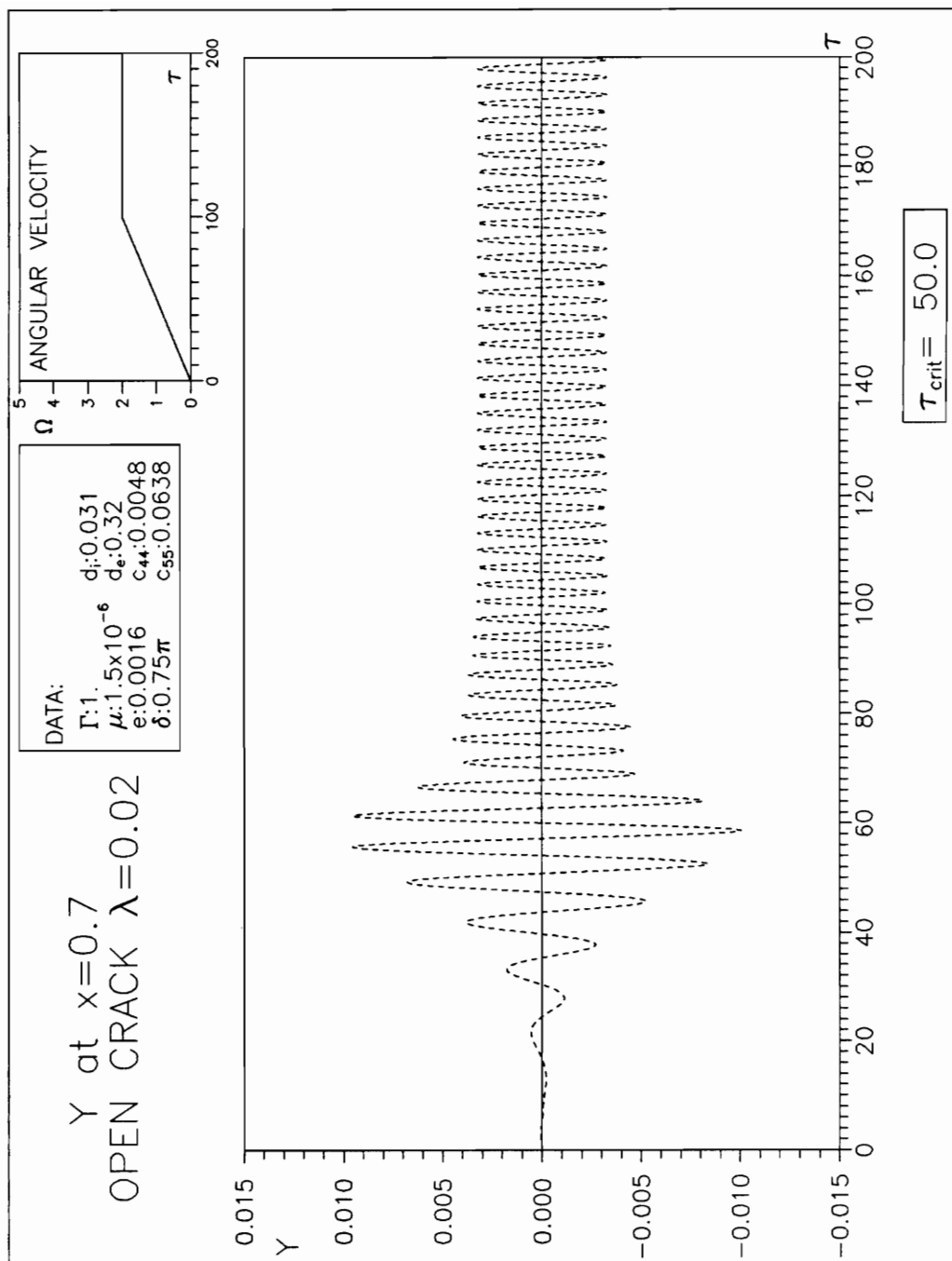
Figure 4.20 Time history of Y displacement at x̃=0.7 for λ=0.02 — Open crack.

Figure 4.21 Time history of V and W displacement at x̄=0.7 for λ=0.02 – Open crack.

Figure 4.22 Orbits Open crack, acceleration: (a) before τ_{max};
(b) after τ_{max}.
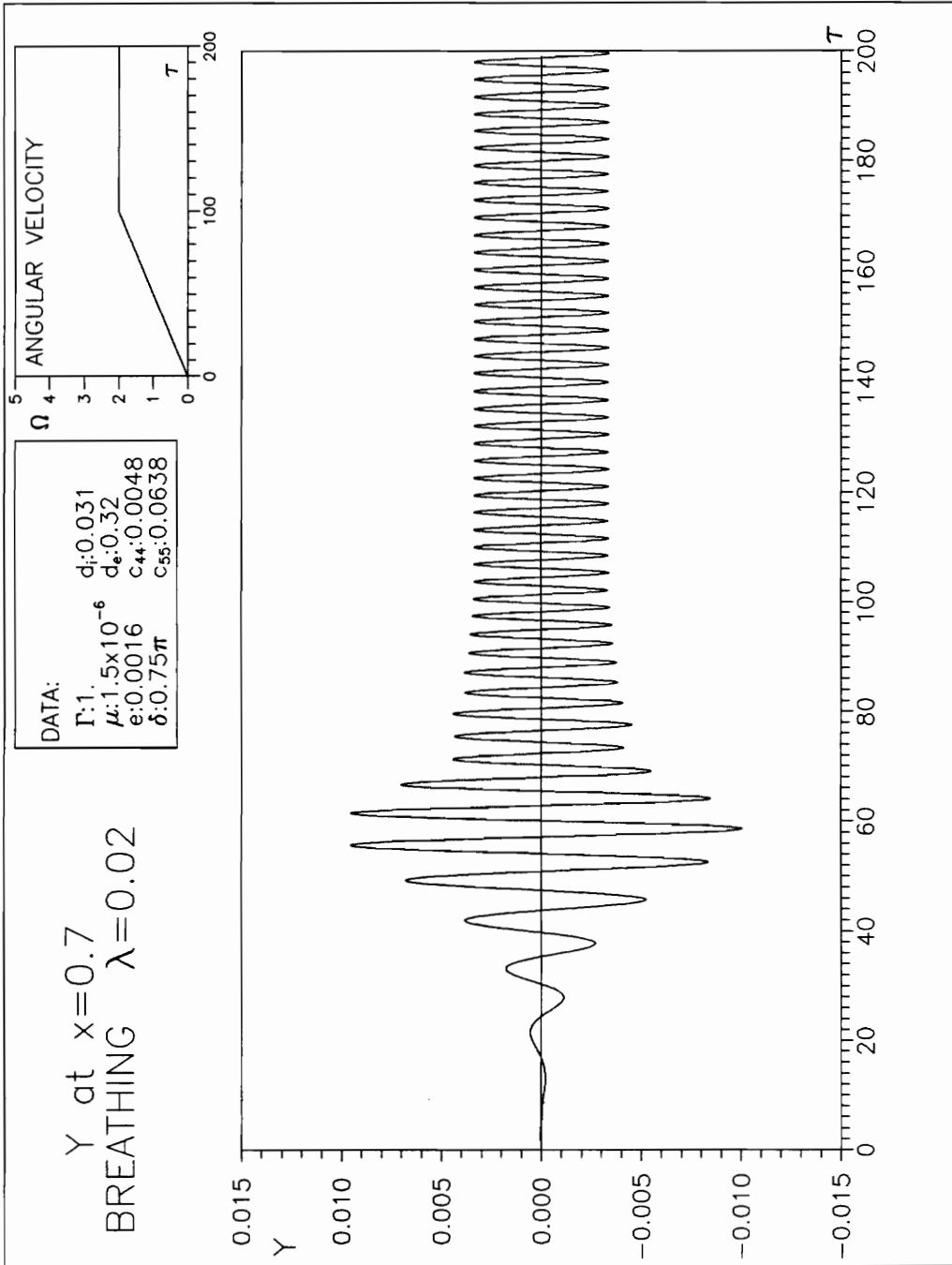
Figure 4.23 Time history of Y displacement at x̃=0.7 for λ=0.02 – Breathing; acceleration.
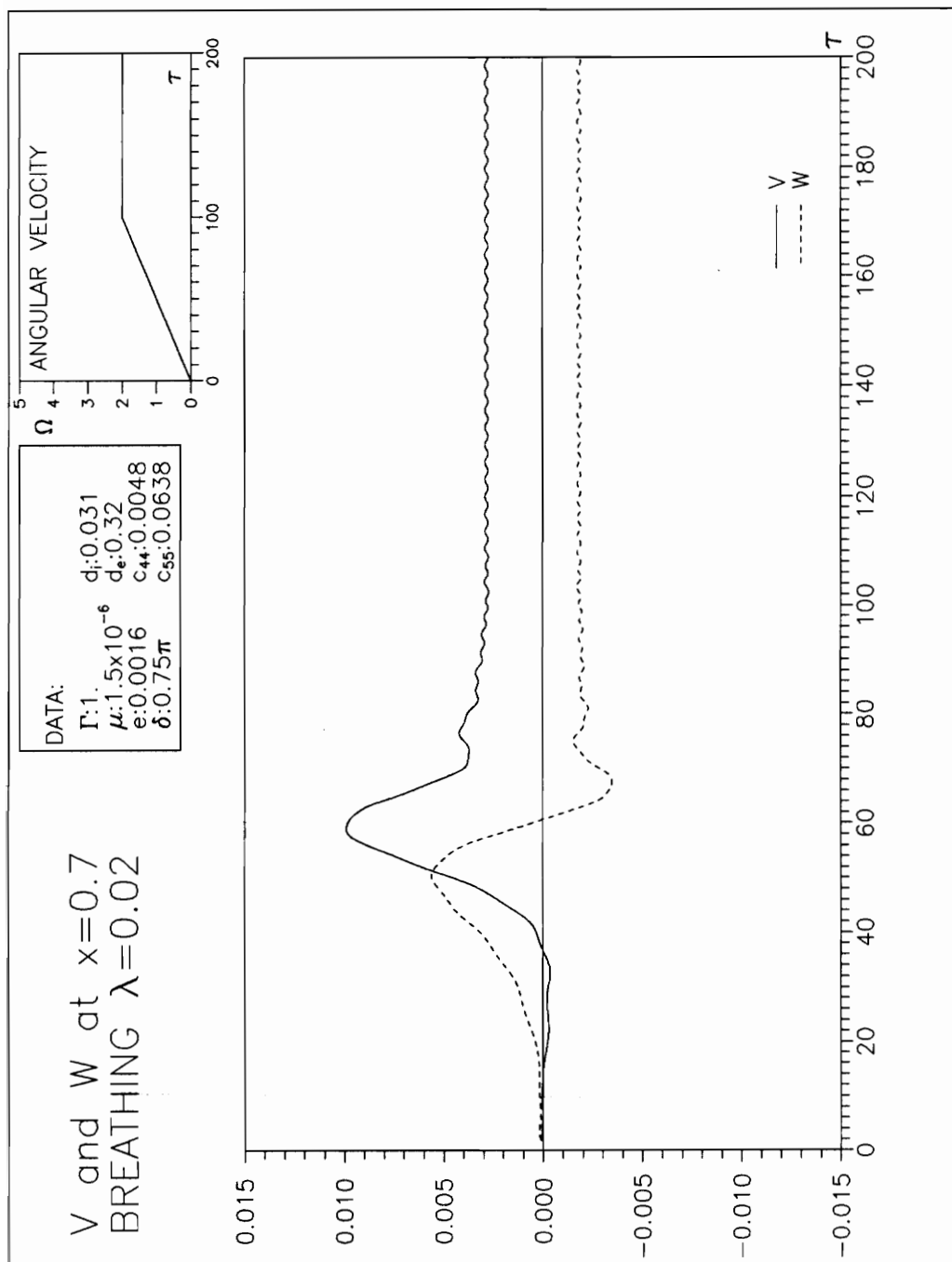
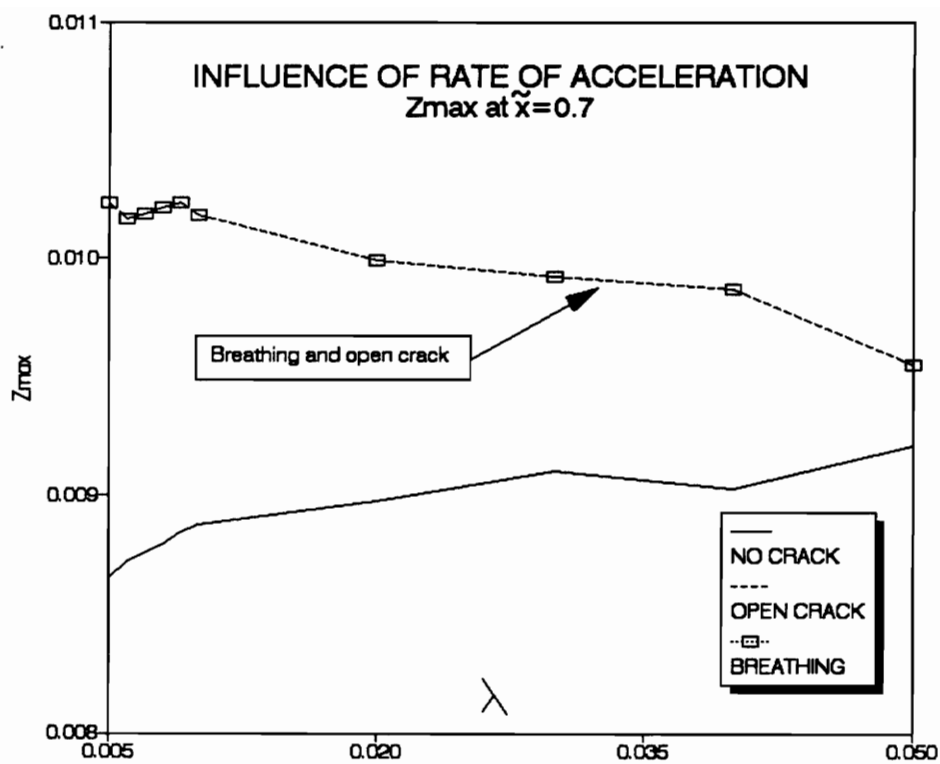**Figure 4.24 Time history of V and W displacement at x̃=0.7 for λ=0.02 - Breathing; acceleration.**

77
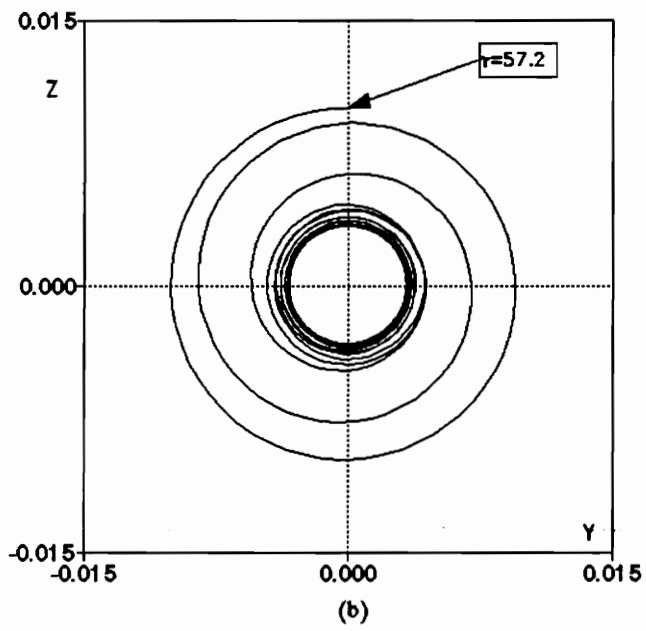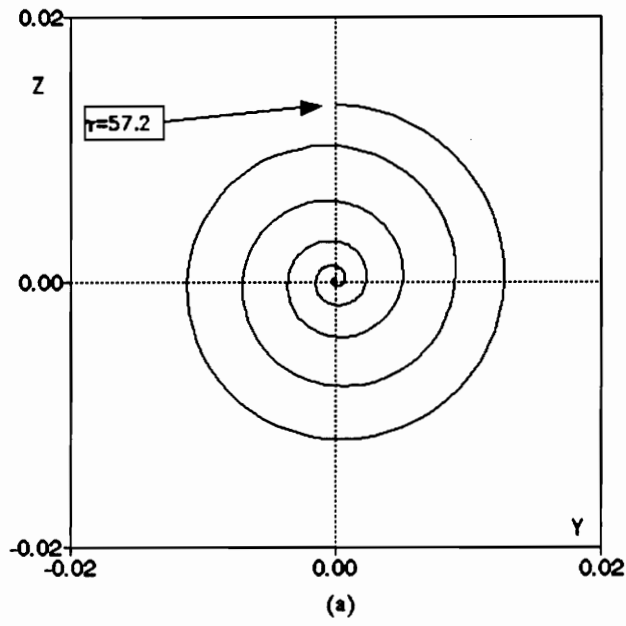
Figure 4.25 Orbits Breathing crack, acceleration: (a) before τ_{max}; (b) after τ_{max}.

Table 4.1 Effect of acceleration on Z displacement at $\tilde{x}=0.7$.

| λ	Z_{max} at x=0.7		
	No crack	**Open crack**	**Breathing**
0.005	0.00865	0.01023	0.01023
0.006	0.00872	0.01017	0.01017
0.007	0.00876	0.01019	0.01019
0.008	0.00879	0.01022	0.01022
0.009	0.00885	0.01023	0.01023
0.010	0.00887	0.01018	0.01018
0.020	0.00898	0.00999	0.00999
0.030	0.00910	0.00992	0.00993
0.040	0.00903	0.00987	0.00987
0.050	0.00921	0.00955	0.00955

Table 4.2 Effect of acceleration on the maximum Z displacement over the whole length.

λ	Z_{max} (Whole length)		
	No crack	Open crack	Breathing
0.005	0.01070	0.01284	0.01284
0.006	0.01078	0.01277	0.01277
0.007	0.01083	0.01271	0.01271
0.008	0.01087	0.01279	0.01279
0.009	0.01094	0.01278	0.01278
0.010	0.01098	0.01273	0.01273
0.020	0.01112	0.01245	0.01245
0.030	0.01127	0.01231	0.01229
0.040	0.01191	0.01224	0.01224
0.050	0.01142	0.01185	0.01189

Figure 4.26 Effect of acceleration on Z displacement at $\tilde{x}=0.7$.
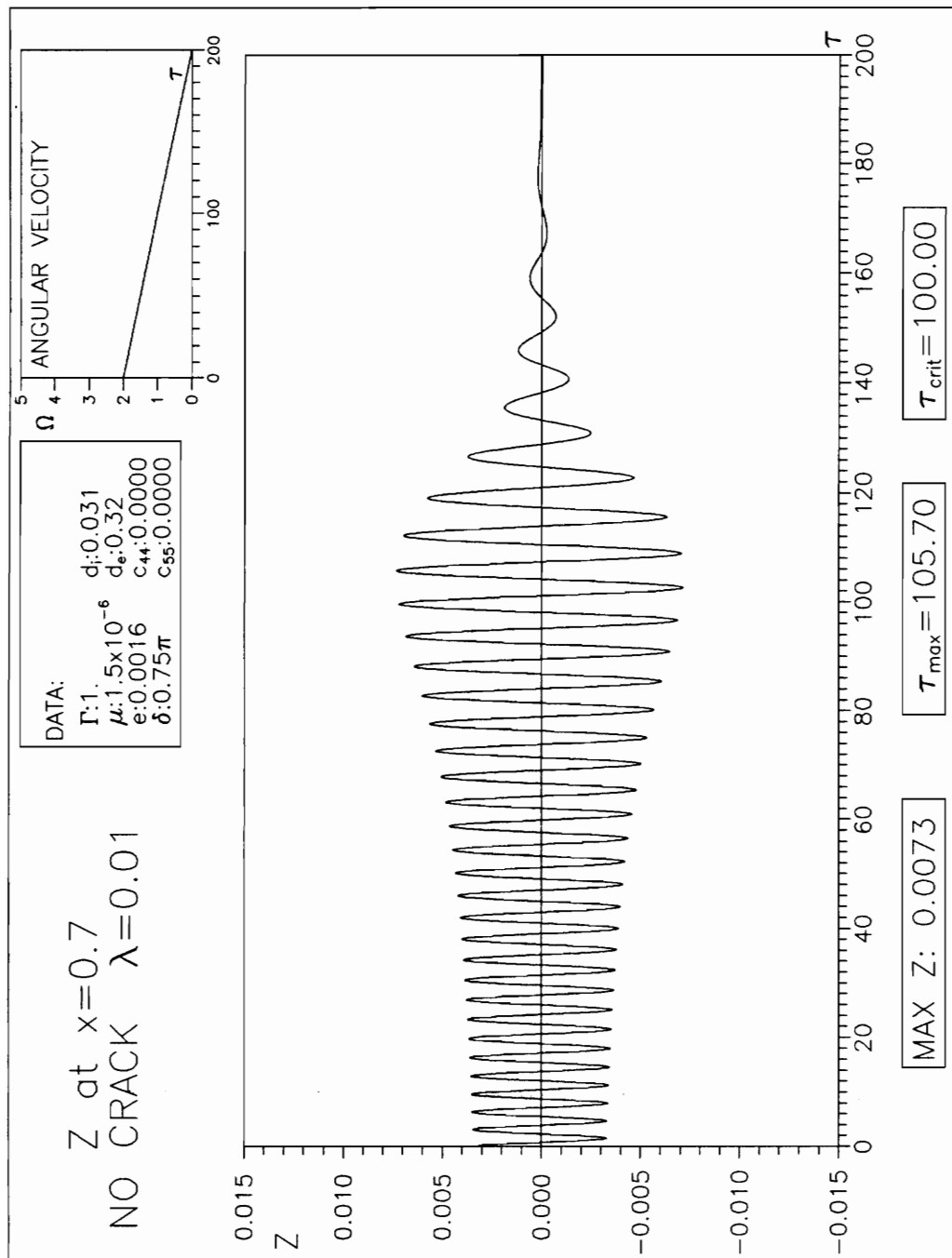
INFLUENCE OF RATE OF ACCELERATION
Zmax (whole length)
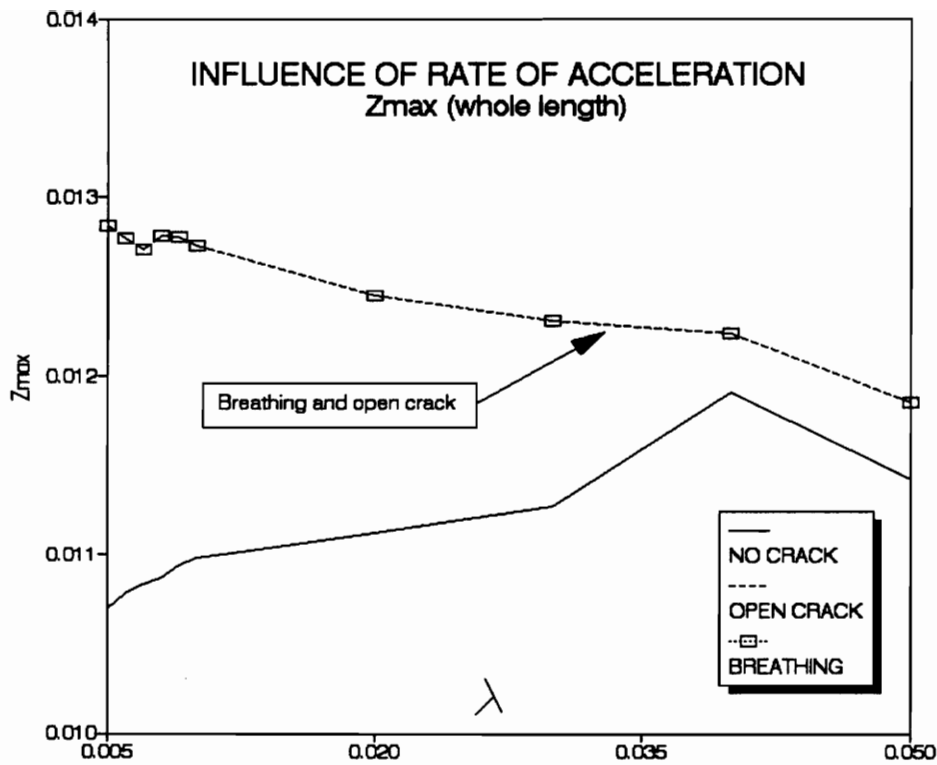
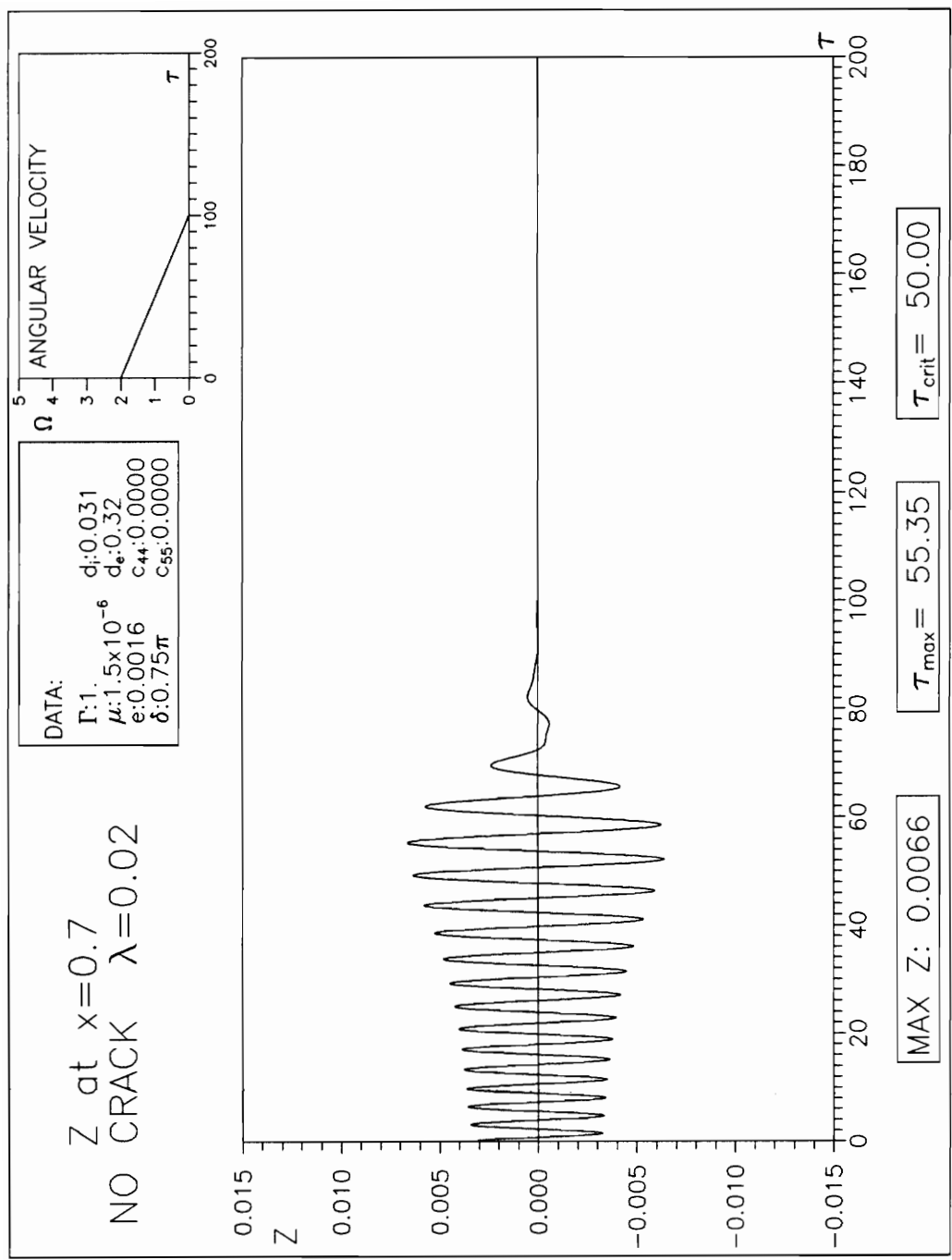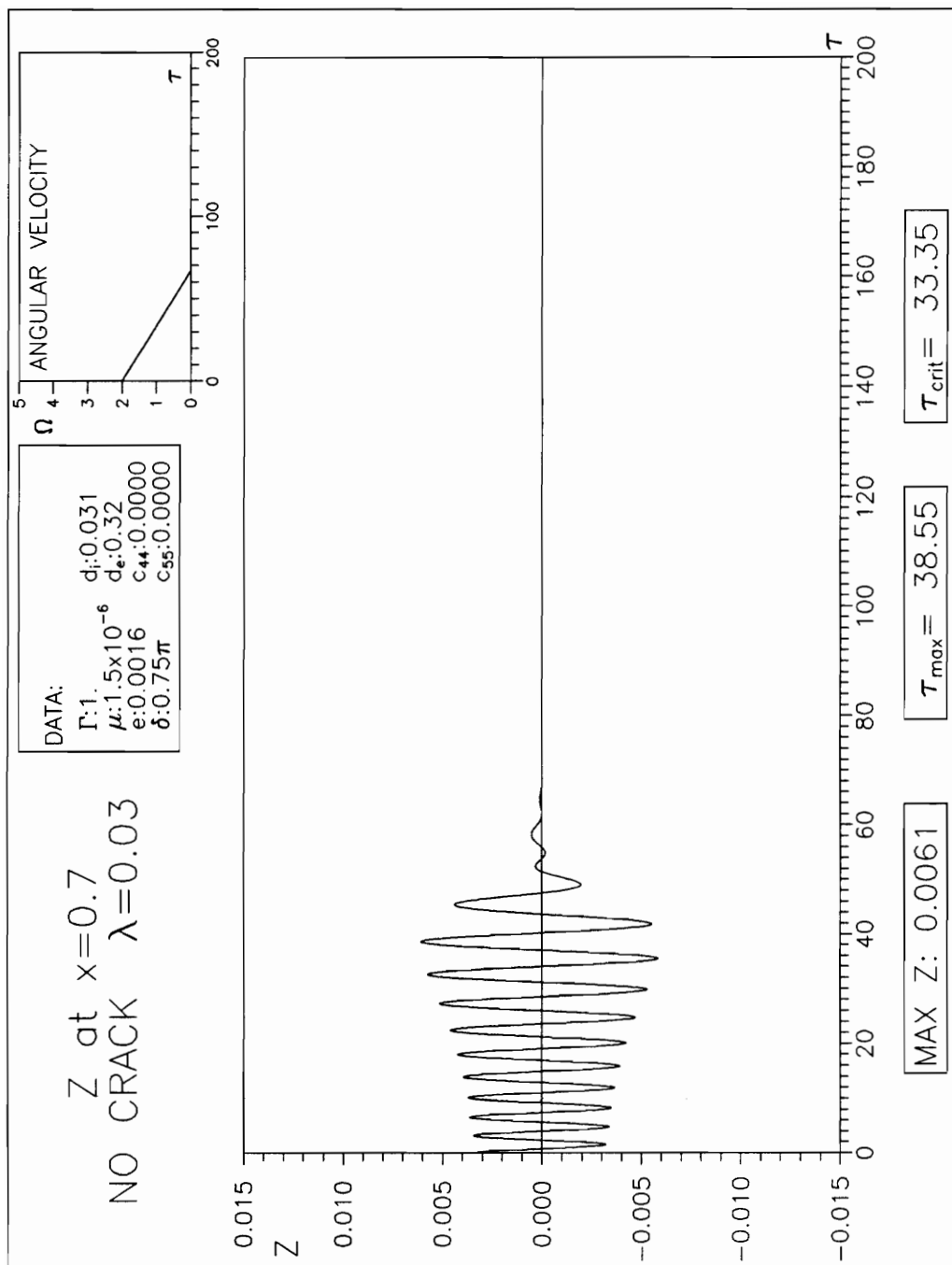Figure 4.27 Effect of acceleration on the maximum Z displace-cent over the whole length.
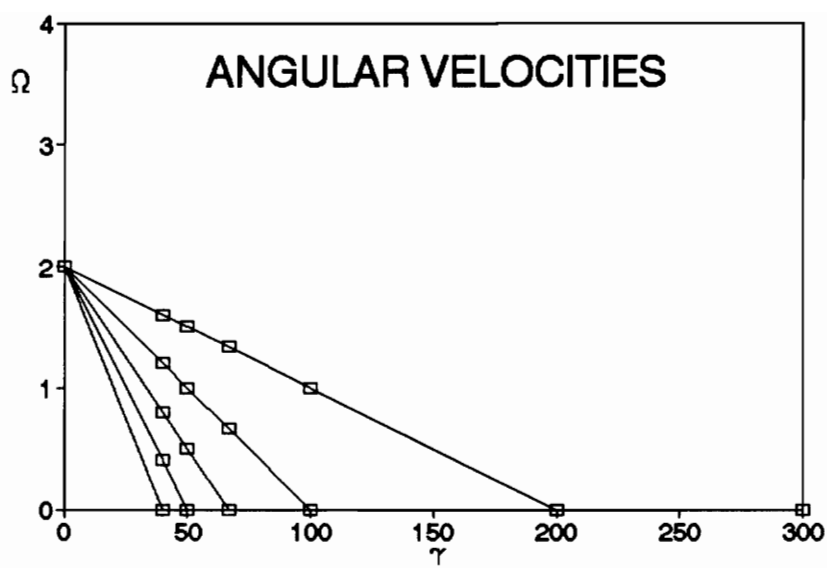
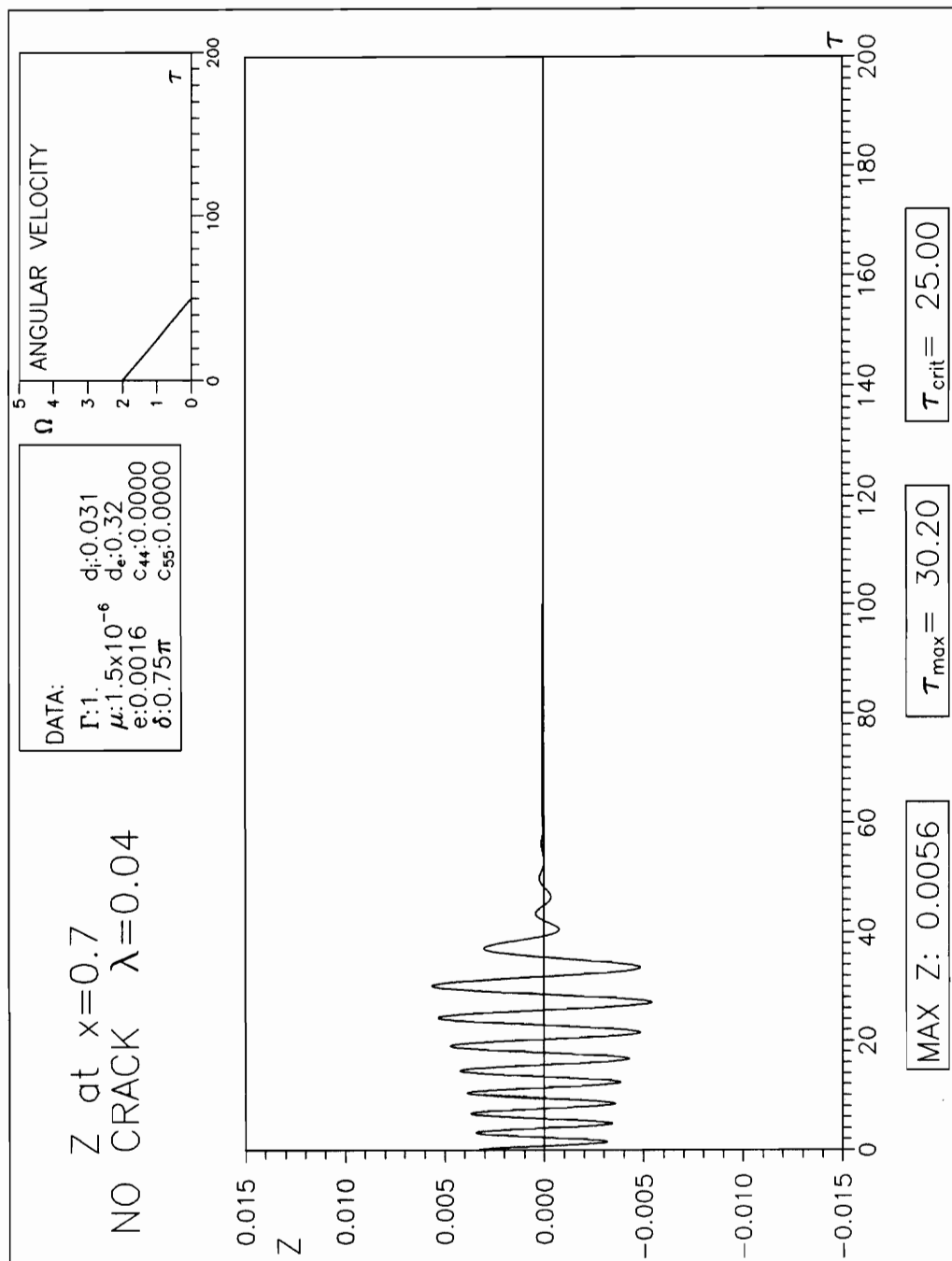Figure 4.28 Rates of deceleration.

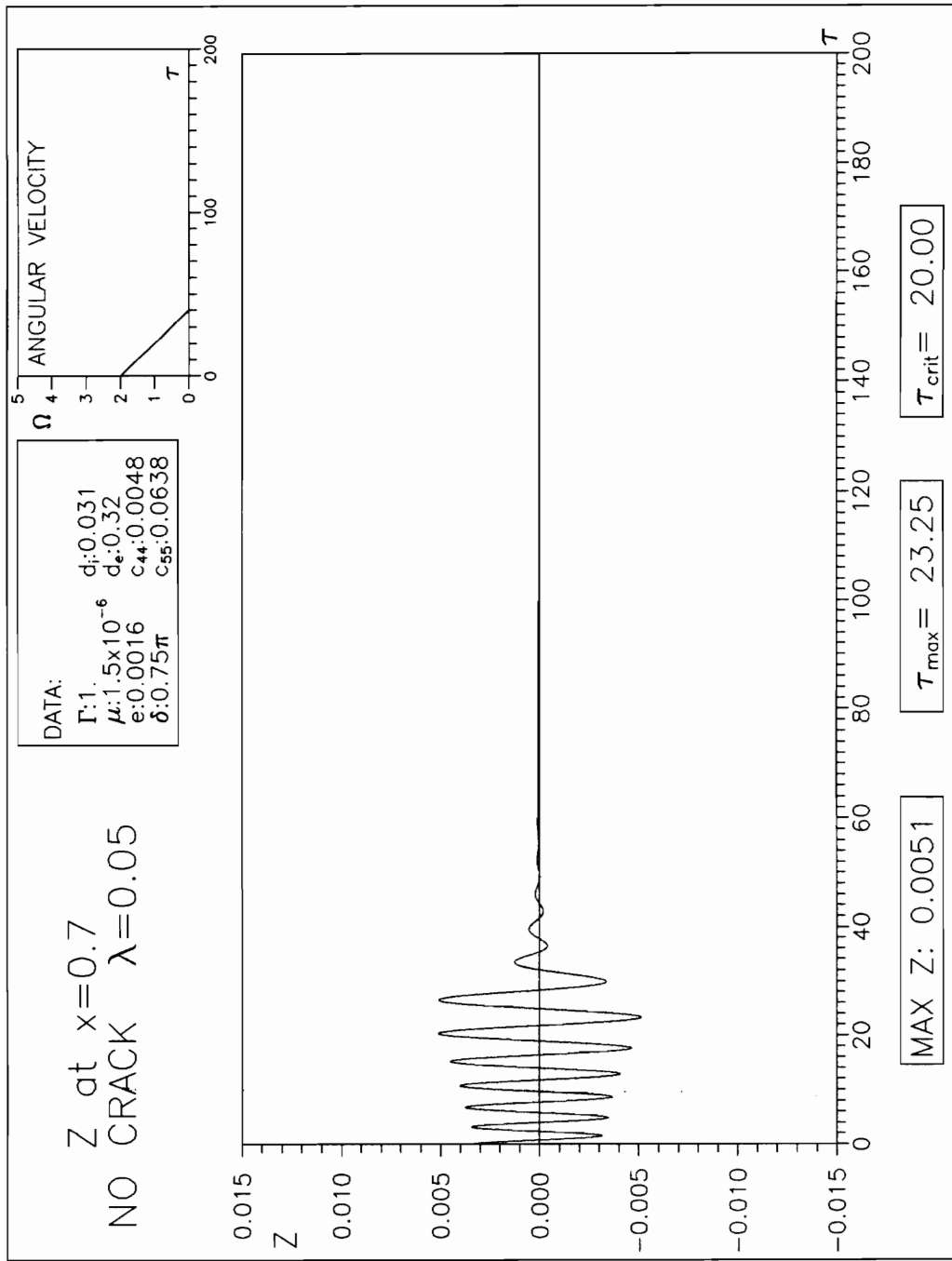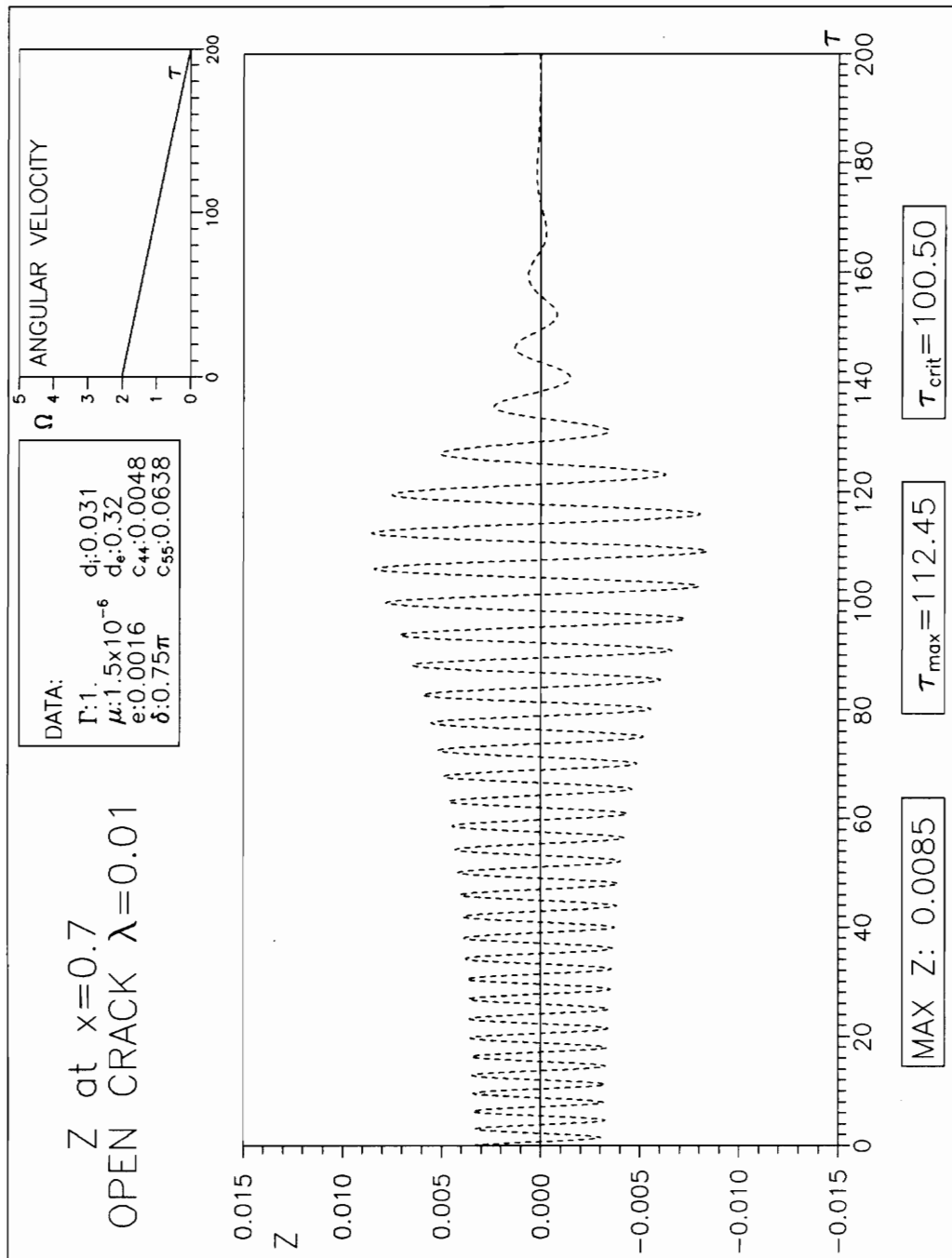**Figure 4.29** Time history of Z displacement at $\tilde{x}=0.7$ for $\lambda=0.01$ — No crack; deceleration.

84

Figure 4.30 Time history of z displacement at x̄=0.7 for λ=0.02 – No crack; deceleration.

Figure 4.31 Time history of Z displacement at x̃=0.7 for λ=0.03 - No crack; deceleration.
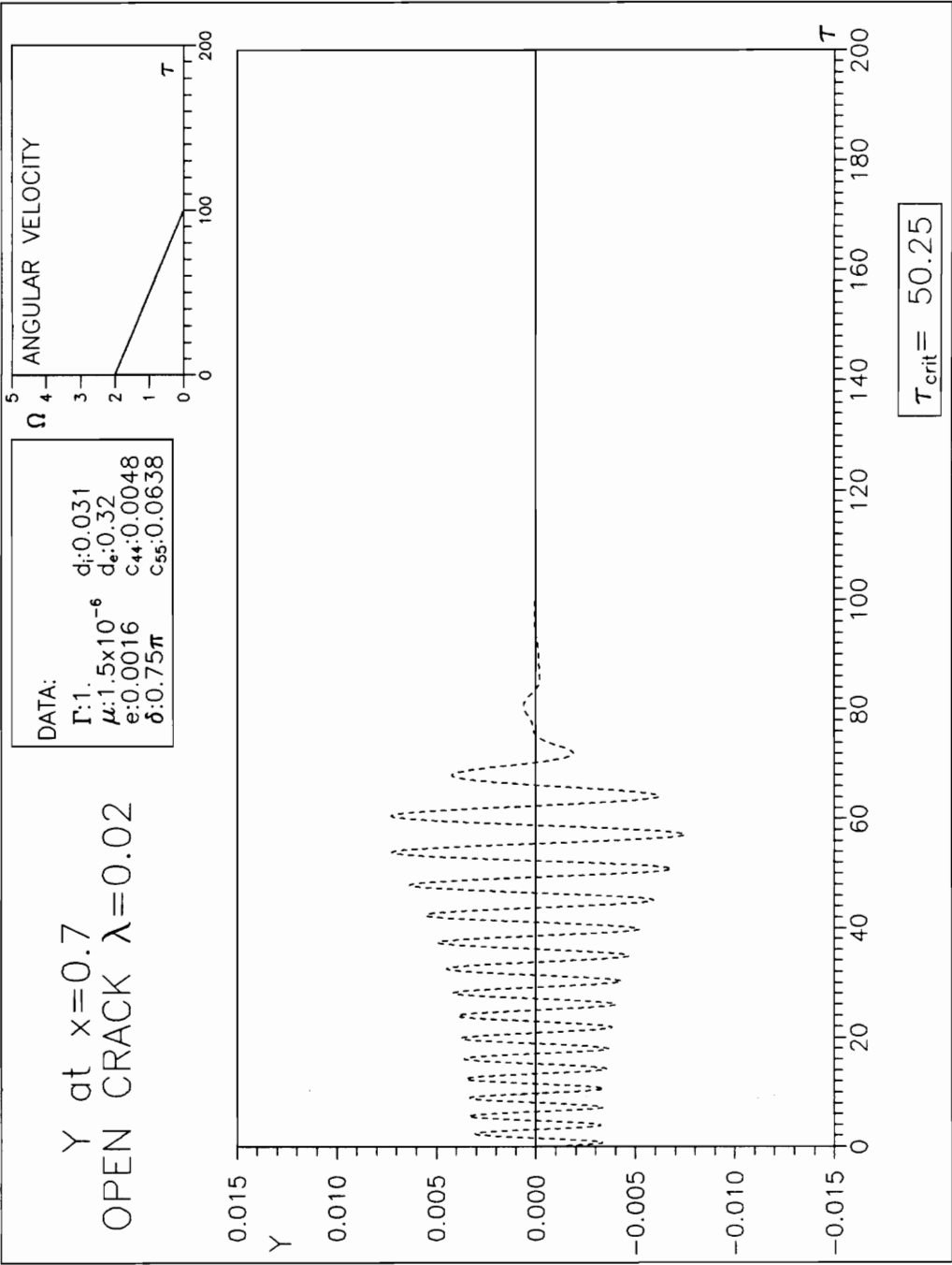
Figure 4.32 Time history of z displacement at x̃=0.7 for λ=0.04 – No crack – Deceleration

Figure 4.33 Time history of Z displacement at x̃=0.7 for λ=0.05 - No crack; deceleration.

Figure 4.34 Time history of z displacement at x̃=0.7 for λ=0.01 – Open crack; deceleration.

Figure 4.35 Time history of Z displacement at x̄=0.7 for λ=0.02 – Open crack; deceleration.

Z at x=0.7
OPEN CRACK λ=0.03

DATA:
Γ:1.
μ:1.5x10^{-6}
e:0.0016
δ:0.75π

d$_i$:0.031
d$_e$:0.32
c$_{44}$:0.0048
c$_{55}$:0.0638

ANGULAR VELOCITY

MAX Z: 0.0068 τ_{max}= 38.70 τ_{crit}= 33.47

Figure 4.36 Time history of z displacement at x̆=0.7 for λ=0.03 – Open crack; deceleration.
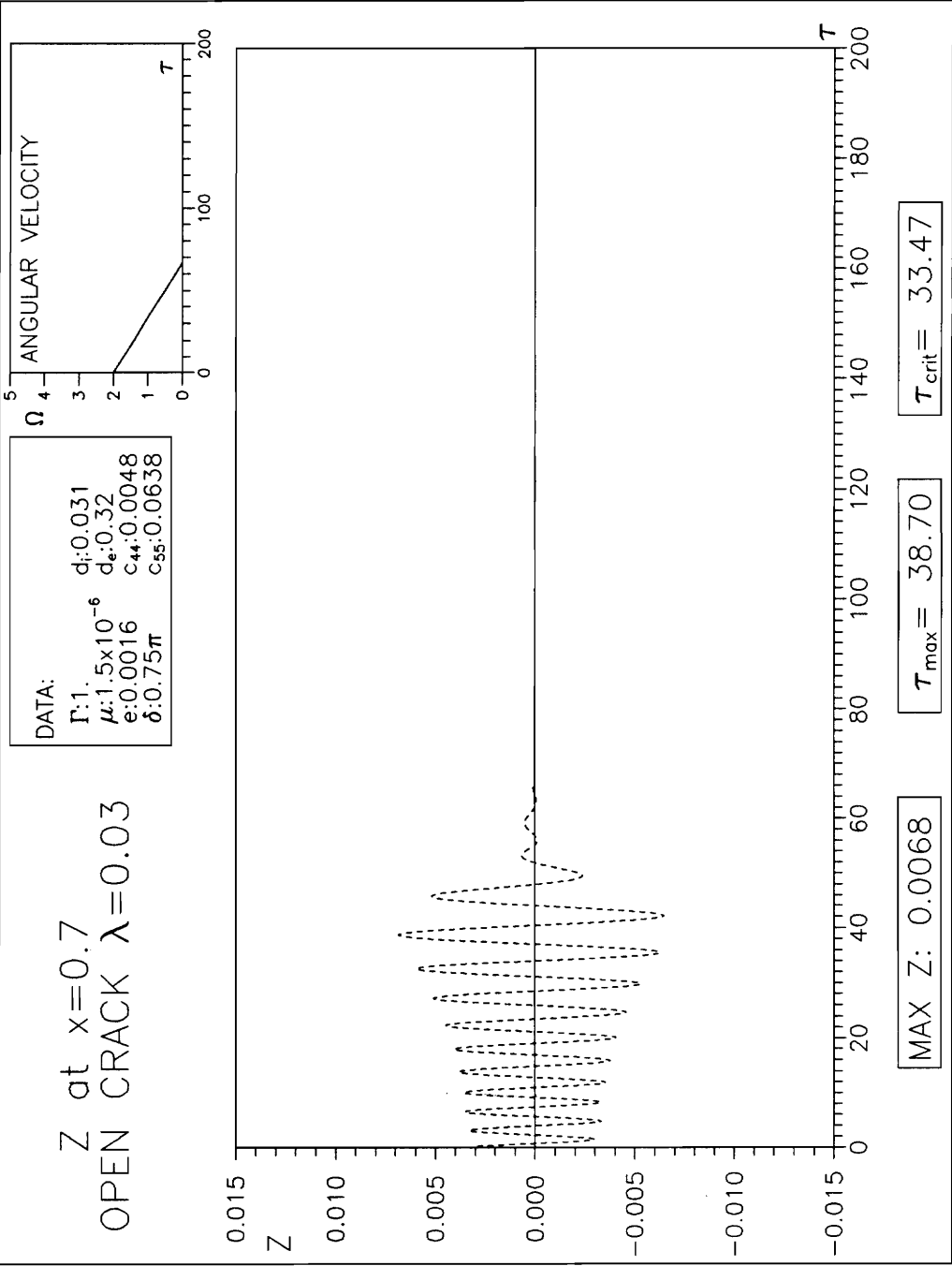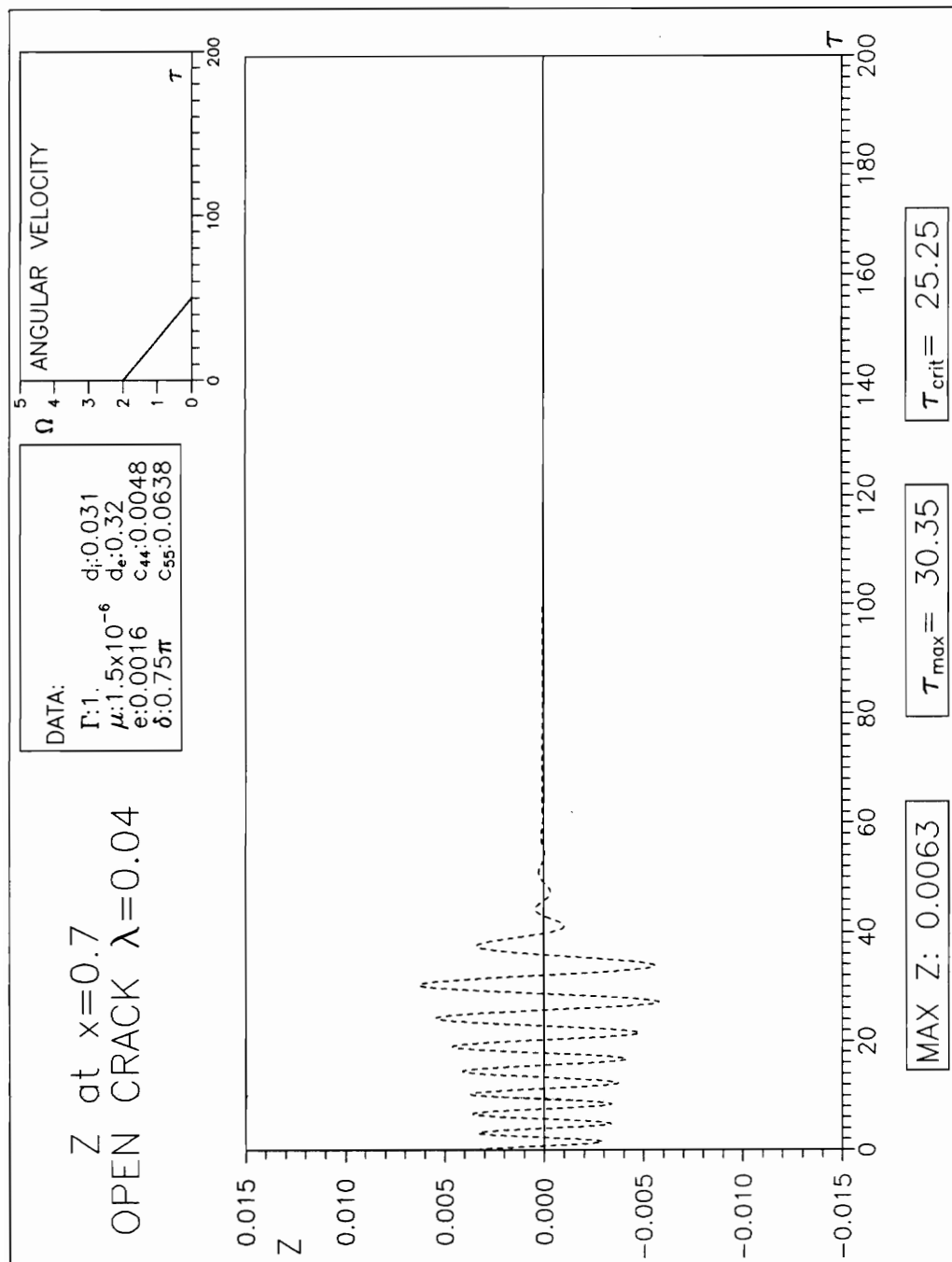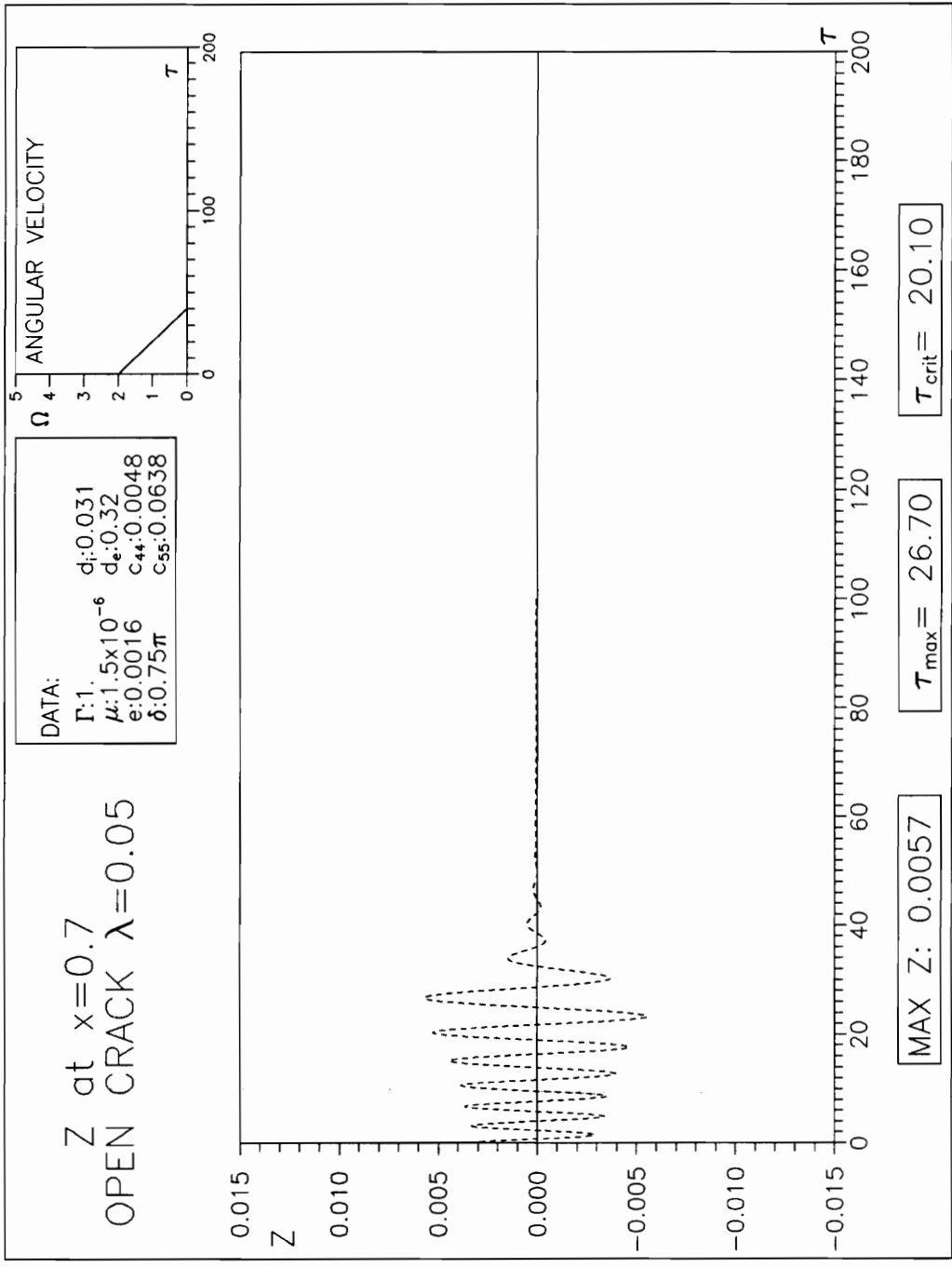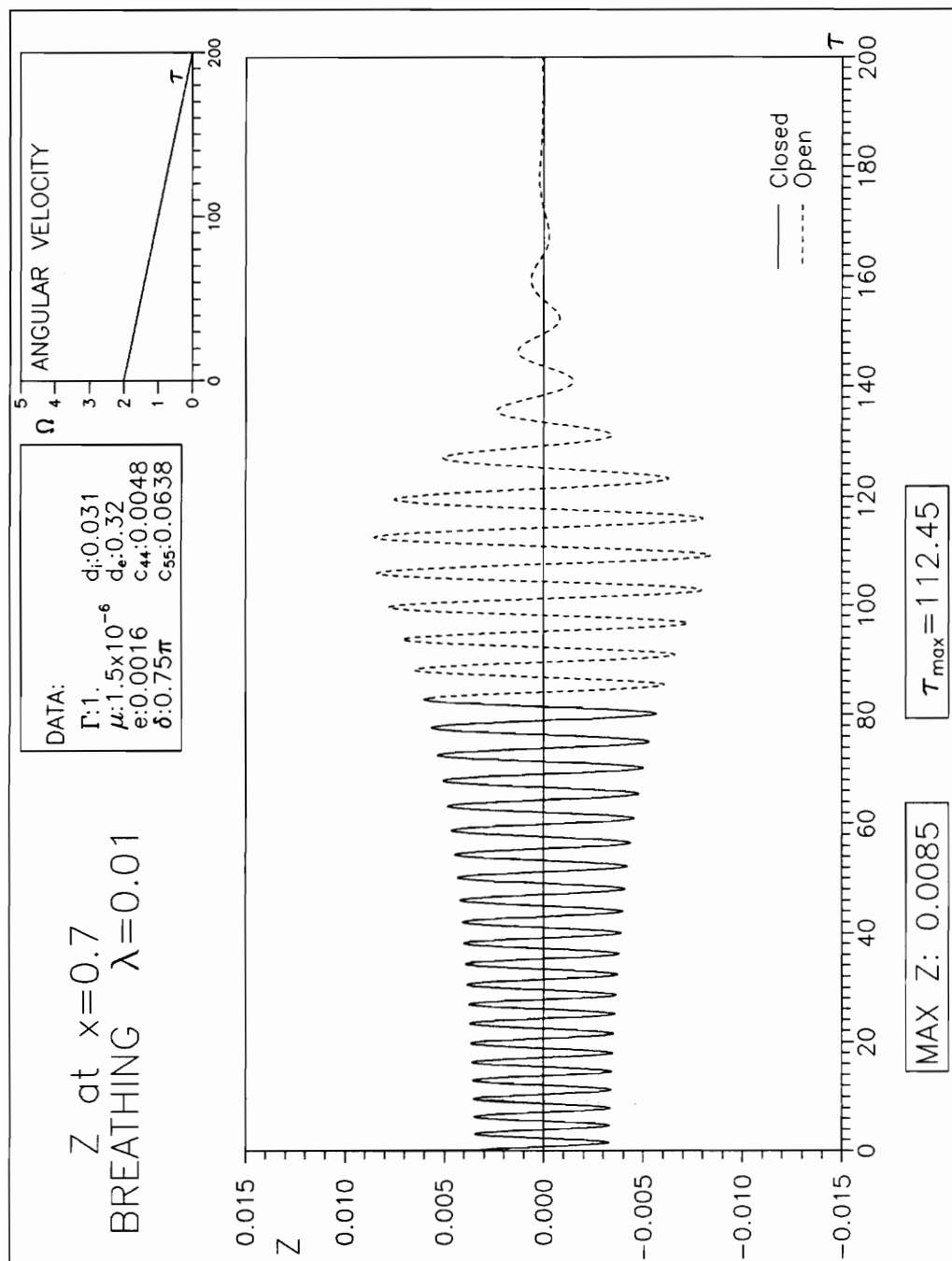
91

Figure 4.37 Time history of Z displacement at $\tilde{x}=0.7$ for $\lambda=0.04$ — Open crack; deceleration.

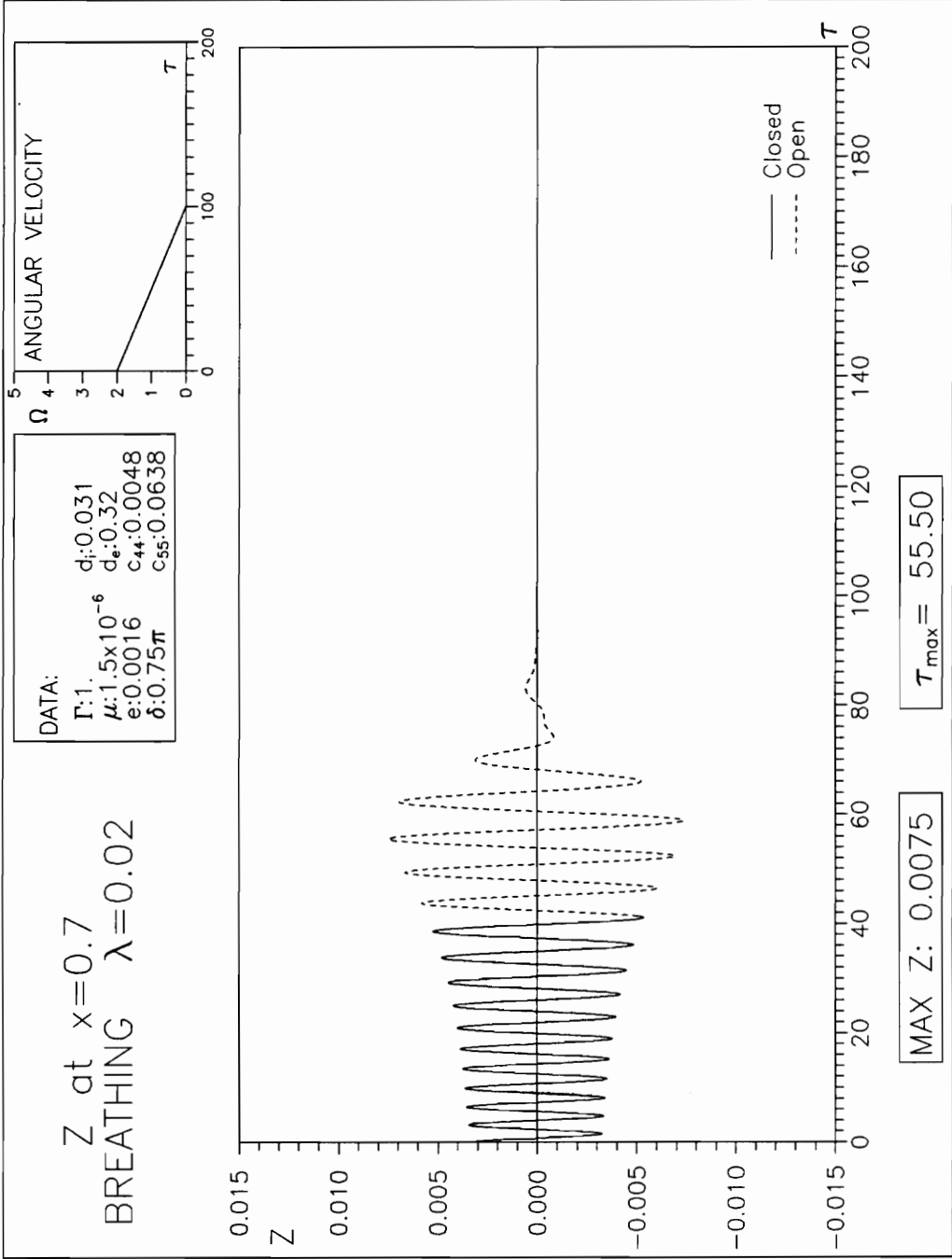**Figure 4.38 Time history of Z displacement at x̃=0.7 for λ=0.05 - Open crack; deceleration.**

Figure 4.39 Time history of z displacement at $\tilde{x}=0.7$ for $\lambda=0.01$ – Breathing; deceleration.

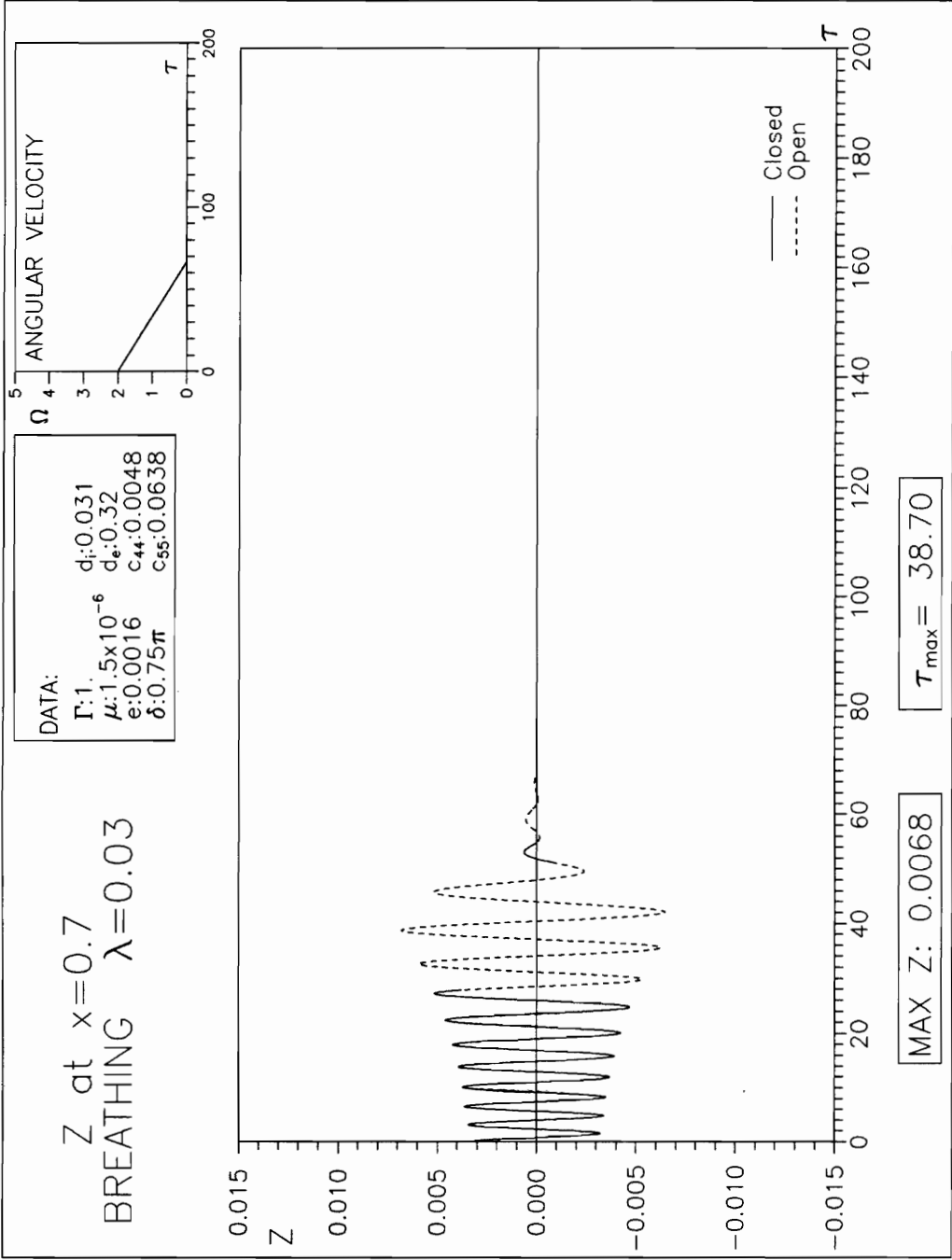**Figure 4.40 Time history of Z displacement at $\tilde{x}=0.7$ for $\lambda=0.02$ – Breathing; deceleration.**

Figure 4.41 Time history of z displacement at x̄=0.7 for λ=0.03 – Breathing; deceleration.

96

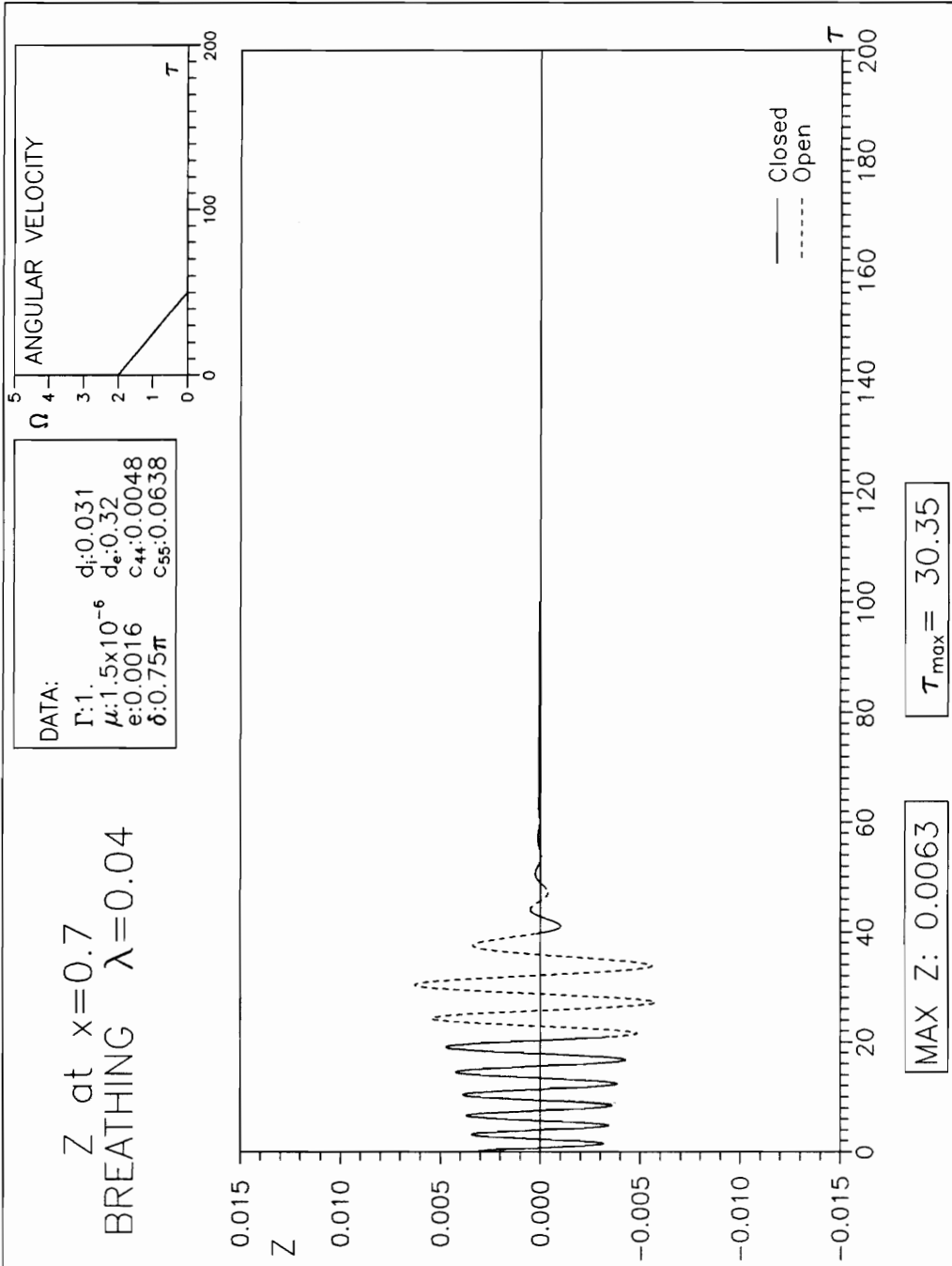**Figure 4.42 Time history of Z displacement at x̄=0.7 for λ=0.04 – Breathing; deceleration.**

Figure 4.43 Time history of Z displacement at x̄=0.7 for λ=0.05 - Breathing; deceleration.
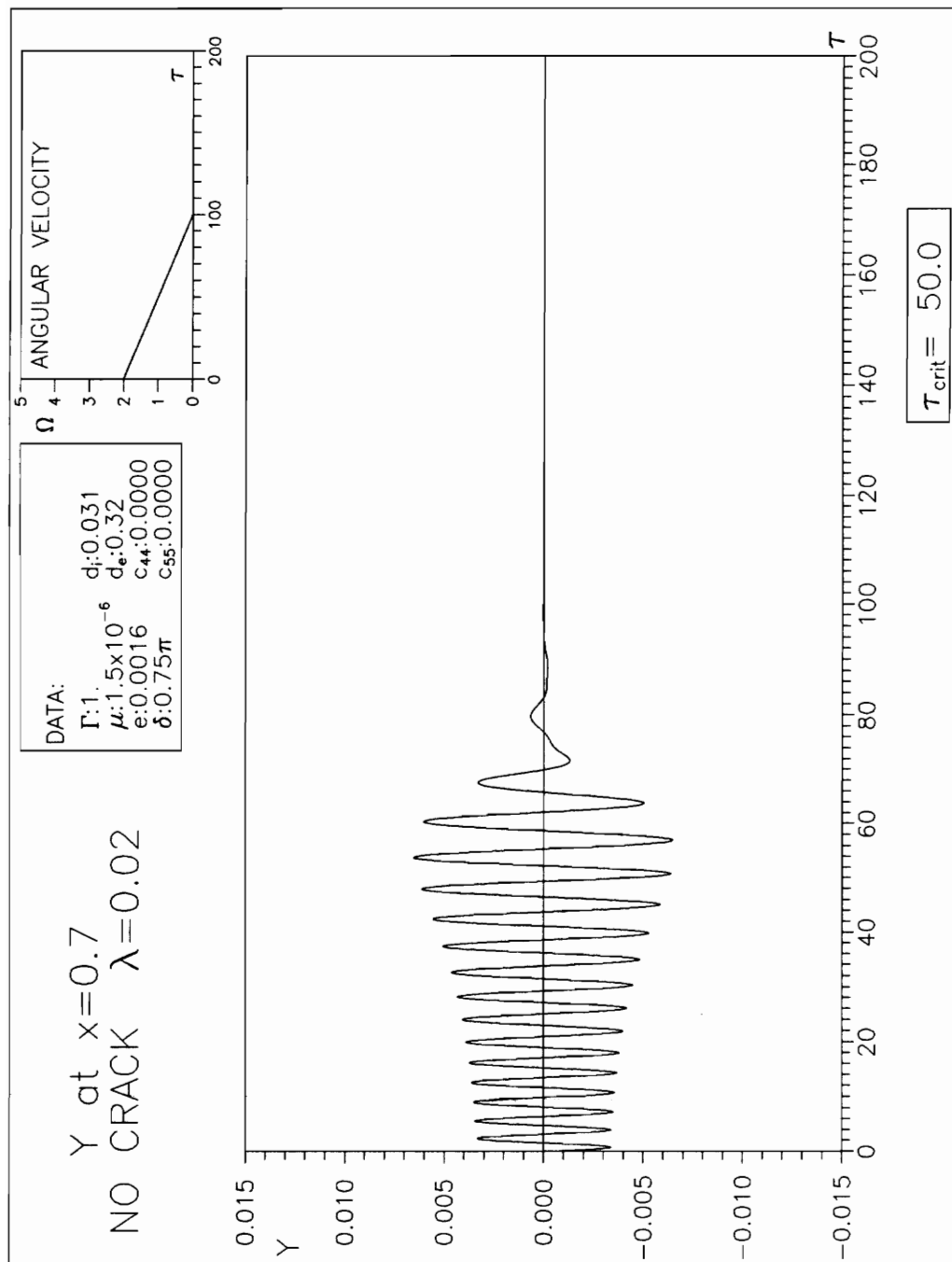
Figure 4.44 Time history of Y displacement at x̃=0.7 for λ=0.02 — No crack; deceleration.
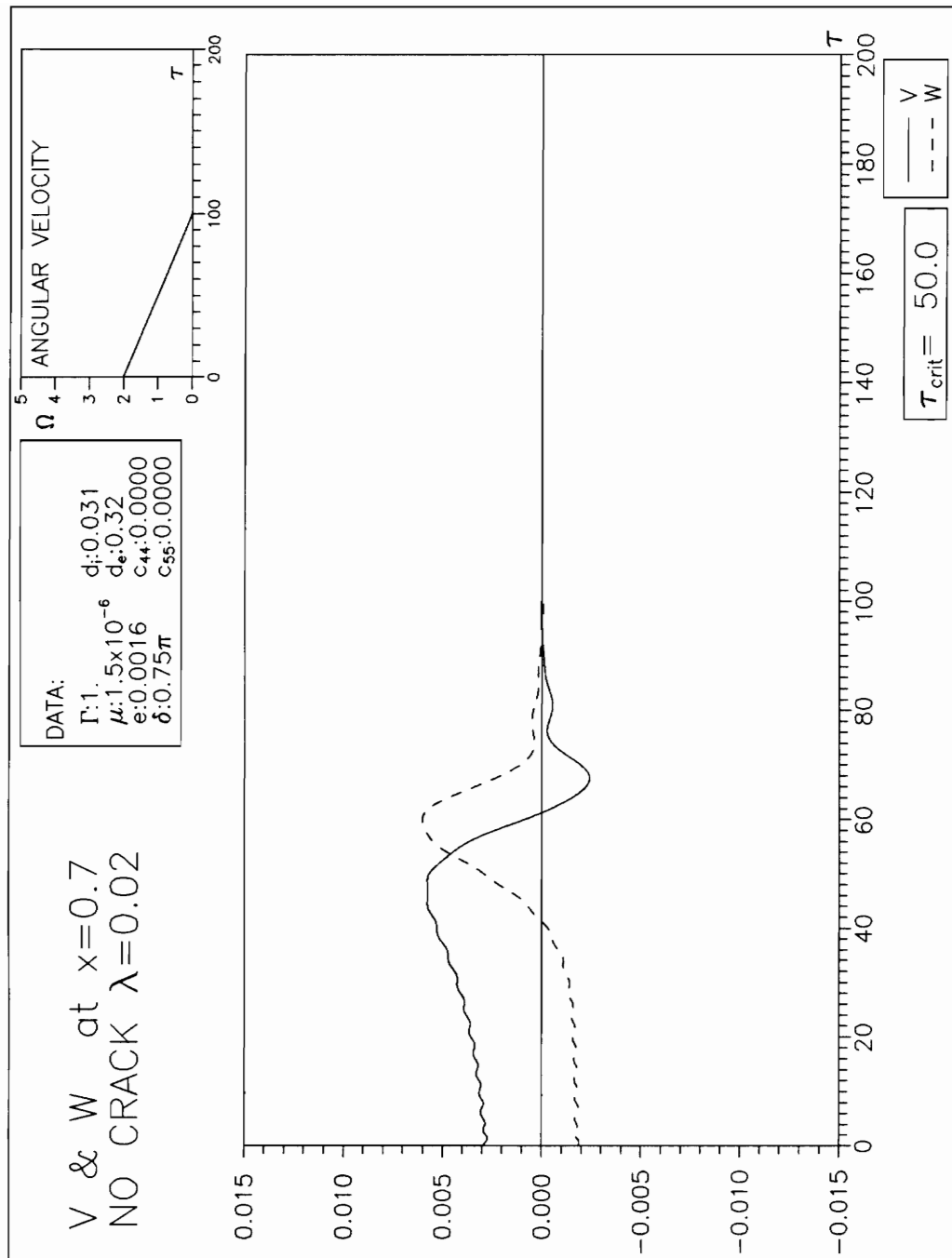
Figure 4.45 Time history of V and W displacement at x̄=0.7 for λ=0.02 – No crack; deceleration.

100
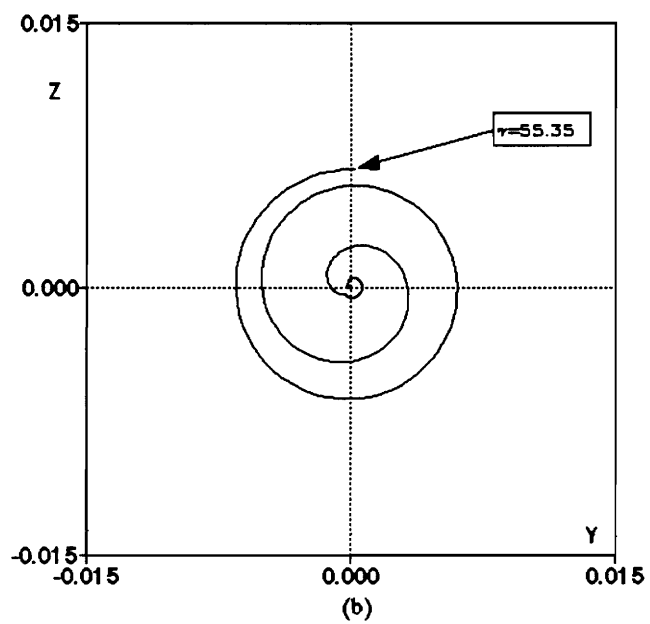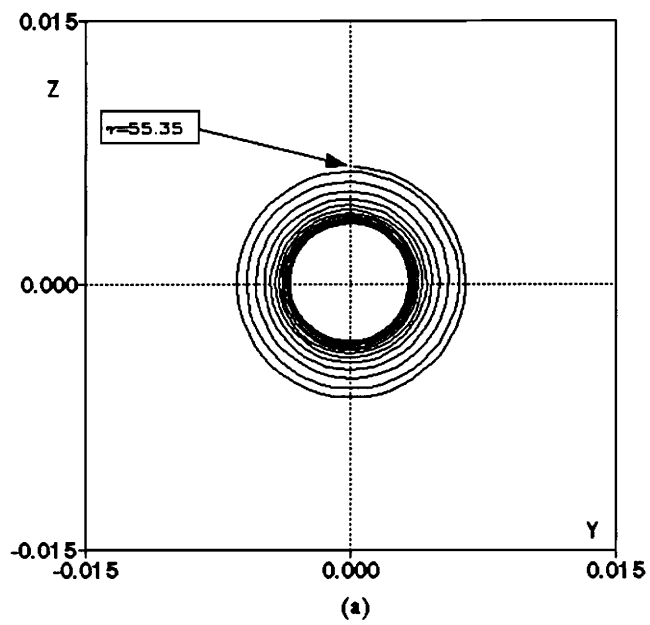
Figure 4.46 Orbits No crack, deceleration: (a) before τ_{max};
(b) after τ_{max}.

101
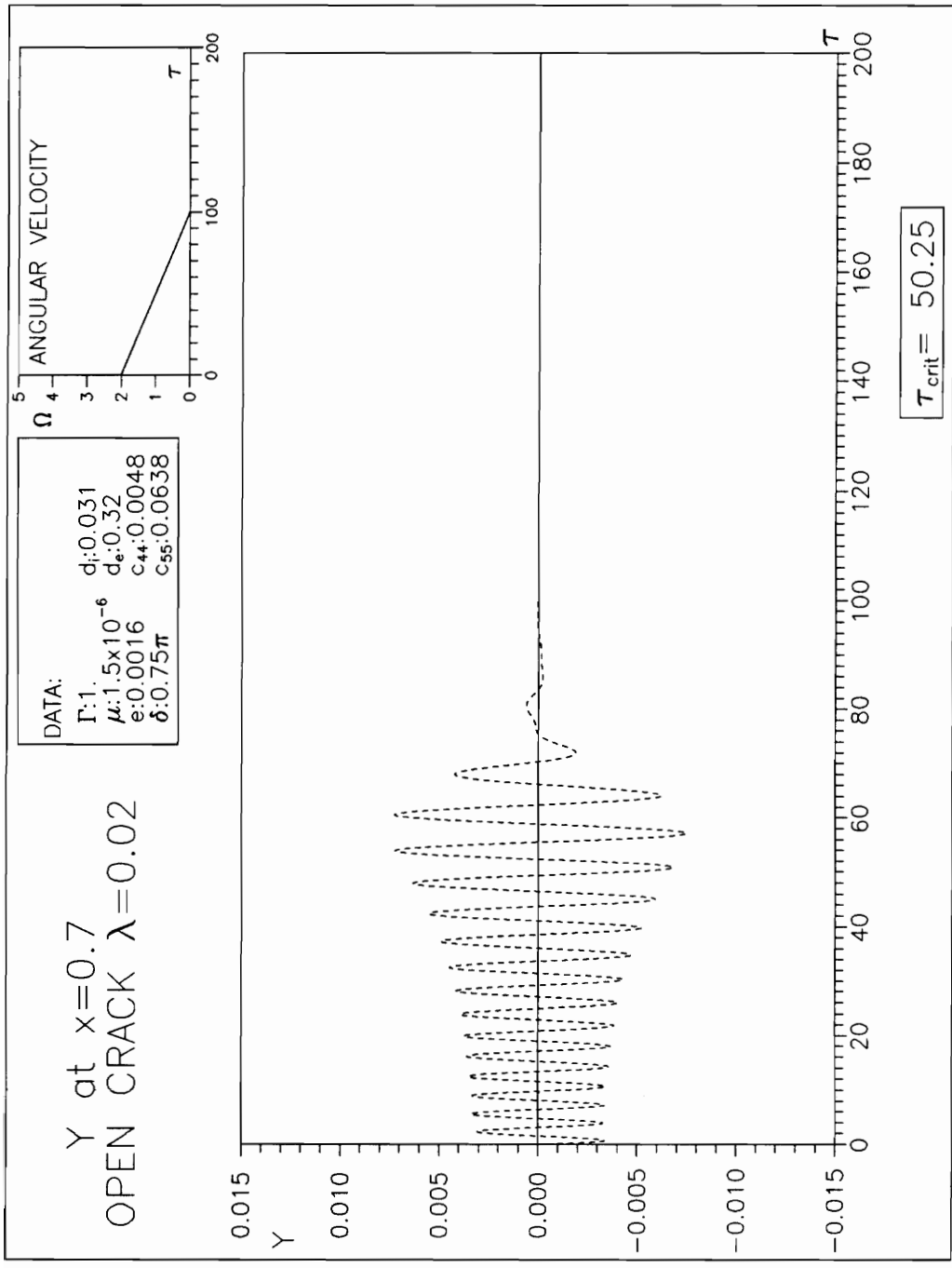
Figure 4.47 Time history of Y displacement at x̃=0.7 for λ=0.02 - Open crack - Deceleration.
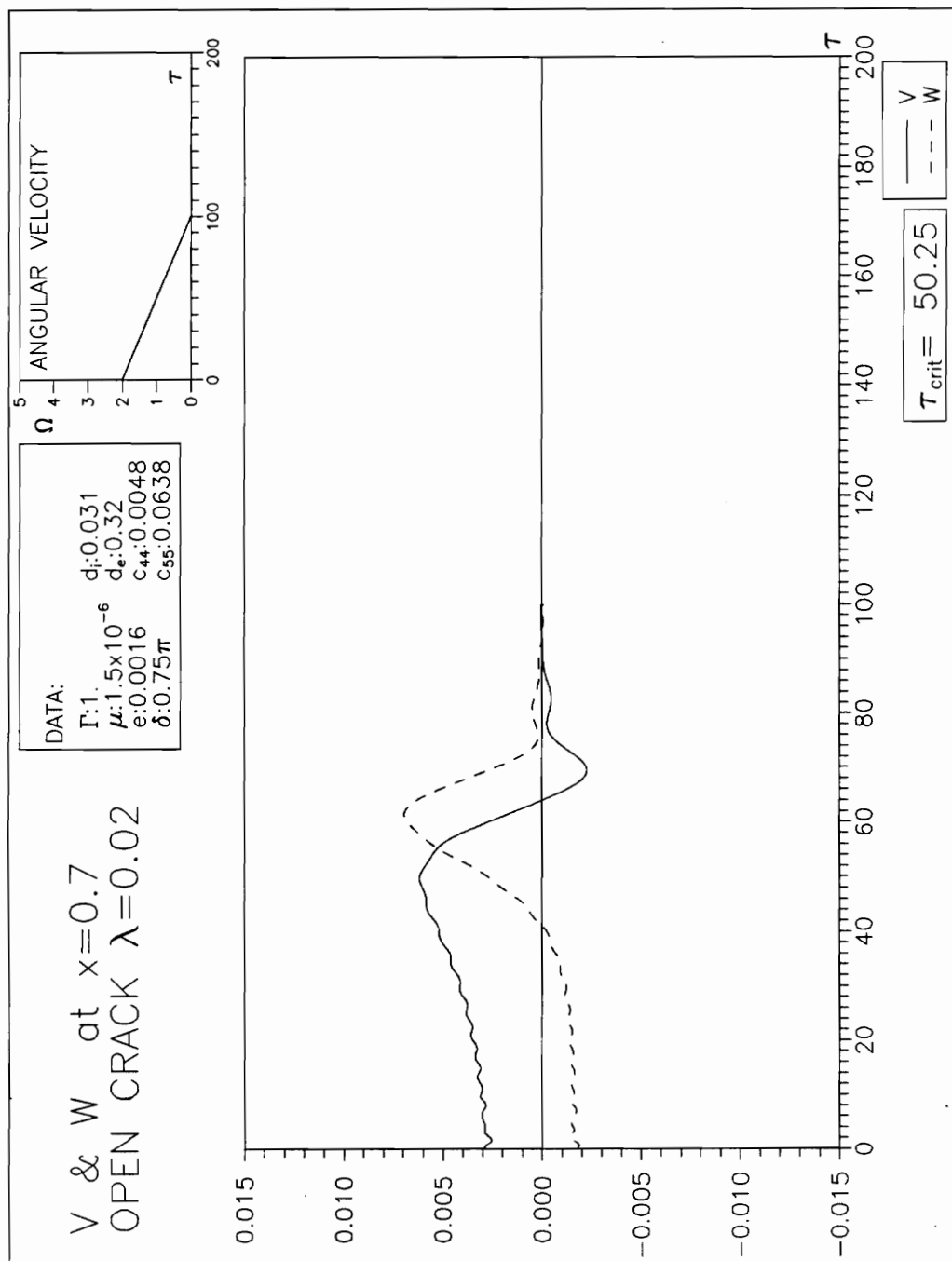
Figure 4.48 Time history of V and W displacement at x̄=0.7 for λ=0.02 – Open crack – Deceleration.
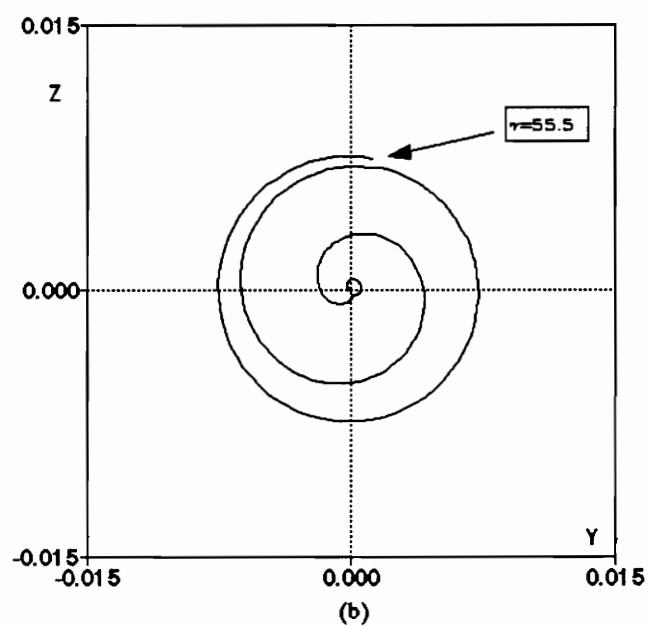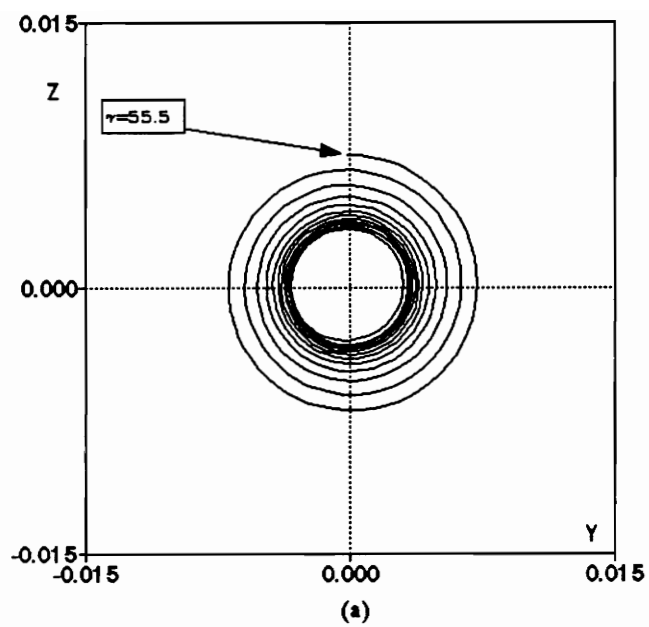
Figure 4.49 Orbits Open crack, deceleration: (a) before τ_{max};
(b) after τ_{max}.
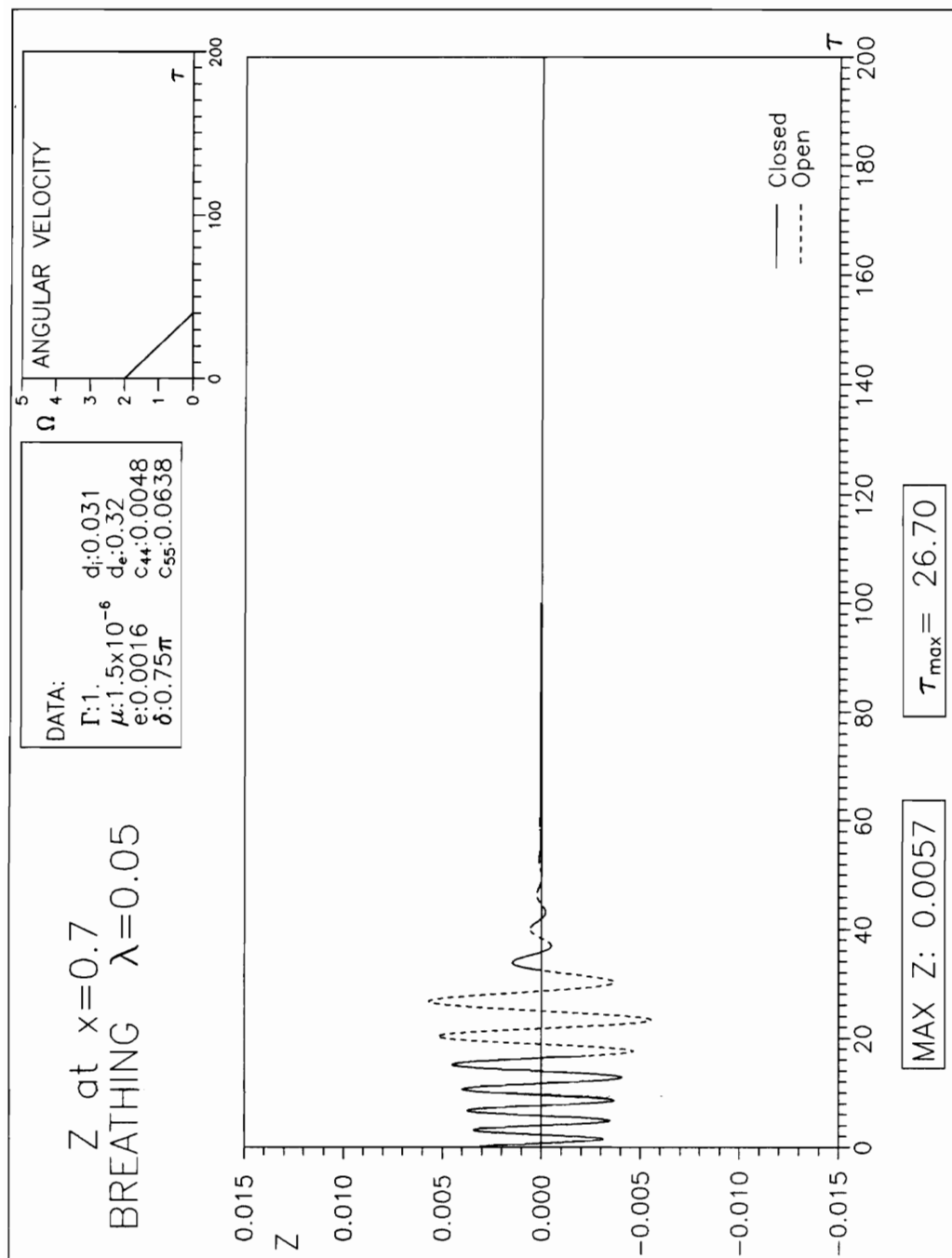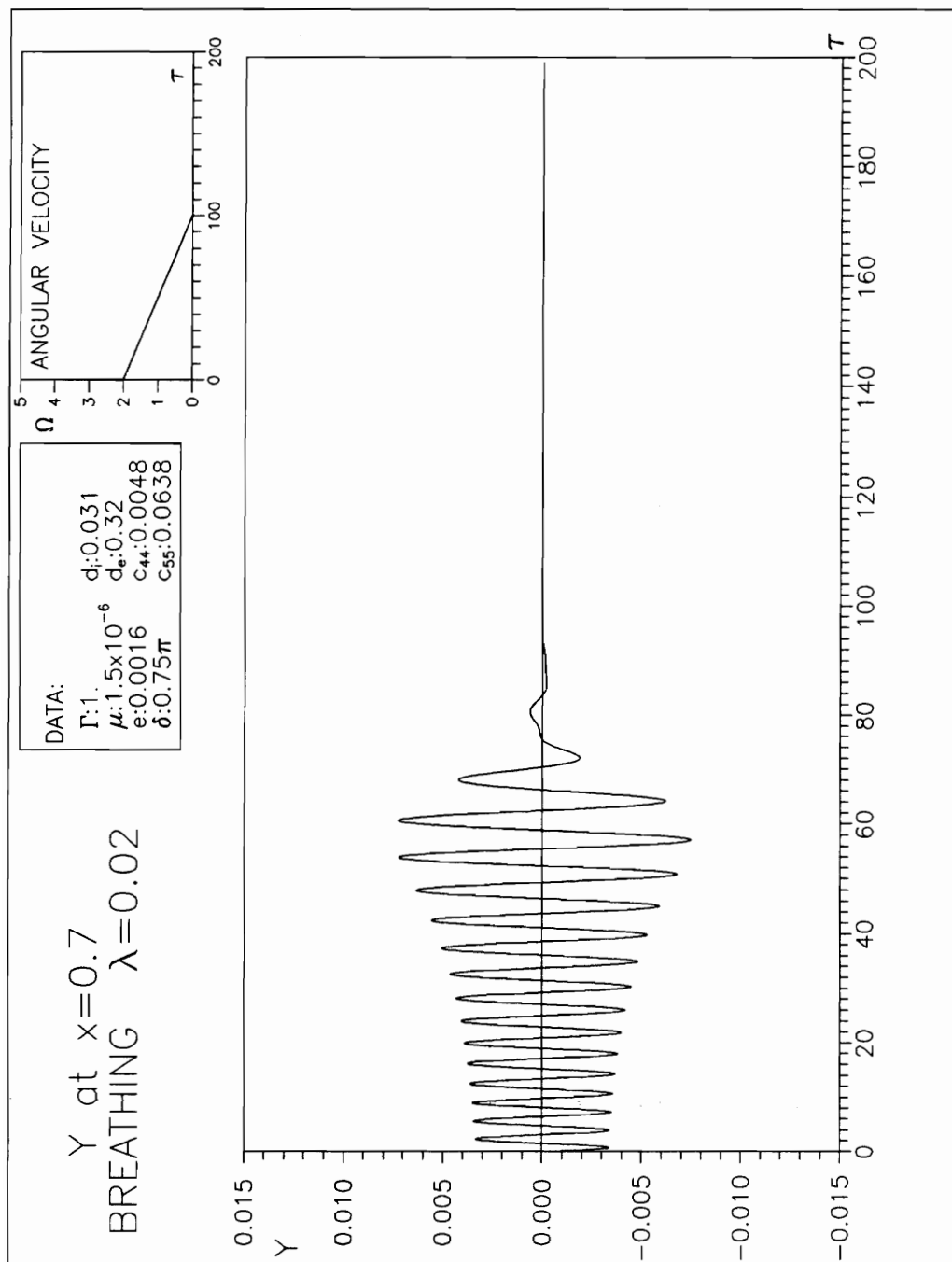
Figure 4.50 Time history of Y displacement at x̃=0.7 for λ=0.02 – Breathing – Deceleration.

Figure 4.51 Time history of V and W displacement at x̄=0.7 for λ=0.02 - Breathing; acceleration.

106

Figure 4.52 Orbits Breathing crack, deceleration: (a) before τ_{max}; (b) after τ_{max}.

Table 4.3 Effect of deceleration on Z displacement at $\tilde{x}=0.7$.

λ	Z_{max} at $\tilde{x}=0.7$		
	No crack	Open crack	Breathing
0.005	0.00775	0.00923	0.00923
0.006	0.00766	0.00908	0.00907
0.007	0.00758	0.00894	0.00894
0.008	0.00749	0.00880	0.00880
0.009	0.00737	0.00864	0.00864
0.010	0.00732	0.00852	0.00852
0.020	0.00663	0.00749	0.00748
0.030	0.00609	0.00683	0.00681
0.040	0.00563	0.00629	0.00630
0.050	0.00513	0.00570	0.00569

Table 4.4 Effect of deceleration on the maximum Z displacement over the whole length.

λ	Z_{max} (Whole length)		
	No crack	Open crack	Breathing
0.005	0.00958	0.01172	0.01172
0.006	0.00947	0.01157	0.01157
0.007	0.00937	0.01137	0.01137
0.008	0.00925	0.01125	0.01125
0.009	0.00911	0.01097	0.01097
0.010	0.00905	0.01093	0.01093
0.020	0.00819	0.00952	0.00951
0.030	0.00752	0.00872	0.00871
0.040	0.00696	0.00808	0.00806
0.050	0.00634	0.00741	0.00739

INFLUENCE OF RATE OF DECELERATION
Zmax at $\tilde{x}=0.7$

Legend:
— NO CRACK
----- OPEN CRACK
···□··· BREATHING

Breathing and open crack
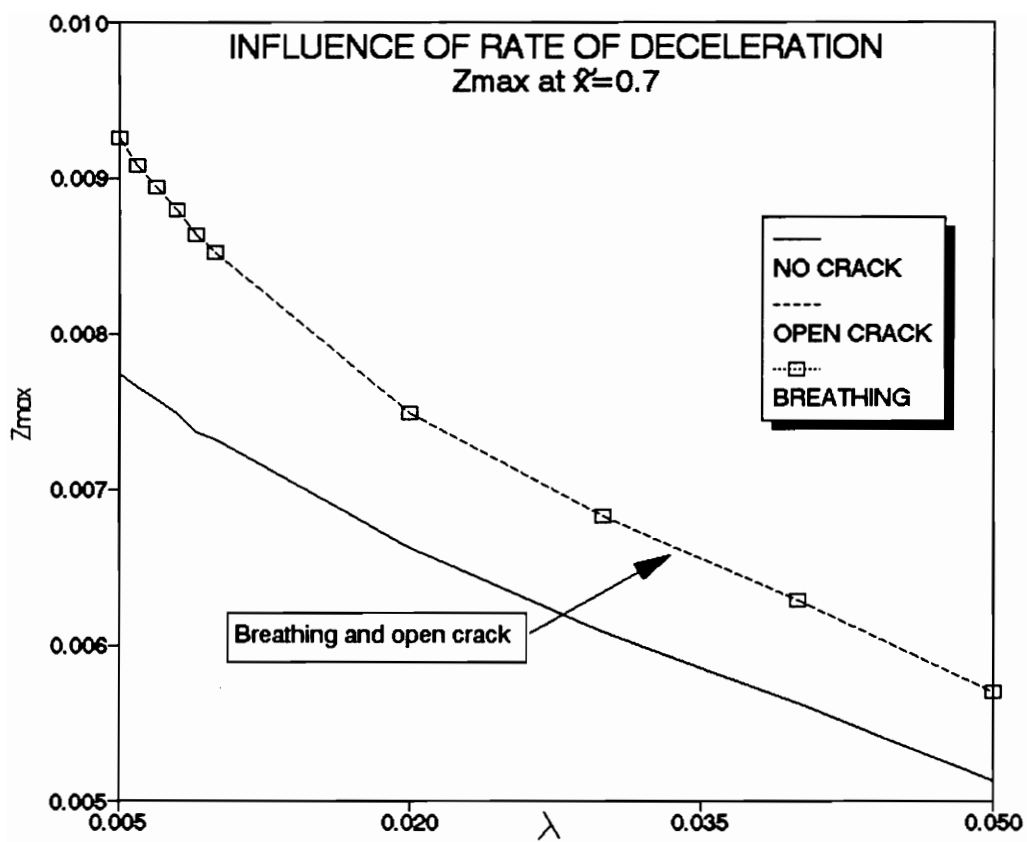
Figure 4.53 Effect of deceleration on Z displacement at $\tilde{x}=0.7$.
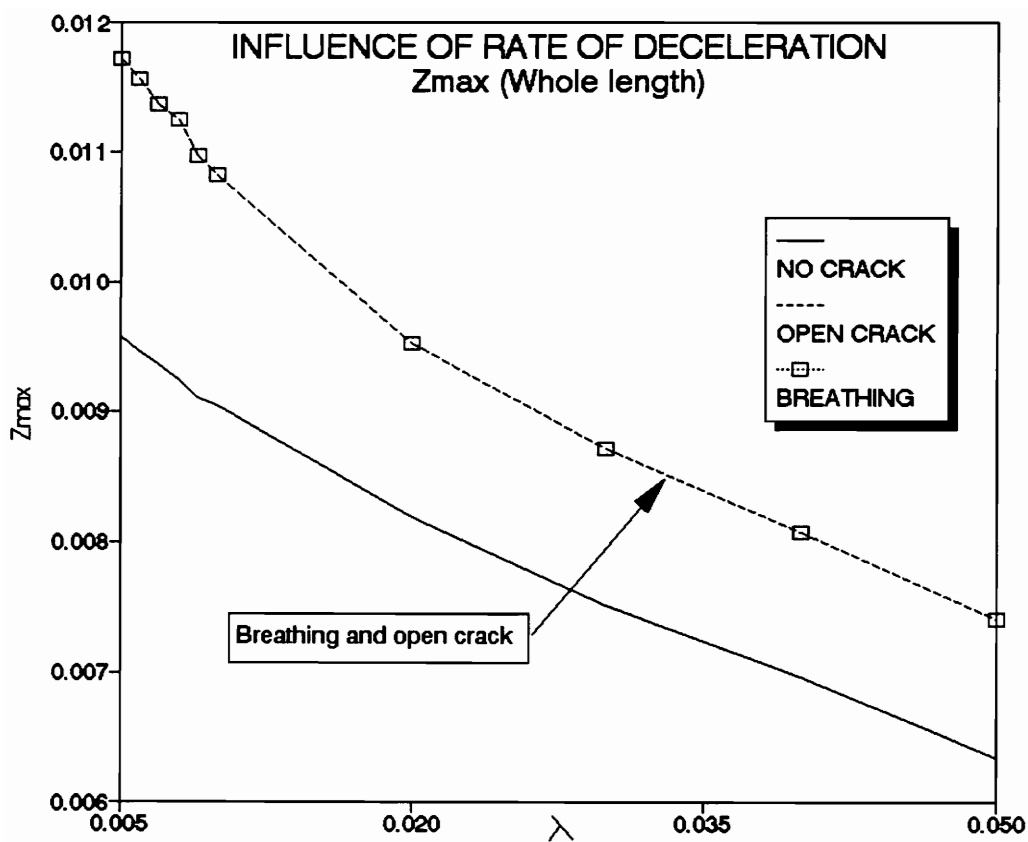
Figure 4.54 Effect of deceleration on the maximum Z displace-ment over the whole length.

Influence of angle δ

Running the program using the standard case parameters and different values of δ in the range 0-2π, several interesting results are found. The runs are made for both cases: acceleration and deceleration with λ=0.02. Table 4.5 and Figures 4.55 to 4.60 contain results for an accelerated rotating shaft including the three conditions uncracked, crack always open and breathing. Z at $\tilde{x}$=0.7 and Zmax were defined previously and the value R_{max} is defined as

$$R_{max} = \max\left\{\sqrt{Z^2+Y^2}\right\} \quad \textit{along} \ \tau \tag{4.4}$$

Table 4.6 and Figures 4.61 to 4.66 also present Z at $\tilde{x}$=0.7, Z_{max}, and R_{max}, but for a decelerated shaft. Similarly as before, an assumed steady motion is achieved before the deceleration starts, using the same criterion as previously.

It is interesting to note that two values of δ geometrically symmetric, like δ=0 and δ=π, do not produce the same result. The possible cause is the direction of the rotating velocity.

Figures 4.58 to 4.60 and 4.64 to 4.66 make clear the fact that an always-open crack and no crack are not always the upper and lower limits of the response, respectively. Note that for δ=π/2, the response given by the breathing case is larger than the response given by the always-open

crack and no crack. This situation is the opposite to that found for $\delta = 3\pi/2$.

These results are very interesting because they are contrary to the primary assumption that the more stiffness the shaft has, the smaller the displacements are. But a quick analysis of a very simple case shows that the results are possible. Let us take the uncracked shaft with constant angular velocity and without damping and eccentricity, and consider just a one-term approximate solution. From equations (2.15) and (2.16):

$$V_1 + \ddot{V}_1 - 2\Omega \dot{W}_1 - \Omega^2 V_1 = 2\bar{\mu}\sin\gamma_1$$

$$W_1 + \ddot{W}_1 + 2\Omega \dot{V}_1 - \Omega^2 W_1 = 2\bar{\mu}\cos\gamma_1 \qquad (4.5)$$

The time histories show that if the shaft reaches a steady state it is possible to assume

$$\dot{V}_1 = \ddot{V}_1 = \dot{W}_1 = \ddot{W}_1 = 0 \qquad (4.6)$$

Then

$$V_1 - \Omega^2 V_1 = 2\bar{\mu}\sin\gamma_1$$

$$W_1 - \Omega^2 W_1 = 2\bar{\mu}\cos\gamma_1 \qquad (4.7)$$

113

Now defining α as a coefficient of stiffness in order to make the stiffness of the shaft variable, the two equations are

$$\alpha V_1 - \Omega^2 V_1 = 2\bar{\mu}\sin\gamma_1$$

$$\alpha W_1 - \Omega^2 W_1 = 2\bar{\mu}\cos\gamma_1$$

and the solutions are

$$V_1 = \frac{2\bar{\mu}\sin\gamma_1}{(\alpha - \Omega^2)}$$

$$W_1 = \frac{2\bar{\mu}\cos\gamma_1}{(\alpha - \Omega^2)}$$
(4.8)

Then the amplitudes of displacements V_1 and W_1 depend on the value of $(\alpha - \Omega^2)$ and not just on α, so an increase in the stiffness can produce a decrease in amplitude.

Influence of crack position

Since not only the detection of the crack but also its probable position are of interest, a study of the effect of the crack position is done.

114

Several runs of the program are made using the standard parameters and making $\bar{b}$ a variable with values ranging between 0 and 1, and λ=0.02 for acceleration and deceleration. The results are presented in Table 4.7 and Figure 4.67 for acceleration, and Table 4.8 and Figure 4.68 for deceleration. As is shown in the figures, there is symmetry in the position of the crack with respect to the maximum displacement Z produced over the whole length. There is no difference between an always-open crack and the more realistic case of breathing. The symmetry is no longer true if the values of the displacement are taken at a particular point, with the exception if that point is in the middle of the shaft. The maximum displacement Z occurs when the crack is in the middle of the shaft.

Influence of crack depth

In order to get an idea of the influence of the depth of the crack on the dynamic response, some runs with different values of the ratio a/D are made. Table 4.9 presents the values of a/D used and the Z displacements obtained for each of them and Figure 4.69 shows the same values graphically for acceleration and Table 4.10 and Figure 6.70 present the same values for deceleration. It is clear that the response changes dramatically with the crack depth, corresponding to an increase in the Z displacement with a/D. It should be noted that the change in the crack depth is modeled as a change in the $\tilde{c}_{44}$ and $\tilde{c}_{55}$ parameters and the

values used for each ratio a/D are presented in Tables 4.9 and 4.10.

Table 4.5 Influence of δ with acceleration. (a) No crack, (b) Crack always open, (c) Breathing crack.

δ	$Z_{at\ \bar{x}=0.7}$	Z_{max}	R_{max}
0	0.00852	0.01055	0.01065
$\pi/2$	0.00919	0.01137	0.01138
π	0.00867	0.01073	0.01074
$3\pi/2$	0.00935	0.01157	0.01157

(a)

δ	$Z_{at\ \bar{x}=0.7}$	Z_{max}	R_{max}
0	0.00874	0.01111	0.01112
$\pi/2$	0.00914	0.01140	0.01140
π	0.00857	0.01089	0.01094
$3\pi/2$	0.00897	0.01118	0.01119

(b)

δ	$Z_{at\ \bar{x}=0.7}$	Z_{max}	R_{max}
0	0.00853	0.01055	0.01065
$\pi/2$	0.00947	0.01172	0.01180
π	0.00857	0.01089	0.01094
$3\pi/2$	0.00852	0.01070	0.01082

(c)
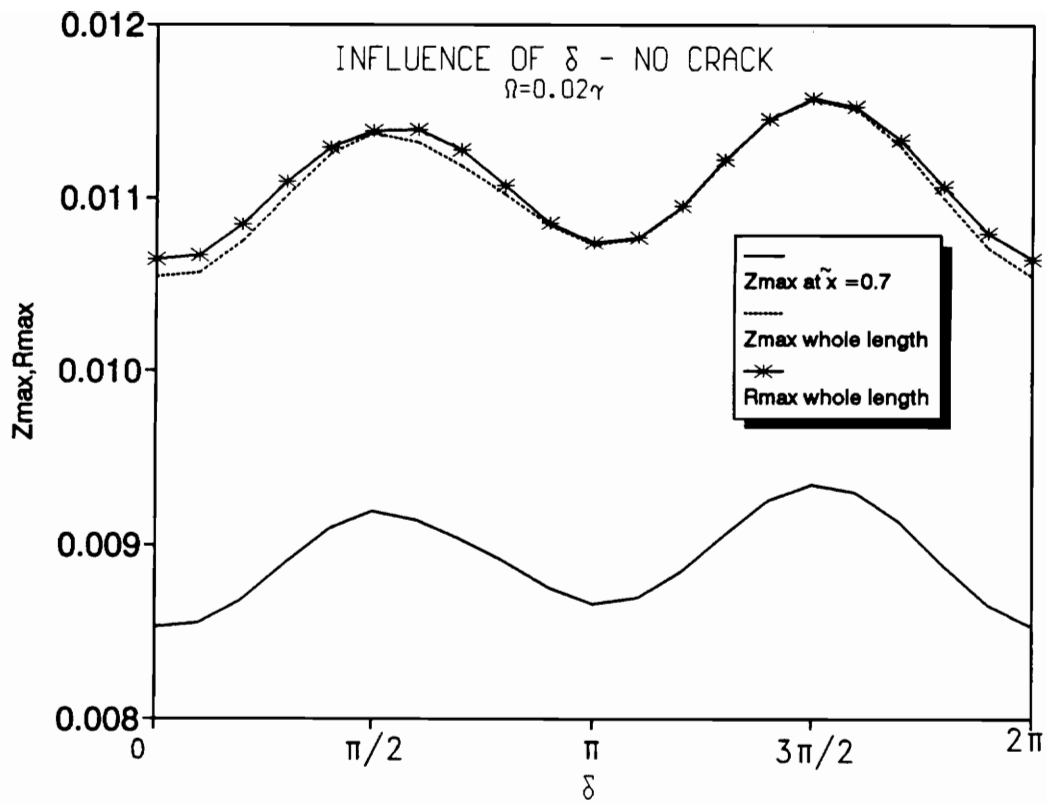
Figure 4.55 Influence of δ; acceleration, no crack.
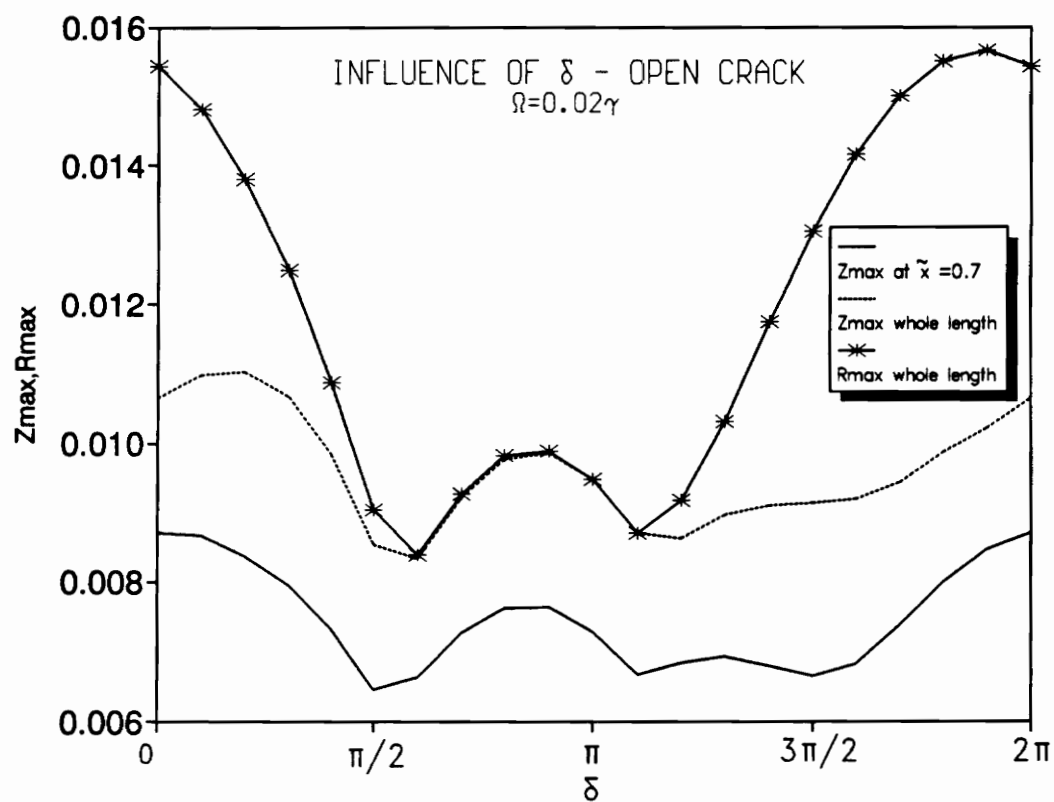
Figure 4.56 Influence of δ; acceleration, open crack.
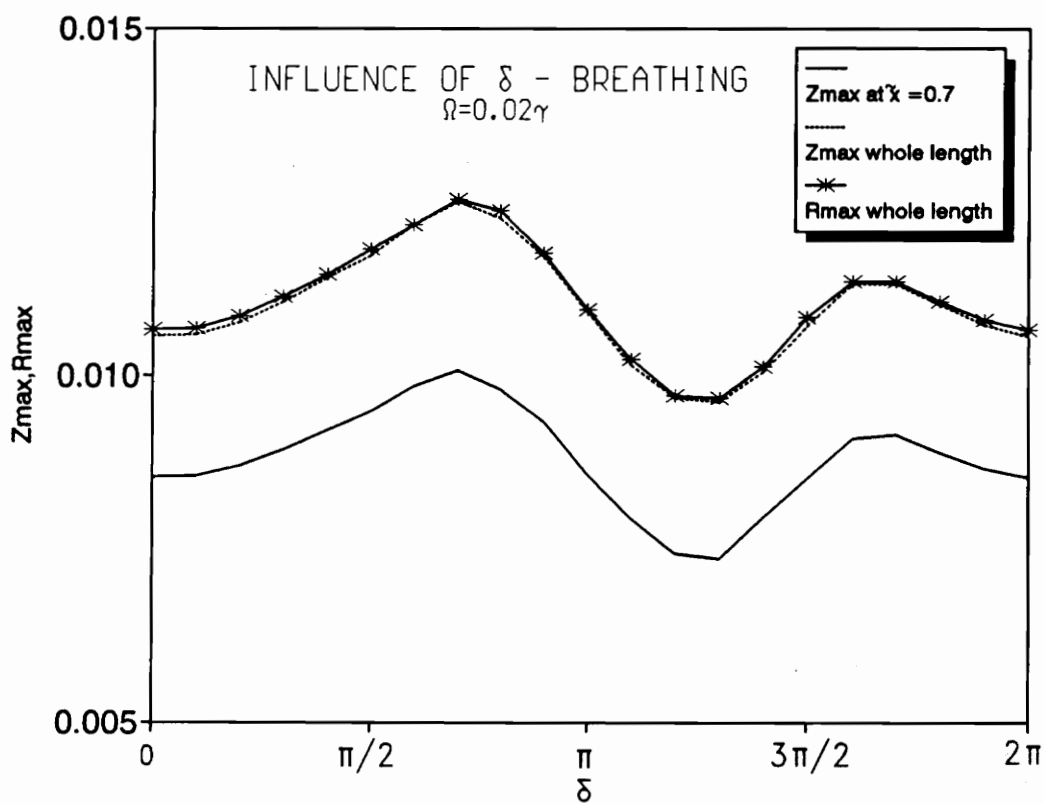
Figure 4.57 Influence of δ; acceleration, breathing crack.

Figure 4.58 Influence of δ; acceleration, Z at x̃ =0.7.

Figure 4.59 Influence of δ; acceleration, Z_{max}.

Figure 4.60 Influence of δ; acceleration, R_max.

Table 4.6 Influence of δ with deceleration. (a) No crack, (b) Crack always open, (c) Breathing crack.

δ	$Z_{at\ \tilde{x}=0.7}$	Z_{max}	R_{max}
0	0.00845	0.01050	0.01476
$\pi/2$	0.00694	0.00865	0.00904
π	0.00709	0.00876	0.00876
$3\pi/2$	0.00759	0.00945	0.01241

(a)

| δ	$Z_{at\ \tilde{x}=0.7}$	Z_{max}	R_{max}
0	0.00869	0.01065	0.01541
$\pi/2$	0.00645	0.00854	0.00904
π	0.00729	0.00947	0.00948
$3\pi/2$	0.00665	0.00915	0.01305

(b)

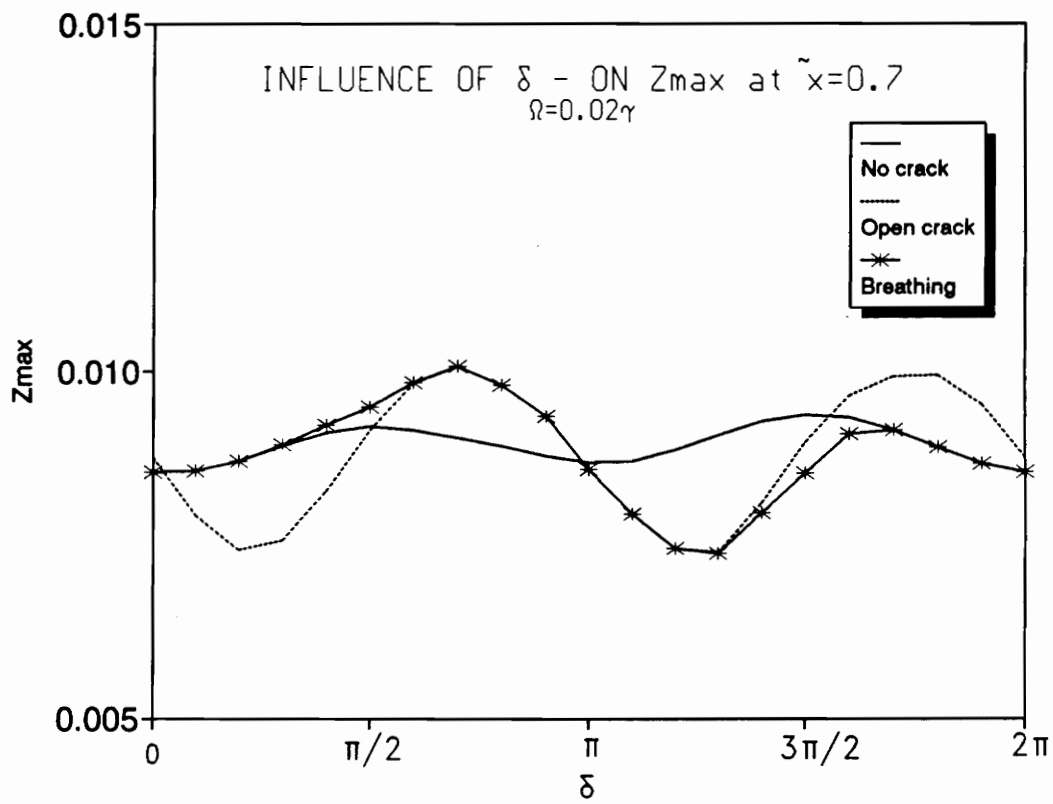| δ	$Z_{at\ \tilde{x}=0.7}$	Z_{max}	R_{max}
0	0.00845	0.01050	0.01476
$\pi/2$	0.00694	0.00865	0.00904
π	0.00729	0.00947	0.00948
$3\pi/2$	0.00682	0.00918	0.01243

(c)
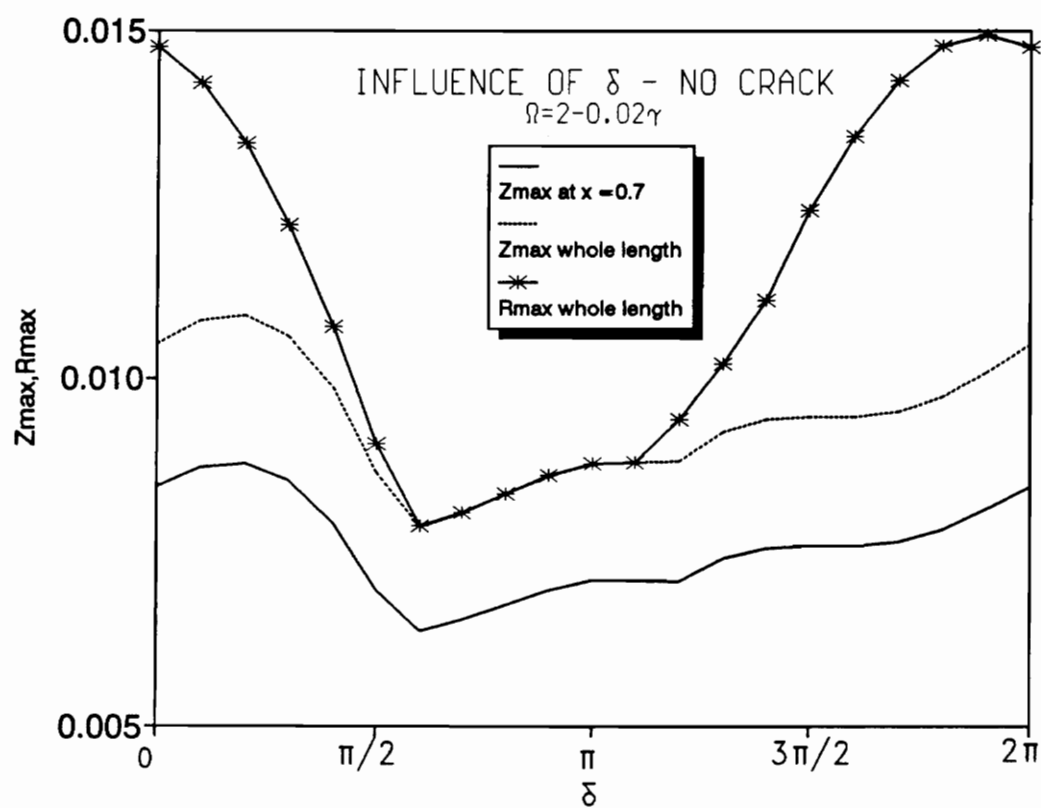
Figure 4.61 Influence of δ; deceleration, no crack.
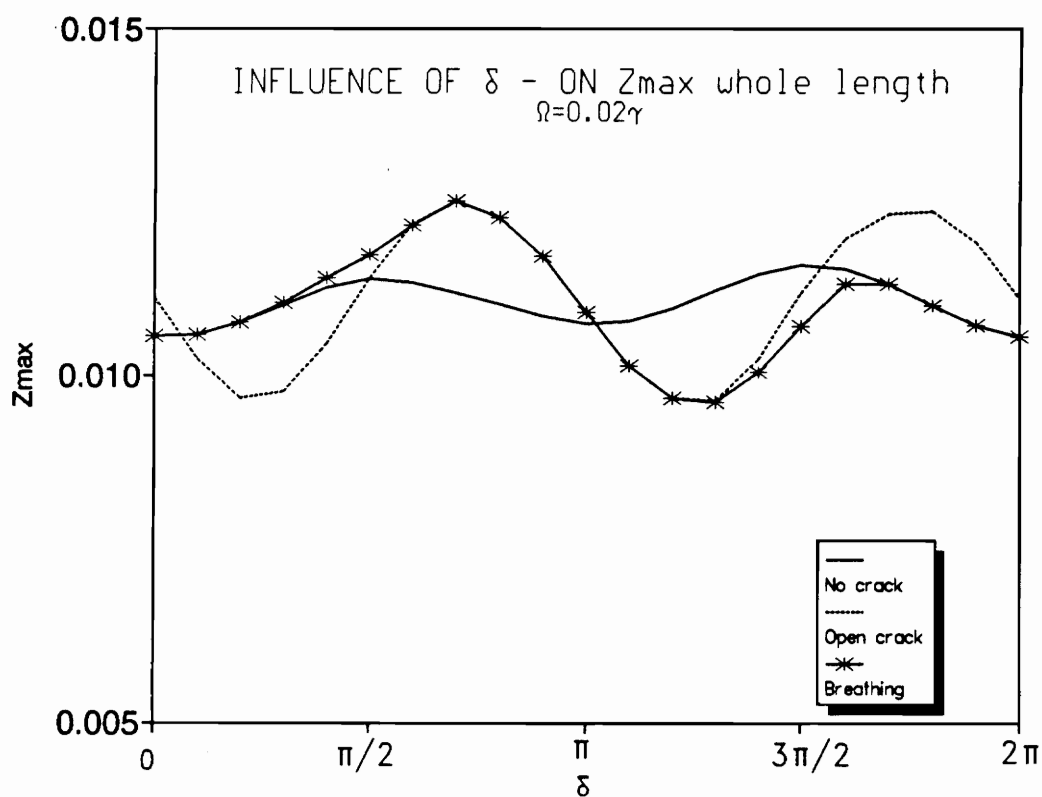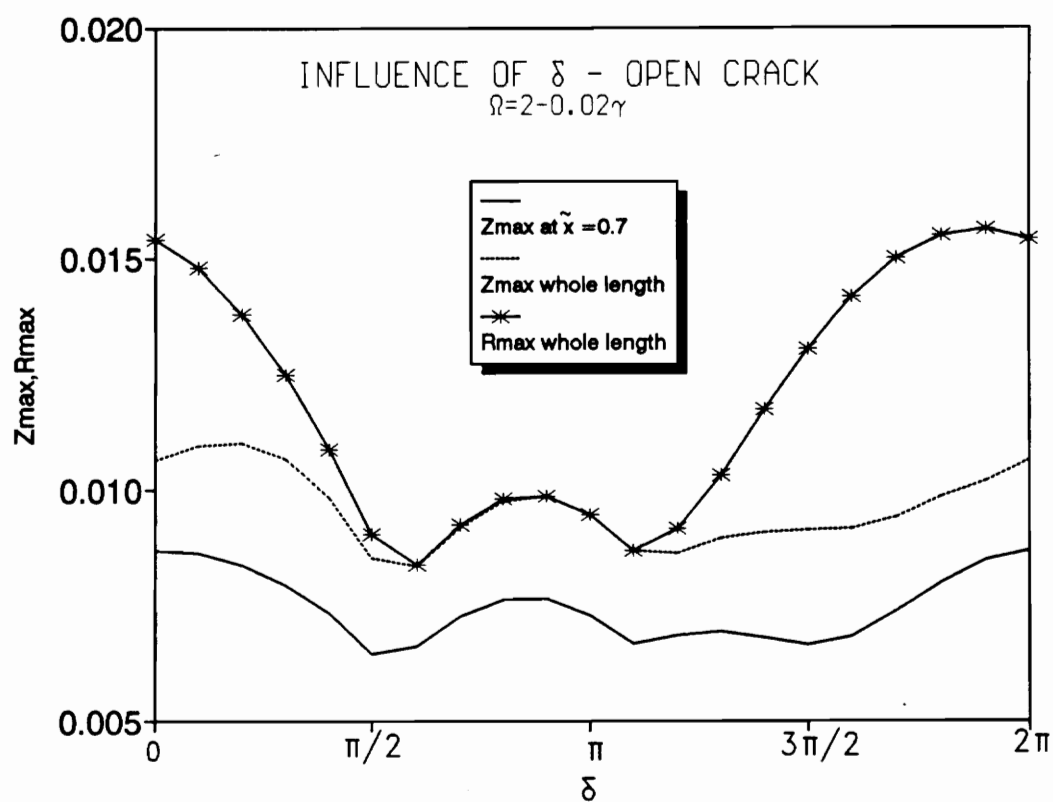
Figure 4.62 Influence of δ; deceleration, open crack.
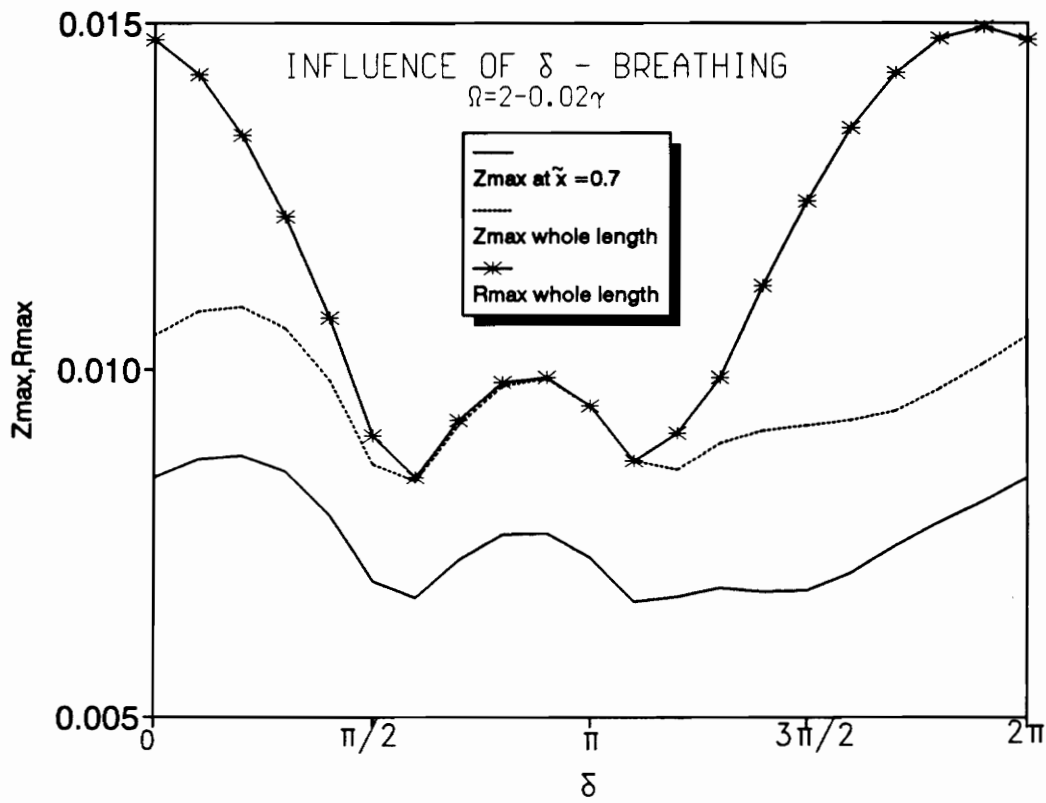
Figure 4.63 Influence of δ; deceleration, breathing crack.
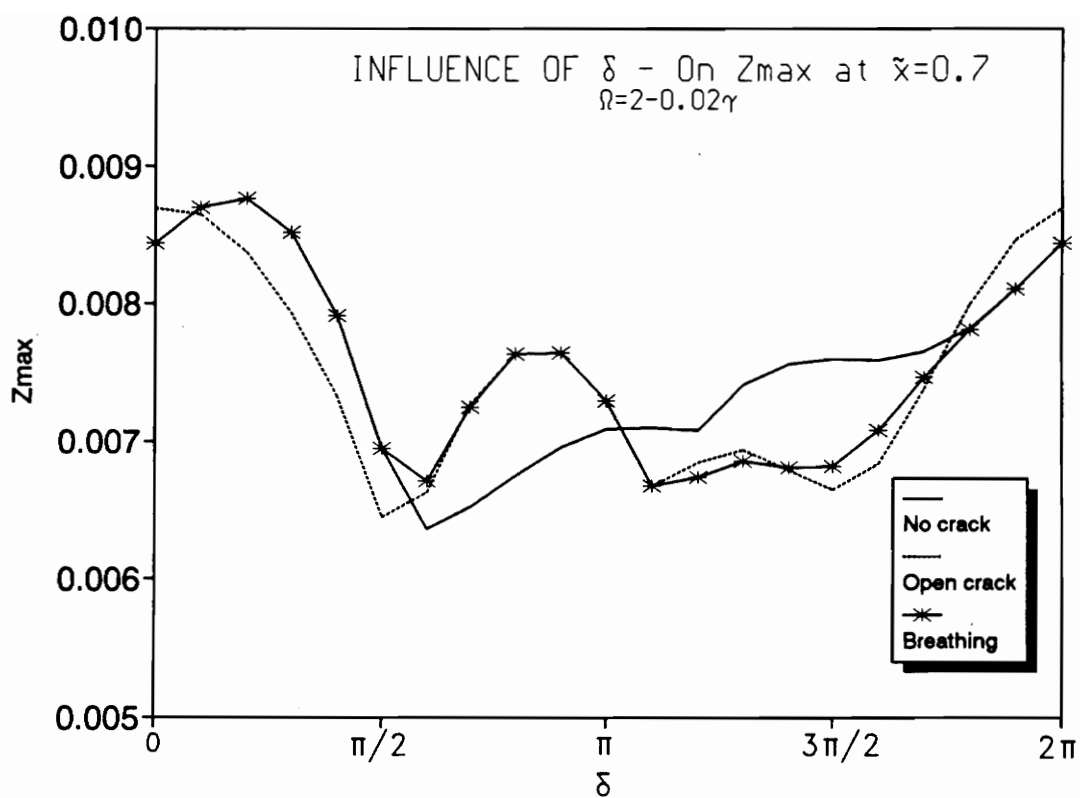
Figure 4.64 Influence of δ; deceleration, Z at $\tilde{x}=0.7$.
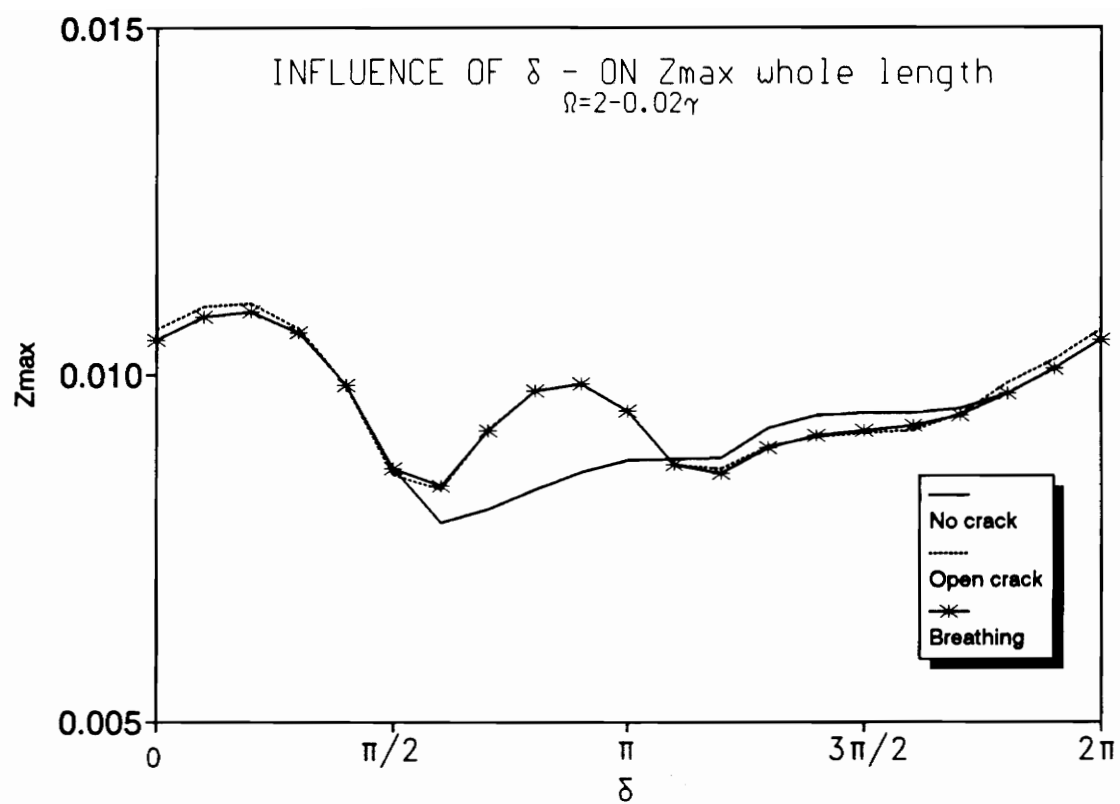
Figure 4.65 Influence of δ; deceleration, Z_{max}.

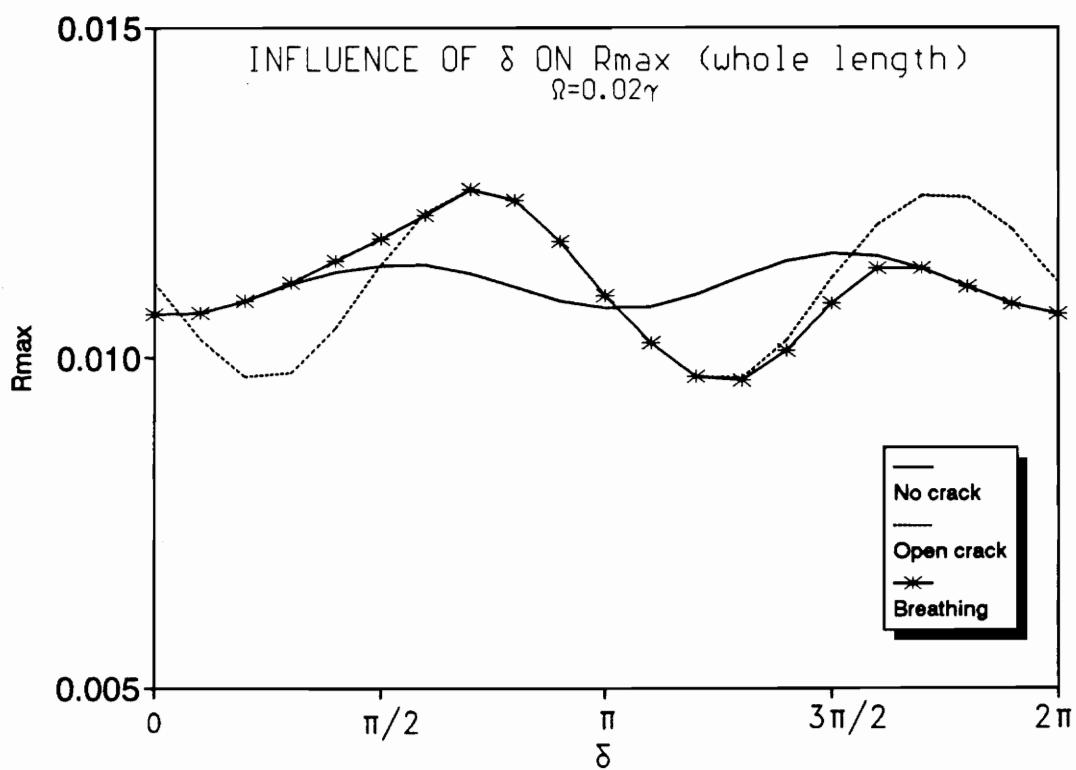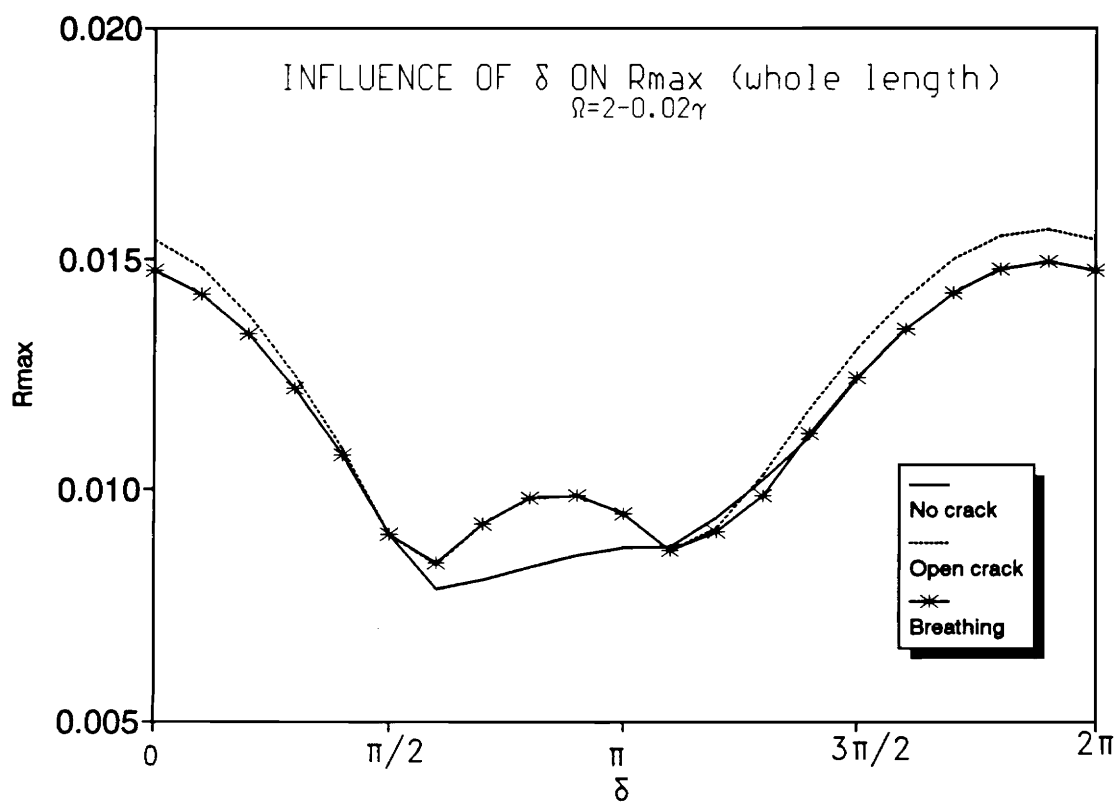**Figure 4.66 Influence of δ; deceleration, R_{max}.**

Table 4.7 Influence of crack position; aceleration: (a) Always open crack; (b) Breathing.

ƀ	Z_{max} at $\tilde{x}=0.7$	Z_{max} (overlength)
0	0.00898	0.01112
0.25	0.00949	0.01175
0.5	0.01035	0.01287
0.75	0.00953	0.01175
1.	0.00898	0.01112

(a)

ƀ	Z_{max} at $\tilde{x}=0.7$	Z_{max}(over length)
0	0.00898	0.01112
0.25	0.00949	0.01175
0.5	0.01035	0.01287
0.75	0.00953	0.01175
1.	0.00898	0.01112

(b)

Figure 4.67 Influence of crack position, acceleration.

Table 4.8 Influence of crack position; deceleration: (a) Always open crack; (b) Breathing.

Б	Z_{max} at $\tilde{x}=0.7$	Z_{max}(over length)
0	0.00663	0.00819
0.25	0.00711	0.00889
0.5	0.00780	0.00996
0.75	0.00745	0.00889
1.	0.00663	0.00819

(a)

Б	Z_{max} at $\tilde{x}=0.7$	Z_{max}(over length)
0	0.00663	0.00819
0.25	0.00711	0.00888
0.5	0.00780	0.00995
0.75	0.00744	0.00888
1.	0.00663	0.00819

(b)
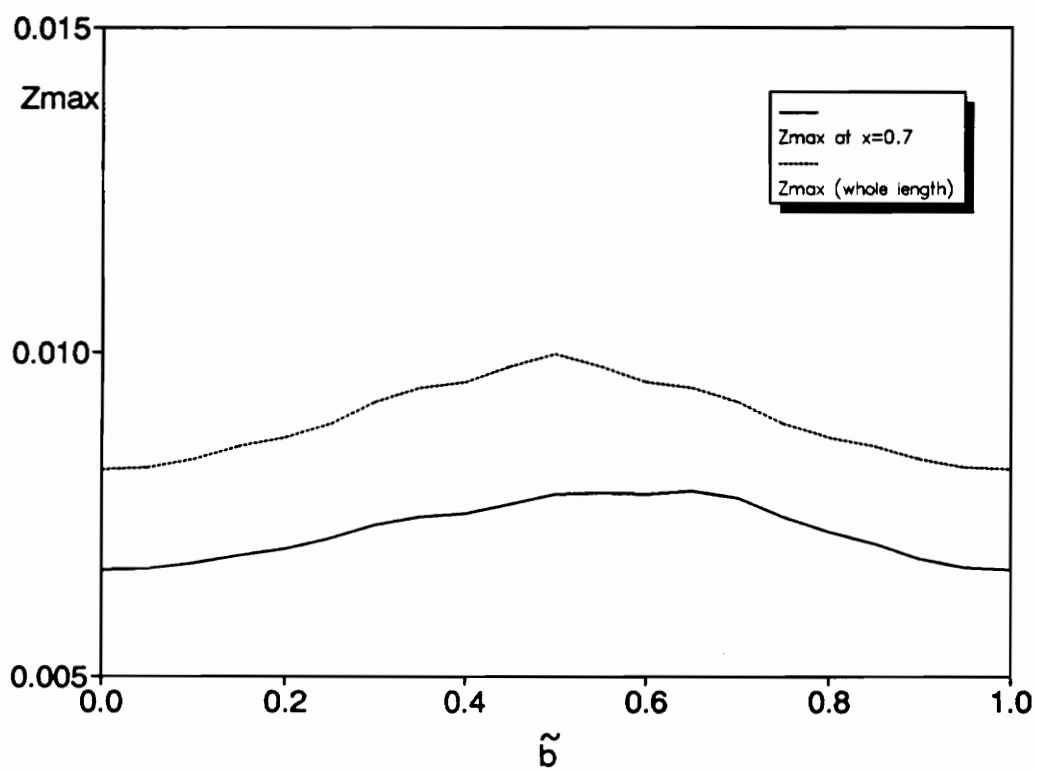
Figure 4.68 Influence of crack position, deceleration.

Table 4.10 Influence of crack depth; acceleration.

a/D	$\tilde{c}_{44}$	$\tilde{c}_{55}$	Z_{max} at $\tilde{x}=0.7$
0.1	0.0023	0.0096	0.0090
0.2	0.0048	0.0638	0.0100
0.25	0.0096	0.1100	0.0120
0.3	0.0172	0.1723	0.0369
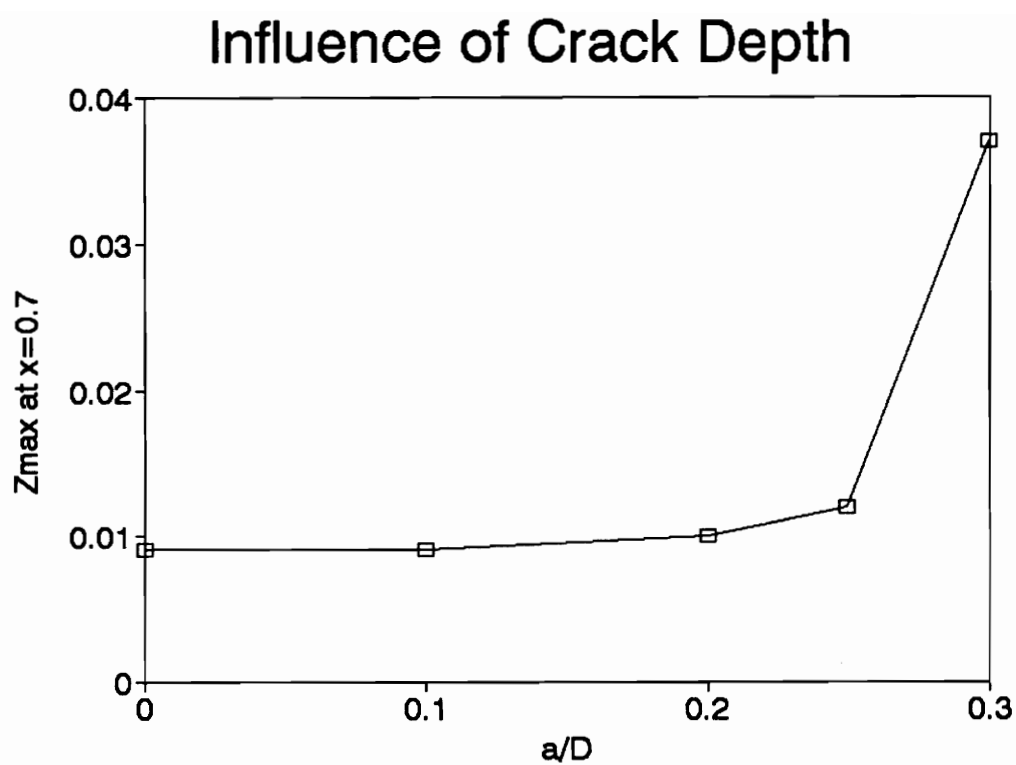
Figure 4.69 Influence of crack depth; acceleration

Table 4.10 Influence of crack depth; decceleration.

a/D	$\tilde{c}_{44}$	$\tilde{c}_{55}$	z_{max} at $\tilde{x}=0.7$
0.1	0.0023	0.0096	0.0070
0.2	0.0048	0.0638	0.0075
0.25	0.0096	0.1100	0.0096
0.3	0.0172	0.1723	0.0364

Influence of Crack Depth
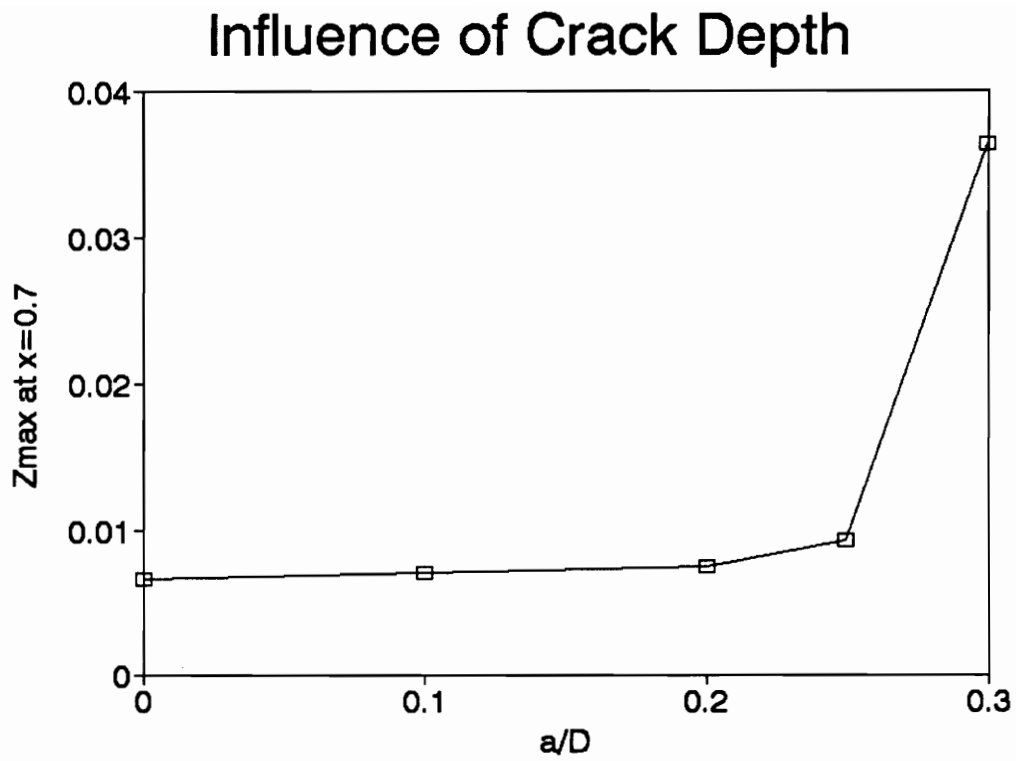
Figure 4.70 Influence of crack depth; decceleration

Chapter 5

Conclusions

The main objective of this thesis has been to find pieces of evidence indicating the presence of cracks in a shaft and methods to evaluate their importance without the need to remove the shaft from the machine or device in which it is placed.

The idea that if the shaft is accelerated or decelerated through a critical angular speed, this may produce appreciable differences in the response if the shaft has a crack or not, was investigated in this work. For that reason, the shaft was subjected to a range of linear accelerations and decelerations, to determine if there was clear evidence of the existence of the crack. Uncracked and always-open cracked shafts were considered as a way to obtain values to be compared against those given by the breathing crack cases.

The results obtained do not provide enough evidence in order to formulate decisive criteria to detect cracks in the shaft. However there are some encouraging findings like the noticeable difference between no crack and breathing crack responses for some cases, as in slow deceleration. But this is counterbalanced by the fact that this result may

not be true for different values of the eccentricity angle δ, as Figures 3.60 - 3.62 and 3.66 - 3.68 show.

Another interesting conclusion is that, since a cracked shaft has a smaller stiffness than an uncracked shaft, the critical speed is slower and then, the maximum amplitude occurs earlier for acceleration and later for deceleration in the cracked shaft than in the uncracked one. But the differences found are not always large enough to be considered encouraging.

The crack position also has influence on the dynamic response of the shaft. The middle of the shaft is the worst, i.e., the position that produces the largest displacements.

The last topic studied was the influence of crack depth. As in Collins (1989), a non-linear relation between crack depth and maximum response was found. This means that a very large shaft displacement can occur as the crack depth increases.

Future Research

Many aspects of the problem still remain to be studied. Among them should be mentioned the following:

Using the mathematical model presented here, many other

combinations of shaft parameters can be investigated. For example: other values of compliances; new acceleration or deceleration functions, like exponential; more than one crack; different values of damping; damping in the crack (note that the damping in the crack, d_c, was considered in the mathematical formulation but for the calculations it was made 0); non-symmetric transverse sections, i.e., $\Gamma \neq 1$; other eccentricities and different ratios L/R (L=length of the shaft, R=radius of the transverse section).

Other forcing systems instead of gravity and unbalance can be modeled with slight modifications of the model.

The shaft modeled in this thesis follows the Euler-Bernoulli theory , so that the shear deformation was not considered. It might prove interesting to develop the equations of motion of the shaft following the Timoshenko theory including angular acceleration or deceleration. Note that this was not done before and for some cases, with small ratio L/R, the results can differ appreciably from those obtained with the model used in this work.

Other boundary conditions can give different results from those obtained in this thesis, where a simply supported shaft was considered. A change in the boundary conditions requires

a definition of a new assumed solution and therefore a change in the final equations of motion.

References

Aiba, S., 1976, "On the Vibration of a Rotating Shaft Passing Through the Critical Speed." *Bulletin of the JSME*, Vol.19, No.128, pp.95–102.

Baker, J.G., 1939, "Mathematical-Machine Determination of the Vibration of an Accelerated Unbalanced Rotor." *Transactions of the ASME*, Vol.61, pp.A145–A150.

Bodger, W.K., 1967, "Deceleration of an Unbalanced Rotor Through a Critical Speed." *Journal of Engineering for Industry*, Vol. 89, pp. 582–586.

Capello, A., 1967, "On the Acceleration of Rotors Through Their Critical Speed." *Meccanica*, vol 2, pp.144–152.

Chang, H.-Y., and Petroski, H.J., 1986, "On Detecting a Crack by Tapping a Beam." *International Journal of Pressure Vessels and Piping*, Vol.22, pp.41–55.

Collins, K.R., 1989, The Effect of Cracks on the Dynamic Behavior of Bars and Shafts" M.S. Thesis, Virginia Polytechnic Institute and State University, Blacksburg, Virginia.

Collins, K.R., Plaut R. H., and Wauer, J., 1991, "Detection of Cracks in Rotating Timoshenko Shafts Using Axial Impulses." *Journal of Vibration and Acoustics*, Vol.113, pp.74–78.

Dornig, A., 1959, "Transients in Simple Undamped Oscillators Under Inertial Disturbances." *Journal of Applied Mechanics*, Vol 26, pp. 217–223.

Gasch, R., Person, M., and Weitz B., 1988, " Dynamic Behaviour of the Laval Rotor with a Cracked Hollow Shaft- A Comparison of Crack Models", *Vibrations in Rotating Machinery*, Mechanical Engineering Publications Ltd., London, pp. 463–472.

Hassenpflug, H.L., Flack, R.D., and Gunter, E.J., 1981, "Influence of Acceleration on the Critical Speed of a Jeffcott Rotor." *Journal of Engineering for Power*, Vol.103, pp.108–113.

Ishida, Y., Ikeda, T., and Yamamoto, T., 1987, "Transient Vibration of a Rotating Shaft with Nonlinear Spring Characteristics during Acceleration through a Major Critical Speed." *JSME International Journal*, Vol.30, Series III, pp.458-466.

Ishida, Y., Ikeda, T., Yamamoto, T., and Murakami, S. 1989, "Nonstationary Vibration of a Rotating Shaft with Nonlinear Spring Characteristics During Acceleration Through a Critical Speed." *JSME International Journal*, Vol.32, Series III, pp. 575-584.

Ishida, Y., 1990, "Lecture Notes on Nonlinear Vibrations of Rotating Shaft Systems" General Electric Company, pp.39-43

Iwatsubo, T., 1976, "Vibration of Rotors Through Critical Speeds." *Shock and Vibration Digest*, Vol.8,No.2, pp.89-98.

Kirmser, P.G., 1944, "The Effect of Discontinuities on the Natural Frequency of Beams." *Proceedings, ASTM*, Vol 44, pp.879-904.

Lewis, F.M., 1932, "Vibration During Acceleration Through a Critical Speed." *Transactions of the ASME*, Vol.54, pp.253-261.

Mayes, I.W., and Davies, W.G.R., 1980, "A Method of Calculating the Vibrational Behaviour of Coupled Rotating Shafts Containing a Transverse Crack." *Vibrations in Rotating Machinery*, Mechanical Engineering Publications Ltd., London, pp.17-27.

Meuser, R.B., and Weibel, E.E., 1948, "Vibration of a Non-linear System During Acceleration Through Resonance." *Journal of Applied Mechanics*, Vol 15, pp.21-24.

Muszynska, A., 1982, "Shaft Crack Detection." *Proceedings, 7th Machinery Dynamics Seminar*, Edmonton, Canada, pp.4.1-4.49.

Naveh, B.M. and Brach, R.M., 1977, ""On the Transition of a Shaft Through Critical Speeds." *Journal of Dynamic Systems, Measurement, and Control*, Vol.99, pp.48-50.

Papadopoulos, C.A., and Dimarogonas, A.D., 1988, "Coupled Longitudinal and Bending Vibrations of a Cracked Shaft." *Journal of Vibration, Acoustics, Stress, and Reliability in Design*, Vol.110, pp.1-8.

Petroski, H.J., and Glazik, J.L.Jr., 1980, "Effects of Cracks on the Response of Circular Cylindrical Shells." *Nuclear Technology*, Vol.51, pp.303-316.

Petroski, H.J., 1981," Simple Static and Dynamic Models for the Cracked Elastic Beam." *International Journal of Fracture*, Vol.17, pp.R71-R76.

Rajab, M.D.,and Al-Sabeeh A., 1991, "Vibrational Characteristics of Cracked Shafts." *Journal of Sound and Vibration*, Vol.147, pp.465-473.

Rogers, J.D., and Hollingshead, J.R., 1988, "Flaw Identification From Forced Vibration Testing." *Proceedings, 6th International Modal Analysis Conference*, Vol. II, Kissimmee, Florida, pp.1414-1419.

Schmied, J., and Krämer, E., 1984, "Vibrational Behaviour of a Rotor with a Cross-Sectional Crack." *Vibrations in Rotating Machinery*, Mechanical Engineering Publications Ltd, London, pp.183-192.

Thomson, W.J., 1949, "Vibration of Slender Bars with Discontinuities in Stiffness." *Journal of Applied Mechanics*, Vol.17, pp.203-207.

Tsuchiya, K., 1982, "Passage of a Rotor Through a Critical Speed." *Journal of Mechanical Design*, Vol.104, pp.370-374.

Wauer, J., 1990a, "On the Dynamics of Cracked Rotors - A Literature Survey." *Applied Mechanics Reviews*, Vol.43, pp.13-17.

Wauer, J., 1990b, "Modelling and Formulation of Equations of Motion for Cracked Rotating Shafts." *International Journal of Solids and Structures*, Vol.26, pp.901-914.

Ying, S.J., 1981, "Transient Whirling of a Rotating Shaft With an Unbalanced Disk.", *Rotating Machinary Dynamics*, DE - Vol.2, ASME, New York, pp.537-543.

Zobnin, A.P.,Kelzon, A.S., and Neigebauer, L.D., 1987, "Influence of Gyroscopic Effect on Resonance Avoidance During Acceleration of Unbalanced Flexible Rotors." *Vibration Engineering*, Vol.1, pp.269-281.

Vita

Raul Horacio Andruet was born on July 14, 1955 in Cordoba, Argentina. He graduated from Universidad Catolica de Cordoba in 1979 with a Bachelor in Civil Engineering degree. He worked in Inconas S.R.L., one of the leading consulting firms in Argentina, from 1979 until 1989. In 1989 he started the Master of Science in Civil Engineering program at Virginia Polytechnic Institute and State University.